Studies on Synthesis and Characterization of Magnesia Based Aggregates Derived from Indian Magnesite

Thesis submitted by

Chandrima Ghosh

Doctor of Philosophy (Engineering)

Department of Chemical Engineering
Faculty Council of Engineering & Technology
Jadavpur University
Kolkata, India

April 2019

JADAVPUR UNIVERSITY
KOLKATA-700032

Index No: I/60/15/E

1. **Title of the thesis:** Studies on Synthesis and Characterization of Magnesia Based Aggregates Derived from Indian Magnesite
2. **Name, Designation & Institution of the Supervisors:**
   i) Prof. Ujjaini Sarkar, Professor, Department of Chemical Engineering, Jadavpur University, Kolkata
   ii) Dr. Himansu Sekhar Tripathi, Senior Principal Scientist, Refractory & Traditional Ceramics Division, CSIR-Central Glass & Ceramic Research Institute, Kolkata
3. **List of Publications:**
   i) Studies on densification, mechanical, microstructural and structure–properties relationship of refractory aggregates prepared from Indian magnesite by changing lime–silica ratio, Chandrima Ghosh, A. Ghosh, H. S. Tripathi, J. Ghosh, M. K. Haldar, Ceram. Int. 40 (2014) 16791-98

   ii) Studies on synthesis and characterization of magnesia based refractory aggregates developed from Indian magnesite, M. K. Haldar, Chandrima Ghosh, A. Ghosh, J. Mat. Sci. Chem. Engg. 2 (2014) 1-8

   iii) Studies on densification, mechanical, micro-structural and structure-properties relationship of magnesium aluminate spinel refractory aggregates prepared from Indian magnesite, Chandrima Ghosh, A. Ghosh, M. K. Haldar, Mat. Char. 99 (2015) 84-91

   iv) Fused magnesia aggregates from Indian magnesite through plasma processing, Chandrima Ghosh, S. K. Singh, S. Sinhamahapatra, Indoceram 4 [2] (2016) 33-36

v) Effect of ZrO_2 on the densification behavior and properties of Indian magnesite, Chandrima Ghosh, S. Sinhamahapatra, H. S. Tripathi, Int. J. Appl. Ceram. Technol. 16 (2019) 410-417

vi) Reverse Flotation of Natural Magnesite and Process Optimization Using Response Surface Methodology, Chandrima Ghosh, S. Sinhamahapatra, H. S. Tripathi, U. Sarkar, Min. Metall. & Explor. (Under Review)

4. List of Patents: None

5. List of Presentations in National/International Conferences & Workshops

i) C. Ghosh, H.S. Tripathi, A.Ghosh, M.K. Haldar, Poster paper presentation entitled "Sintering and characterisation of refractory aggregates developed from off grade indigenous magnesite" in *National Seminar on Advances in Refractory Raw materials and Monolithics (ARMM 2013), November'2013*

ii) C. Ghosh, M.K. Haldar, H.S. Tripathi, A. Ghosh, Oral paper presentation entitled "Densification and property studies of inferior grade Indian magnesite for refractory application" in *10th India International Refractory Congress-2014 (IREFCON'14), Kolkata, January'2014*

iii) C. Ghosh, Poster paper presentation entitled "Plasma fused magnesium aluminate spinel from Indian natural magnesite" in *International Conference on Advances in Engineering and Technology (ICAET, 2016), Kolkata, April'2016*

iv) C. Ghosh, A.Ghosh, H.S. Tripathi, S. Sinhamahapatra, Poster paper presentation entitled "Plasma Assisted preparation of fused magnesium aluminate spinel from Indian Magnesite" in *2nd International Conference on Alumina and Other Functional Ceramics (AOFC-2017), Kolkata, February'2017*

v) C. Ghosh, Oral paper presentation entitled "Improvement of High Temperature Properties of Refractory Aggregates Developed from Low Grade Indian Magnesite" in *CGCRI-WUST Post Graduate Seminar on Refractories, CSIR-CGCRI, Kolkata, April'2019*

CERTIFICATE FROM THE SUPERVISORS

This is to certify that the thesis entitled "Studies on Synthesis and Characterization of Magnesia Based Aggregates Derived from Indian Magnesite" submitted by Smt. Chandrima Ghosh, who got her name registered on 28.01.2015 for the award of Ph.D (Engg) degree of Jadavpur University is absolutely based upon her own work under the supervision of Prof. Ujjaini Sarkar and Dr. Himansu Sekhar Tripathi and that neither her thesis nor any part of the thesis has been submitted for any degree/diploma or any other academic award anywhere before.

1._____

(Prof. Ujjaini Sarkar)
Professor
Department of Chemical Engineering
Jadavpur University

2._____

(Dr. H. S. Tripathi)
Senior Principal Scientist
Refractory & Traditional Ceramics Division, CSIR-Central Glass and Ceramic Research Institute

Acknowledgement

This thesis is a testament to my long, arduous journey towards receiving the Ph.D degree. The journey was hardly an individual effort, but the result of contributions and sacrifices made by numerous people including my family, well-wishers, friends and colleagues from different organizations. Hence, I take this opportunity at the onset to express my sincerest thanks to all those who contributed in myriad ways to the success of this endeavour and made it a memorable experience for me.

First, I would like to thank my supervisors, Dr. Himansu Sekhar Tripathi, Senior Principal Scientist & Head, Refractory & Traditional Ceramics Division (RTCD), CSIR-Central Glass & Ceramic Research Institute (CSIR-CGCRI), Kolkata and Prof. Ujjaini Sarkar, Professor, Department of Chemical Engineering, Jadavpur University, Kolkata. I would like to express my profound gratitude towards them for their astute supervision and immeasurable guidance for the enrichment of the thesis. Here, it would be a grave injustice if I do not mention the priceless contribution of Late Dr. Manas Kamal Haldar, Principal Scientist, RTCD, CSIR-CGCRI during the initial stage of my work as my supervisor, whose guidance was instrumental to the development of this research.

I am indebted to Council of Scientific & Industrial Research (CSIR), for bestowing the prestigious CSIR-Senior Research Fellowship to enable me to carry out my work. My sincere thanks go to the Director, CSIR-CGCRI, Kolkata for providing state-of-the-art laboratory facilities.

I would like to express my heartiest gratitude to Mr. Somnath Sinhamahapatra, Senior Scientist, RTCD, CSIR-CGCRI for his constant support and persistent guidance. I am also thankful to Dr. Koushik Dana, Senior Scientist, RTCD, CSIR-CGCRI and Dr. Shirshendu Chakraborty, Senior Scientist, Glass Division, CSIR-CGCRI for their valuable suggestions at crucial junctures of my research.

I am thankful to all the students of RTCD, CSIR-CGCRI for their endearing presence and constant encouragement, especially to Mr. Pintu Kumar for his tireless help. My thanks go out to all the staff members of RTCD, CSIR-CGCRI.

I thank the HOD, Department of Chemical Engineering, Jadavpur University and all other professors, students and technical staff for their help and support.

Finally, this section would not be complete without acknowledging the support of my family for their patience and understanding when I was too engrossed with my work and for the sacrifices that they made during this time.

I apologize to anyone I may have inadvertently omitted to acknowledge and express my deepest gratitude for their support.

Chandrima Ghosh

Date:

Table of Contents

		Page No.
Abstract		1-2
1. Introduction		3-4
2. Literature Survey		5-36
2.1 Application of magnesia		7
2.2 Magnesite-Introduction		8
2.2.1	Crystal structure of magnesia	9
2.2.2	Occurrences	10
2.2.3	Thermal behaviour of magnesite	12
2.2.4	Sintering behaviour of magnesite	16
2.3 Beneficiation of magnesite		21
2.4 Modification in phase assemblage		28
2.4.1	Changing C/S ratio	28
2.4.2	Zirconia addition	31
2.5 Development of magnesium aluminate spinel		32
3. Methodology		37-40
3.1 Methodology 1: Controlling the high temperature phase formation by changing the lime/silica ratio		37
3.2 Methodology 2: Addition of zirconia to modify the high temperature phase formation		38
3.3 Methodology 3: Preparation of magnesium aluminate spinel		38
3.4 Methodology 4: Beneficiation by reverse flotation and process optimization using RSM		38

Page No.

4. Experimental 41-56

4.1 Raw magnesite characterization 41

4.1.1 Chemical analysis 41

4.1.2 X-ray diffraction 42

4.1.3 Infrared spectroscopy 43

4.1.4 Differential thermal analysis & thermo-gravimetric analysis 44

4.1.5 Particle size distribution 45

4.1.6 Surface area measurement 46

4.2 Sample preparation 47

4.2.1 Batch composition 47

4.2.2 Powder preparation 47

4.2.3 Fabrication of bars 48

4.2.4 Sintering 48

4.3 Characterization of sintered aggregates 48

4.3.1 Linear shrinkage on firing 49

4.3.2 Bulk density and apparent porosity 49

4.3.3 True density 49

4.3.4 Phase analysis by XRD 50

4.3.5 Flexural strength at ambient temperature 50

4.3.6 Flexural strength at elevated temperature 51

4.3.7 Thermal shock resistance 51

4.3.8 Microstructure analysis 51

4.4 Beneficiation through froth flotation 52

4.4.1 Froth flotation principles 53

4.4.2 Flotation experiment 54

4.5 Process optimization by Response Surface Methodology 54

4.5.1 Box-Behnken Design 55

4.6 Phase analysis 56

Page No.

5. Results & Discussion 57-123

5.1 Raw material characterization 57

5.1.1 Chemical analysis 57

5.1.2 Phase analysis 57

5.1.3 Thermal decomposition behaviour 58

5.1.4 Infrared spectroscopy 59

5.1.5 Particle size analysis 60

5.1.6 Surface area analysis 61

5.2 Characterization of sintered aggregates 61

5.2.1 Densification behaviour 61

5.2.2 Phase analysis 63

5.2.3 Mechanical/thermo-mechanical properties 64

5.2.4 Microstructure analysis 66

5.3 Methodology 1 72

5.3.1 Densification behaviour 72

5.3.2 Phase analysis 73

5.3.3 Mechanical/thermo-mechanical properties 75

5.3.4 Microstructure analysis 78

5.3.5 Summary 86

5.4 Methodology 2 88

5.4.1 Densification behaviour 88

5.4.2 Phase analysis 90

5.4.3 Mechanical/thermo-mechanical properties 91

5.4.4 Microstructure analysis 94

5.4.5 Summary 100

5.5 Methodology 3 103

5.5.1 Densification behaviour 103

5.5.2 Phase analysis 106

5.5.3 Mechanical/thermo-mechanical properties 107

Page No.

5.5.4 Microstructure analysis 108

5.5.5 Summary 114

5.6 Methodology 4 116

5.6.1 Particle size analysis 116

5.6.2 Box-Behnken Design (BBD) and analysis 117

5.6.3 Characteristic of processed magnesite 121

5.6.4 Summary 123

6. Summary and Conclusions 124-125

7. References 126-139

List of Figures

Figure No.	Title	Page No.
Figure 2-1	Crystal structure of magnesia	7
Figure 2-2	Crystal structure of magnesite	10
Figure 2-3	CaO-SiO_2-MgO phase diagram	30
Figure 2-4	Structure of magnesium aluminate spinel	33
Figure 2-5	Magnesia-alumina phase diagram	34
Figure 3-1	Process Flow for methodologies 1, 2 & 3	39
Figure 3-2	Process Flow for methodology 4	40
Figure 4-1	Schematic of X-Ray Diffractometer	43
Figure 4-2	Schematic diagram of IR spectroscope	44
Figure 4-3	Thermal analyzer apparatus	45
Figure 4-4	Schematic diagram of froth flotation cell	53
Figure 5-1	XRD pattern of as received magnesite	58
Figure 5-2	TG-DTA thermogram of as received magnesite	59
Figure 5-3	Infrared spectroscopy of as received magnesite	60
Figure 5-4	Particle size distribution of milled slurry	61
Figure 5-5	Variation in bulk density and apparent porosity of magnesite samples (M0) as a function of sintering temperature	62
Figure 5-6	Variation in linear shrinkage and percentage densification of magnesite samples (M0) as a function of sintering temperature	63
Figure 5-7	XRD pattern of magnesite samples (M0) sintered in the temperature range of 1550-1700 °C	64
Figure 5-8	Variation in CMOR and HMOR (at 1300 °C) of magnesite samples (M0) as a function of sintering temperature	65
Figure 5-9	Retained flexural strength of magnesite samples (M0) with thermal cycles	65
Figure 5-10	FESEM images of magnesite samples (M0) sintered at (a) 1550 °C, (b) 1600 °C, (c) 1650 °C and (d) 1700 °C	66

Figure No.	Title	Page No.
Figure 5-11	Elemental mapping of magnesite sample (M0) sintered at 1550 °C	67
Figure 5-12	Line scan of magnesite sample (M0) sintered at 1600 °C	68
Figure 5-13	Line scan of magnesite sample (M0) sintered at 1650 °C	69
Figure 5-14	Elemental mapping of magnesite sample (M0) sintered at 1700 °C	70
Figure 5-15	Variation in bulk density and apparent porosity of M0 (as received), M1 (C/S ratio 1:1) and M2 (C/S ratio 2:1) samples as a function of sintering temperature	72
Figure 5-16	XRD pattern of M1 samples (C/S ratio 1:1) sintered in the temperature range of 1550-1700 °C	73
Figure 5-17	XRD pattern of M2 samples (C/S ratio 2:1) sintered in the temperature range of 1550-1700 °C	74
Figure 5-18	Variation in CMOR and HMOR (at 1300 °C) of M1 samples (C/S ratio 1:1) as a function of sintering temperature	75
Figure 5-19	Variation in CMOR and HMOR (at 1300 °C) of M2 samples (C/S ratio 2:1) as a function of sintering temperature	76
Figure 5-20	Retained flexural strength of M1 samples (C/S ratio 1:1) with thermal cycle	77
Figure 5-21	Retained flexural strength of M2 samples (C/S ratio 2:1) with thermal cycle	77
Figure 5-22	FESEM images of M1 samples (C/S ratio 1:1) sintered at (a) 1550 °C, (b) 1600 °C, (c) 1650 °C and (d) 1700 °C	78
Figure 5-23	FESEM images of M2 samples (C/S ratio 2:1) sintered at (a) 1550 °C, (b) 1600 °C, (c) 1650 °C and (d) 1700 °C	79
Figure 5-24	Elemental mapping of M1 sample (C/S ratio 1:1) sintered at 1550 °C	80
Figure 5-25	Line scan of M1 sample (C/S ratio 1:1) sintered at 1600 °C	81
Figure 5-26	Line scan of M1 sample (C/S ratio 1:1) sintered at 1650 °C	81
Figure 5-27	Elemental mapping of M1 sample (C/S ratio 1:1) sintered at 1700 °C	82
Figure 5-28	Elemental mapping of M2 sample (C/S ratio 2:1) sintered at 1550 °C	83

Figure No.	Title	Page No.
Figure 5-29	Elemental mapping of M2 sample (C/S ratio 2:1) sintered at 1600 °C	84
Figure 5-30	Line scan of M2 sample (C/S ratio 2:1) sintered at 1650 °C	85
Figure 5-31	Line scan of M2 sample (C/S ratio 2:1) sintered at 1700 °C	85
Figure 5-32	Variation in apparent porosity of the samples with sintering temperature and zirconia content	89
Figure 5-33	Variation in bulk density of the samples with sintering temperature and zirconia content	89
Figure 5-34	Phase development of samples sintered at 1600 °C with different zirconia content	90
Figure 5-35	Variation in flexural strength at room temperature with zirconia content of the samples sintered at 1550 °C	92
Figure 5-36	Variation in flexural strength at room temperature with zirconia content of the samples sintered at 1600 °C	92
Figure 5-37	Retained flexural strength of the samples sintered at 1550 °C with varying amount of zirconia after different thermal shock cycles	93
Figure 5-38	Retained flexural strength of the samples sintered at 1600 °C with varying amount of zirconia after different thermal shock cycles	93
Figure 5-39	FESEM images of (a) MZ0, (b) MZ1, (c) MZ3 and (d) MZ5 samples sintered at 1550 °C	94
Figure 5-40	FESEM images of (a) MZ0, (b) MZ1, (c) MZ3 and (d) MZ5 samples sintered at 1600 °C	95
Figure 5-41	Average grain size of the samples sintered at 1550 °C and 1600 °C	96
Figure 5-42	Elemental mapping of MZ1 sample sintered at 1550 °C	97
Figure 5-43	Point analysis of MZ3 sample sintered at 1550 °C	98
Figure 5-44	Point analysis of MZ3 sample sintered at 1550 °C	98
Figure 5-45	Point analysis of MZ3 sample sintered at 1550 °C	99
Figure 5-46	Point analysis of MZ3 sample sintered at 1600 °C	99
Figure 5-47	Line scan of MZ5 sample sintered at 1550 °C	100
Figure 5-48	Variation in bulk density and apparent porosity of magnesium aluminate spinel samples as a function of sintering temperature	104

Figure No.	Title	Page No.
Figure 5-49	Variation in linear shrinkage and volume shrinkage of magnesium aluminate spinel samples as a function of sintering temperature	104
Figure 5-50	Variation in true density and densification (%) of magnesium aluminate spinel samples as a function of sintering temperature	105
Figure 5-51	Variation in total porosity and closed porosity of magnesium aluminate spinel samples as a function of sintering temperature	105
Figure 5-52	XRD pattern of magnesium aluminate spinel samples sintered at different temperatures	106
Figure 5-53	Variation in CMOR and HMOR (at 1300 °C) of magnesium aluminate spinel samples as a function of sintering temperature	107
Figure 5-54	Variation in retained flexural strength of magnesium aluminate spinel samples with thermal cycles	108
Figure 5-55	FESEM images of magnesium aluminate spinel samples sintered at (a, b) 1550 °C, (c, d) 1600 °C, (e, f) 1650 °C and (g, h) 1700 °C	109
Figure 5-56	Variation in grain size of magnesium aluminate spinel samples with sintering temperature	110
Figure 5-57	Line scan of magnesium aluminate spinel sample sintered at 1550 °C	111
Figure 5-58	Line scan of magnesium aluminate spinel sample sintered at 1600 °C	112
Figure 5-59	Line scan of magnesium aluminate spinel sample sintered at 1650 °C	113
Figure 5-60	Line scan of magnesium aluminate spinel sample sintered at 1700 °C	113
Figure 5-61	Particle size distribution in (a) froth and (b) tailing	116
Figure 5-62	Correlation between experimental and predicted data	120
Figure 5-63	Normal plot of studentized residuals	120
Figure 5-64	Response surface plots showing the interactive effect of C/F ratio, amount of depressant and air pressure in various combinations; (a) effect of C/F ratio and air pressure (b) effect of amount of depressant and air pressure (c) effect of amount of depressant and C/F ratio on the silica content of forth	122
Figure 5-65	XRD pattern of raw magnesite and processed magnesite (PM)	123

List of Tables

Table No.	Title	Page No.
Table 2-1	Properties of magnesia	6
Table 2-2	World production of magnesite and reserves	11
Table 2-3	Year wise production of magnesite in India (by states)	11
Table 2-4	Year wise consumption of magnesite in India in 2014-2015 and 2015-2016 (by industries)	12
Table 2-5	Activation energy for magnesite decomposition using different methods	15
Table 4-1	Methodology wise batch code and composition	47
Table 5-1	Chemical analysis results of raw magnesite	57
Table 5-2	Quantification of the crystalline phases of magnesite sample (M0)	64
Table 5-3	Quantification of the crystalline phases of M1 samples (C/S ratio 1:1) sintered at different temperatures	74
Table 5-4	Quantification of the crystalline phases of M2 samples (C/S ratio 2:1) sintered at different temperatures	75
Table 5-5	Quantification of the crystalline phases of the samples sintered at 1600 °C with varying amount of zirconia	91
Table 5-6	Details of microstructural analysis of MZ0, MZ1, MZ3 and MZ5 samples sintered at 1550 °C and 1600 °C	96
Table 5-7	Variation in spinel content with increase in sintering temperature	106
Table 5-8	Experimental design matrix and results (as per BBD)	117
Table 5-9	Summary of models tested for the response	117
Table 5-10	Analysis of variance (ANOVA) for the quadratic model	118
Table 5-11	Goodness of fit parameters of the suggested quadratic model	119
Table 5-12	Quantification of the crystalline phases of raw and processed magnesite	123

List of Abbreviations/Symbols

XRD	X-ray diffraction
DTA	Differential thermal analysis
TGA	Thermo-gravimetric analysis
IR	Infrared spectroscopy
BS	British standard
ASTM	American society for testing and materials
FESEM	Field emission scanning electron microscope
EDX	Energy dispersive X-ray analysis
BD	Bulk density
AP	Apparent porosity
C/S	Lime/silica ratio
MOR	Modulus of rupture
MPa	Mega Pascal
θ	Bragg's angle
SHMP	Sodium hexametaphosphate
RSM	Response surface methodology
BBD	Box-Behnken design
C/F	Collector/frother ratio
ANOVA	Analysis of variance

Abstract

Natural magnesite is the primary source for the production of magnesia based refractory materials. India has vast deposit of magnesite in Salem and Almora region. However due to the presence of large amount of impurities which form low melting phases on sintering, high temperature applications of Indian magnesite are restricted. In this background, an attempt has been made to synthesize and characterize magnesite based refractory aggregates and to improve its mechanical & thermo-mechanical properties using different methodologies. Natural magnesite of Salem region was used as the starting material.

Raw magnesite was characterized in terms of chemical analysis, differential thermal analysis, thermo gravimetric analysis, phase assemblage and Infrared spectroscopy. The sintering temperature range across methodologies was chosen to be 1550-1700 °C. All sintered samples were characterized in terms of densification, flexural strength, thermal shock resistance, phase assemblage and microstructural evolution.

In the first methodology, lime/silica ratio of the system was changed by adding $CaCO_3$ in the raw magnesite. It was observed that when the lime/silica ratio was modified into 1:1, only low melting monticellite phase was formed as a secondary phase. However, when the ratio was changed into 2:1, dicalcium silicate phase was formed which was high melting in nature. This helped in improvement of thermo-mechanical properties.

In the second methodology, 1 to 5 wt % zirconia was added to the raw magnesite to reduce the low melting phase formation at high temperatures. It was found that addition of zirconia minimized the formation of low melting monticellite phase as zirconia utilized one of the impurities (lime) to stabilize its tetragonal form at room temperature. As the low melting phase formation was reduced, high temperature mechanical properties were improved.

In the third methodology, magnesium aluminate spinel samples were prepared using the raw magnesite and calcined alumina in one stage sintering. Developed spinel aggregates showed good mechanical and thermo-mechanical properties. Quantification of the crystalline phases showed that the spinel content increased with sintering temperature.

In the fourth and final methodology, the raw magnesite was beneficiated using reverse froth flotation technique. Pine oil was used as frother, Flotigam EDA as collector and sodium hexametaphosphate as depressant of carbonate groups. Various process parameters were optimized using Response Surface Methodology (RSM). A quadratic model equation was formulated for the experiment. The effect of different process parameters was analyzed using Box-Behnken Design. The model was significant as suggested by statistical analysis. Optimum process conditions were predicted by RSM after analyzing the experimental data. The beneficiated sample for which the highest silica in froth was achieved was characterized in terms of X-ray diffraction analysis. Quantification of the crystalline phases showed that amount of quartz was reduced from 2.3 % in the raw magnesite to 1.8 % in the processed magnesite. A new experiment was carried out using optimized values of process parameters. The results of the new experiment and the software predicted data are in good agreement with each other.

1. Introduction

Magnesite is a carbonate of magnesium having the chemical formula $MgCO_3$. Theoretically it contains 52.4% CO_2 and 47.6% MgO. It is mostly found as irregular veins in an alteration product of ultramafic rocks, serpentinite and other magnesium rich rock types and is formed by replacement of dolomite and dolomitic lime stone. These magnesites often are cryptocrystalline and contain silica and lime as impurities along with Fe_2O_3 and Al_2O_3.

Magnesite finds its application in various fields. However, the most important use of magnesite is as a refractory raw material. Magnesite is burnt to produce magnesia which is used in steel, cement, glass, non ferrous metal and calcium carbide industries in the form of MgO-C, MgO-chrome and fired magnesia bricks. The primary features which make magnesia an attractive choice are its high melting point (~2800°C), good resistance to attack by iron oxides, alkalis and high lime containing fluxes formed at the working temperature of steel melting furnaces and environment friendly nature.

Magnesite is mainly mined in Russia, China, North Korea, Turkey, Australia, Austria, and Brazil etc. Though India has vast reserve of naturally occurring magnesite, Indian refractory industries are mostly dependant on imported ones. This is because of the high level of impurities present in Indian magnesite. The major two deposits of magnesite in India are Salem of Tamil Nadu and Almora of Uttarakhand. Salem magnesite contains silica and lime as impurities while Almora magnesite contains iron oxide. These impurities form low melting phases like monticellite and merwinite (in case of Salem magnesite) and di-calcium ferrite (in case of Almora magnesite) at elevated temperatures which degrade high temperature refractory properties of Indian magnesite.

For past many years researchers have been trying to improve the quality of Indian low grade magnesite using different approaches like bio leaching, froth flotation, gravity separation, additive incorporation etc. However, detailed study on Salem magnesite and synthesis of good quality refractory aggregates from low grade magnesite have not been achieved yet. In this background, an attempt has been made to synthesize and characterize

magnesite based refractory aggregates and to improve its mechanical & thermo-mechanical properties using different methodologies which are as follows:

- Controlling the high temperature phase development by changing the lime/silica ratio
- Addition of monoclinic zirconia (ZrO_2) with an aim that it will react with the impurities present in Salem magnesite to form different high melting phases or will use the impurities for its tetragonal phase stabilization
- Development of magnesia rich magnesium aluminate spinel ($MgAl_2O_4$) by reaction sintering with calcined alumina for the maximum utilization of low quality magnesite
- Beneficiation of raw magnesite by reverse flotation and process optimization using RSM

2. Literature Survey

The word “refractory” has its origin in Latin word refrāctārius which means stubborn. According to the ASTM C71 specification, refractories are “nonmetallic materials having those chemical and physical properties that make them applicable for structures or as components of system that are exposed to environments above 1000 °F (538 °C)” [1]. The concept of refractories is known to exist since ancient times i.e. Bronze and Iron Ages. With time and evolution of society and technology, the refractory industry too, has advanced itself. Most of the scientific and technological developments of the past 100 years would not have been possible without refractories. Refractories are widely used in industries like metal, glass, petrochemicals and cement [2]. Out of the total world’s refractory production 70% is consumed by the iron & steel industries [3].

Based on their physical appearance, refractories are broadly classified into two categories- shaped and unshaped or monolithics [4]. Irrespective of whether the refractory is shaped or not, it requires a stable aggregate surrounded by a matrix. Moreover, depending on the chemical nature, refractories can be divided into three classes- acidic, basic and neutral. Basic refractories are widely used in iron & steel industries and non-ferrous industries like copper, lead, zinc, alumina and cement [5]. Magnesite, dolomite and chromite are the major raw materials for the manufacture of different types of basic refractories. Out of these, magnesite is the most important one and the main source of magnesia, the most widely used basic refractory material. Raw magnesite is also used in industries like mosaic tiles, electrodes, chemicals, manufacture of magnesium metals, fertilizers and food processing [6].

The occurrence of magnesia (also referred to as periclase) or magnesium oxide (MgO) in its natural form is rare. Periclase was discovered by A. Scacchi in 1840 in Italy as a mineral contaminated with ferrous oxide. The word ‘periclase’ is derived from the Greek word ‘peri’, which means ‘around’ and the word ‘klao’, which means ‘to cut’. Some general properties of magnesia are shown in Table 2-1 [7].

Table 2-1: Properties of magnesia

Color	Mainly colorless to grayish white
Crystal structure	Face centered cubic
Density	3.581 g/cc
Hardness (Mohs scale)	5.5
Refractive index (at 633nm)	1.7350
Thermal conductivity (at 1600 °C)	0.016 cal s^{-1} cm^{-1} $^oC^{-1}$
Melting point	2800 °C
Thermal expansion coefficient (at 1000 °C)	13.6 × 10^{-6} /°C
Heat of formation	-601.241 kJ/mol
Elastic modulus	210-317 GPa
Modulus of rupture	96.5-103.4 GPa
Flexural strength	89.6 GPa

Magnesia has a face centered cubic (FCC) crystal lattice similar to sodium chloride & calcium oxide which was first proposed by W. A. Hull [8] and further substantiated by Davey and Hoffman [9]. R. W. G. Wyckoff studied the crystal structure of magnesium oxide using Laue photographs and X-ray spectrum measurements. He remarked that the only possible simple structure for magnesium oxide is 'sodium chloride' arrangement. More complicated arrangement having 32 molecules is also possible [10].

Periclase belongs to space group of Fm3m (point group $4/\mathrm{m}\,\bar{3}\,2/\mathrm{m}$). The cubic closed-packed arrangement is formed by the O^{2-} anions and the resultant octahedral coordination sites are fully occupied by Mg^{2+} cations and form [MgO_6] octahedral. These [MgO_6] octahedras are connected with each other by edge sharing. In periclase structure, Mg^{2+} ions are centrosymmetric and [MgO_6] octahedras are remained undistorted [11].

R. M. Hazen studied the effect of temperature and pressure on lattice parameters of periclase using a synthetically prepared fine single crystal of periclase. Crystal structure of magnesia is shown in Figure 2-1. Magnesium and oxygen occupied fixed special positions; 4a and 4b respectively in periclase and the site symmetry was reported as $4/\mathrm{m}\,\bar{3}\,2/\mathrm{m}$. The

unit cell dimension of periclase at room temperature and normal atmospheric pressure was obtained as a=4.2110 Å. Lattice parameter increases with increase in temperature, at 1040 °C it became 4.264Å and at higher pressure it decreases [12].

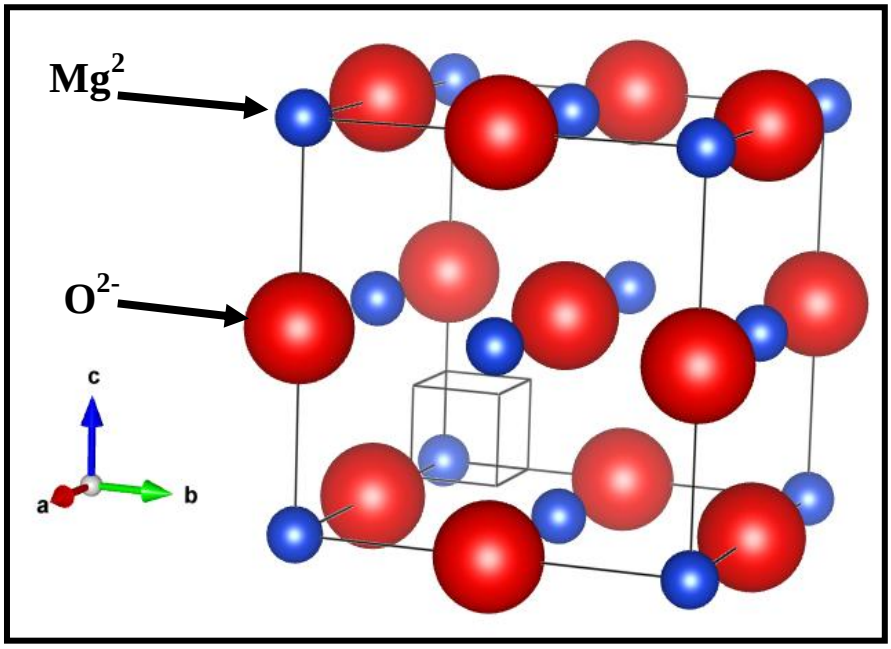

Figure 2-1: Crystal structure of magnesia [12]

2.1 Applications of magnesia

Magnesia has long been considered as an important industrial material for its use in refractories [13]. Approximately, two-third of the total consumption of magnesium compounds is used for refractory applications [14, 15]. The remaining one-third has various uses like environmental pollution abatement, manufacturing, construction, agriculture and pharmaceuticals [16-20]. It is used in the form fused magnesia, dead burnt magnesia or as caustic calcined magnesia. Dead burnt magnesite (DBM) is produced in the rotary kiln by calcining raw magnesite at a controlled temperature of 1750 °C and it is chemically inert. Light burnt or caustic calcined magnesia is produced by calcining magnesite ore at temperature ranging from 700 °C to 1000 °C [21]. Magnesia can also be extracted from sea-water by precipitation in which $Mg(OH)_2$ is precipitated by the addition of alkali [22]. The hydroxide is washed, filtered and dead-burned in the temperature range of 1700-2000 °C to produce refractory grains [23]. In addition to it, extraction from inland brine is also considered as a source of magnesia [24].

Fused magnesia is used as insulating material in electrical industries and refractory brick linings in steel furnaces. Magnesia in dead burnt form is used to make basic refractory bricks, mortars, ramming masses, tar/pitch impregnated magnesite, magnesia-carbon bricks, slide-gate plates and other refractories. On the other hand, caustic calcined form of magnesite is used in manufacturing sorel cement, castable refractories and extraction of magnesium metal [25].

Magnesia based shaped and unshaped refractories are used worldwide for lining industrial furnaces, particularly primary and secondary steel making furnaces [26]. These refractories are good candidates for the lining of cement and steel furnaces owing to the high melting point of MgO (~2800 °C) and to the fact that it has excellent resistance to attack by iron oxide, alkalis and high lime containing fluxes at working temperature of steel melting furnaces (1700 °C) [27, 28]. Unlike its competitors (lime & dolomite), it has better resistance to hydration and also is non toxic. However, the main disadvantages which limit their applications are its poor thermal shock resistance and high thermal conductivity[28, 29]. Due to poor thermal shock resistance they cannot tolerate several thermal cycles [30].

2.2 Magnesite - Introduction

Magnesite is the major source of magnesia. The name ‘magnesite’ is derived from Magnesia, a prefecture in Thessaly, Greece. Magnesia alba, also known to the alchemists as white magnesia or mild magnesian earth, is nothing but today’s magnesite or magnesium carbonate. The mineralogical term magnesite was first applied to a series of magnesium salts (carbonate, sulfate, nitrate and chloride) by J. C. Delaméthrie in 1795. The same name was also being used to describe magnesium carbonates and silicates by A. Brongniart [31]. The use of the term magnesite was first restricted to the carbonate minerals by D. L. G. Karsten in 1808 [32].

In nature, magnesite occurs in veins and masses combined with serpentine and other magnesium rich igneous and metamorphic rocks from which it is formed by alteration [33]. G. W. Bain [34] described four types of magnesite deposits and they are as follows:

i) as a sedimentary rock
ii) as an alteration of serpentine

iii) as a vein filling

iv) as a replacement of limestone and dolomite

Magnesite can be found in two physical forms, one is cryptocrystalline or amorphous and the other is crystalline, macrocrystalline or bone magnesite.

Sedimentary deposits of cryptocrystalline magnesite occur in lagoons, salt lakes and fresh water lakes. The formation of magnesite in salt water occurs under specific conditions like a reducing alkaline environment, a high concentration of magnesium sulphate and a concentration of CO_2 above 380 mg/L and the presence of H_2S, ammonia, or organic salt and a high temperature. At first the magnesium precipitates as hydroxide and then it is altered by reaction with carbonate ion to form $MgCO_3 \cdot xH_2O$ followed by dehydration to form $MgCO_3$.

Amorphous magnesite deposits occur in serpentized ultrabasic rocks which have gone through a hydrothermal leaching of magnesium from the serpentine. The reaction is as follows:

$$H_4Mg_3Si_2O_9 + 2H_2O + 3CO_2 \rightarrow 3MgCO_3 + 4H_2O + 2SiO_2 \qquad \textbf{(Equation 2-1)}$$

(Serpentine)

The magnesium carbonate thus formed, is deposited in veins and the silica is carried away in solution. Magnesite can also be formed by the serpentization of ultrabasic rock under low temperature and low pressure conditions. Deposits of cryptocrystalline magnesite in cracks and fissures are the result of weathering of serpentine by CO_2 containing water. Crystalline magnesite, on the other hand, is formed through the hydrothermal metasomatic replacement of older dolomite or limestone formations.

2.2.1 Crystal structure of magnesite

Magnesite ($MgCO_3$) has a specific gravity of 3.0-3.12 and a Mohs scale hardness of 3.5-4.5 [35]. In its pure form, magnesite is white in color with an opaque cast. In the native form, it is yellow, brown or gray. Crystal system of magnesite is hexagonal or rhombohedral, though crystals are rare [7]. The crystal structure of magnesite was determined by Oh et al [36] using X-ray and infrared methods. Single crystals of magnesite were synthesized using a hydrothermal method. The crystal structure was reported as trigonal having space

group of $R\bar{3}C$ and the lattice parameters are a=4.637Å, c=15.023Å and z=6. The bond length of C-O and Mg-O in magnesite are 1.283Å and 2.105 Å respectively and inter atomic bond angles of O-Mg-O are 88.25°, 91.75° and 180° and forms an near ideal octahedron structure.

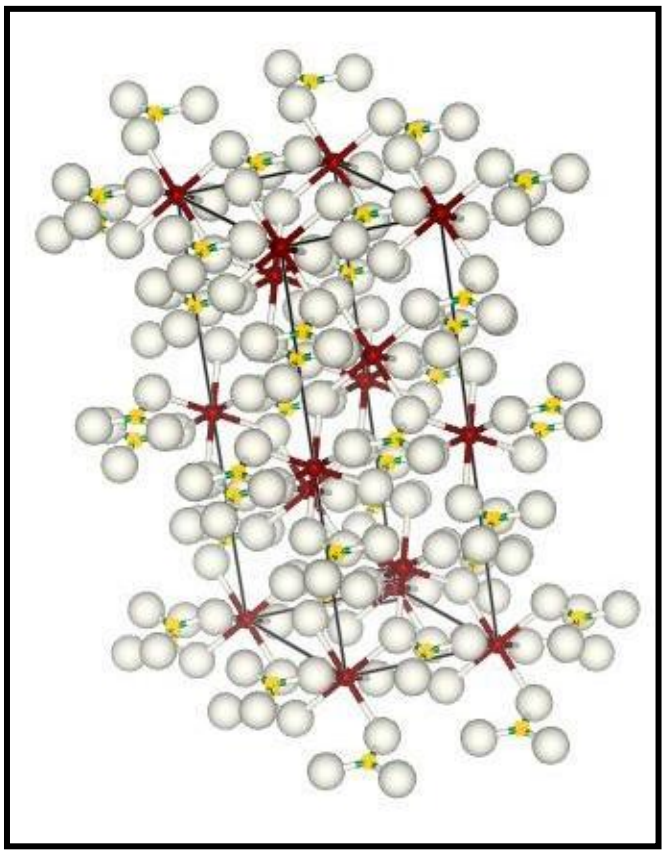

Figure 2-2: Crystal structure of magnesite [36]

(Where maroon balls represent magnesium, yellow balls represent carbon and grey balls represent oxygen atoms)

In a separate study, crystal structure of magnesite was investigated by means of X-ray diffraction of synthetically prepared single crystal of high quality pure magnesite. The crystal structure was reported as rhombohedral having space group symmetry of $R\bar{3}C$. The unit cell dimensions obtained were a=4.6255Å, c =14.987Å [37].

2.2.2 Occurrences

Magnesite reserves are found all over the world (Table 2-2). Though Russia has the largest reserve of magnesite mines, China is the main exporter of raw magnesite followed by other

countries like Turkey, Russia, U.S.A., Australia, Austria, Spain, Brazil, Greece, North Korea, India etc [22, 38].

Table 2-2: World production of magnesite and reserves [38]

Country	**Mine Production (2016)**	**Reserve**
Australia	440	330,000
Austria	750	50,000
Brazil	500	390,000
China	19,000	1,000,000
Greece	410	280,000
India	240	90,000
North Korea	250	1,500,000
Russia	1,350	2,300,000
Slovakia	620	120,000
Spain	620	35,000
Turkey	2,800	390,000
Other Countries	680	1,400,000

Adopted from Mineral Commodity Summaries, U. S. Geological Survey, January, 2017

India has vast reserves of natural magnesite in different localities. According to the Indian Minerals Handbook, 2018, substantial resources of magnesite are at Uttarakhand (59%), Rajasthan (14%) and Tamil Nadu (25%) (Table 2-3). Other resources are located in Andhra Pradesh, Himachal Pradesh, Jammu & Kashmir, Karnataka & Kerala [25].

Table 2-3: Year wise production of magnesite in India (by states)[25]

State	**2014-2015**		**2015-2016**		**2016-2017**	
	Quantity (tonnes)	**Value (‘000)**	**Quantity (tonnes)**	**Value (‘000)**	**Quantity (tonnes)**	**Value (‘000)**
Karnataka	9129	40910	8161	39962	8391	35562
Tamil Nadu	225694	637938	264913	705318	223424	612564
Uttarakhand	50186	69944	54589	81792	67352	87529

Adopted from Indian Minerals Yearbook 2018, Part- III: Mineral Reviews, Govt. of India, Ministry of Mines, Indian Bureau of Mines [25]

Magnesite is mostly used in calcined form which found applications in magnesia refractory, sorel cement etc. Raw magnesite is used in chemical, fertilizer, food processing industries and also for extraction of magnesium metal. About 86% of the magnesite mined is used for calcinations, 9 % is used in ferro-alloy industries and only 4 % is used in refractories (Table 2-4)

Table 2-4: Year wise consumption of magnesite in India in 2014-2015 and 2015-2016 (by industries)

Industry	**2014-15 (In tonnes)**	**2015-16 (In tonnes)**
Calcination	171400	155100
Chemicals	2,300	3000
Ferro-alloys	10700	14500
Refractories	67500	69000
Others	23400	23400

Adopted from Indian Minerals Yearbook 2017, Part-III: Mineral Reviews, Govt. of India, Ministry of Mines, Indian Bureau of Mines [25]

Magnesite of Tamil Nadu (Salem region), India is found mainly as encrustations, veins and stringers in ultra basic rocks like dunite and peridotite. Magnesite deposits of South India are located in the amphibolites-granulite facies transition zone, which lies between the low-grade granite-greenstone terrain in the north and the high-grade granulite terrain to the south. Mineralization of magnesite is observed at different places along the shear zone. Chalk hills, Salem, Tamil Nadu, host the major magnesite deposit in south India. Magnesite at Salem is generally considered to be formed due to the reaction of late stage co-magmatic hydrothermal fluids with the host ultramafic rocks, though the source of CO_2 still remains uncertain [39].

2.2.3 Thermal behavior of magnesite

In ceramics, all the carbonate minerals are decomposed before being used or during firing of the product. Therefore the decomposition of the carbonates, particularly limestone, dolomite and magnesite had been investigated thoroughly for many years. Various researchers have studied the decomposition behavior of magnesite by thermal analysis.

C. W. Beck [40] interpreted the differential thermal analysis curves of forty eight carbonate samples including magnesite from two different regions. The magnesite specimen from Styria, Austria, showed slow decomposition starting at 470 °C, followed by an endothermic peak at 660 °C and then it rapidly ended at 685 °C. The other magnesite sample was taken from California and the chemical analysis showed the presence of 15.31 % $FeCO_3$. In this case, decomposition started slowly at 500 °C and then after 590 °C, it went on rapidly to the peak at 755 °C finally overlapping with the exothermic peak at 785 °C representing the oxidation of ferrous oxide to ferric oxide.

Differential thermal analysis of forty three samples of various carbonates including magnesite samples from different sources were carried out by R. M. Gruver [41]. Magnesite samples from California, Greece and Washington were studied. Magnesite sample from California and Greece showed sluggish decomposition near 700 °C. In case of the sample from the state of Washington, the decomposition peak was at 750 °C followed by a strong exothermic peak at 780 °C.

Rao et al [42] studied the DTA curves of different carbonates including $MgCO_3$ and found that all of them showed large endothermic peaks followed by small exothermic peaks at temperatures 40-80 °C higher than the endothermic ones. The endothermic peaks corresponded to the decomposition of carbonates into oxides and the exothermic peaks were the results of the transformation of disordered metastable oxides into ordered crystalline ones.

Khan et al [43] studied the thermal analysis of basic magnesium carbonate by thermogravimetry (TGA), derivative thermogravimetry (DTGA) and differential thermal analysis (DTA). The decomposition peaks were endothermic but a constant exothermic peak was also noticed. This exothermic peak was found to be strongly dependent on the rate at which the samples were heated, sample size and atmospheric conditions.

Cuthbert and Rowland [44] also studied the differential thermal analysis of some carbonate minerals. According to their study, the thermal curve of magnesite showed a broad range of endothermic reaction starting from 400° to 690° having the peak at 650°. They found a

small endothermic peak after the major one. They believed that the second peak was due to the presence of small amount of calcite.

The effect of temperature and particle size in the decomposition kinetics of magnesite using thermal analysis was studied by D. Sheila [45]. The first endothermic peak in DTA was found at 873 K due to the decomposition of magnesium carbonate followed by another endothermic peak at around 1073-1123 K corresponding to the decomposition of calcium carbonate. Isothermal TG analysis at four different temperatures was carried out to identify the reaction mechanism and the kinetics of the reaction. Activation energy values were calculated by different methods and it was in the range of 95-104 kJ/mol.

Samtani et al [46] studied the thermal behavior and the decomposition kinetics of magnesite, calcite and dolomite using the Arrhenius equation. They observed that calcite and dolomite decomposed via a zero order mechanism. However, magnesite decomposed via a 1^{st} order process. They further calculated the activation energy for the each decomposition reaction and the values are 226.34, 192.50 and 175.05 kJ/mol for magnesite, calcite and dolomite respectively. These values are higher than the findings of others due to the difference in experimental conditions resulting in a modified reaction process.

Thermal decomposition kinetics of magnesite were investigated using non-isothermal TG-DSC technique by Liu et al [47] at different heating rate of 15, 20, 25, 35 and 40 K min^{-1}. They used a combination of Friedman equation and Kissinger equation to calculate the E (activation energy) and log A (A is the pre-exponential factor) values. Thermal decomposition mechanism function of magnesite was determined by a new multiple rate iso-temperature method, based on the assumption of a series of mechanism functions. They further used the Malek method[48] to study the magnesite decomposition kinetics. Their research showed that the decomposition of magnesite was controlled by three-dimension diffusion. They got an activation energy value of 156.12 kJ mol^{-1}.

Tian et al [49] studied the thermal decomposition of magnesite by using a TG-MS. Different methods namely Coats–Redfern, Flynn–Wall–Ozawa, and Kissinger–Akahira–Sunose were used to investigate the decomposition kinetics. Almost similar activation energy values were obtained for different methods as shown in Table 2-5:

Table 2-5: Activation energy for magnesite decomposition using different methods

Method	**Activation Energy (kJ/mol^{-1})**
Coats–Redfern	199.99
Flynn–Wall–Ozawa	206.37
Kissinger–Akahira–Sunose	202.58
Average	202.98

Maitra et al [50] investigated the decomposition of Indian magnesite of Almora region using TG analysis under non-isothermal condition. They used the Coats and Redfern integral approximation to determine the kinetics parameters and got an activation energy value of 145.56 kJ/mol^{-1}. It was observed that the decomposition reaction followed a contracting sphere kinetic mechanism.

The kinetic parameters of the thermal decomposition of magnesite were investigated by Demir et al [51] using TG analysis. They used Coats–Redfern and Suzuki methods for the analysis. They proposed a first order kinetic model for the process and calculated the activation energy values for the range of particle size fractions used. They observed that activation energy values decreased with decreasing particle size. For their sample they obtained activation energy values in the range of 236.25 to 302.21 kJ/mol^{-1}.

L'. Turčániová et al [52] studied the influence of mechanical activation and decrepitation on the process of formation of active MgO in the course of the thermal decomposition of magnesite. The kinetic study results confirmed the importance of specifying the stimulation factors i.e. mechanical activation and decrepitation. The process of forming active MgO during the decomposition of magnesite was described by the KEKAM equation with a changing exponential factor. They also observed that both the apparent rate constant and the exponential factor of the process of magnesite decomposition increased with the activation in the grinding process.

Four types of Egyptian magnesite were studied for their chemical and mineralogical composition by Serry et al [53]. Characterization was done in terms of XRD, TG-DTA and wet chemical analysis. Suitability of these magnesites to manufacture shaped and unshaped

MgO-CaO refractories was studied. They recommended pure dolomitic magnesite ore for the said refractory production with the addition of MgO rich and/or Fe_2O_3 rich materials.

2.2.4 Sintering behavior of magnesite

Sintering characteristics of magnesia has been studied by different researchers using different source of magnesia. Sintering is a thermal process which reduces surface area by grain-boundary formation, neck growth between particles and densification [54, 55]. In the sintering process, a powder material, already formed into a required shape, is converted into a dense solid [56]. In case of crystalline materials, mass transport mechanisms responsible for sintering are bulk diffusion, surface diffusion, grain-boundary diffusion with neck surface redistribution, plastic flow, evaporation/condensation or any other combination of these mechanisms. However, the driving force is always the reduction of surface free energy [54, 57]. Primarily, sintering process can be divided into two broad categories: solid state sintering and liquid phase sintering. In solid state sintering the green body is heated to a temperature that is usually 0.5-0.9 of its melting point. Solid state sintering occurs when the green body is densified by atomic diffusion in solid state without the presence of any liquid phase [56, 58, 59]. However, a typical difficulty in solid state sintering is that coarsening may dominate the sintering process which hinders high densification. Use of an additive which forms small amount of liquid phase in the grain boundaries at the sintering temperature can give solution to this problem [59].

W. S. Treffner [60] studied the sintering behavior and the microstructure of magnesia grains obtained from coarse crystalline, cryptocrystalline magnesites and from seawater & brines. Upon heating, magnesium carbonate is first decomposed to magnesia which due to its small crystal size, is in a very reactive state. The decomposition of magnesite can be represented as follows:

$$MgCO_3 \xrightarrow{\Delta} MgO + CO_2 \qquad \textbf{(Equation 2-2)}$$

This is known as low calcined magnesia or low burnt magnesia. Further heating converts it to dense, dead burnt magnesia. He concluded that impure magnesites sinter to strong, dense structures at relatively low temperatures. The presence of iron, lime and silica containing impurities assist the process of sintering the magnesite. Whereas, in purer magnesia, a

defective periclase crystal structure is essential to achieve the desirable periclase–periclase bonding. He suggested that such defects can be created by high temperatures or by addition of other materials like sesquioxides which form solid solutions with MgO.

Electron microscope and electron diffraction studies of chemically pure and natural magnesite was done by Pande and Singh [61] to assess their sintering characteristics at temperatures in the range of 400 °C to 1050 °C. It was observed that small MgO particles were formed at lower temperatures which at higher temperatures grew into large secondary aggregates showing higher porosity. It was also detected that the sintering initiated at 850 °C and completed at 1050 °C.

The effect of pre-calcination temperatures on the sinterability of high purity magnesia powders was investigated by Allison et al [62]. They observed a significant decrease in the density of the sintered products when petrographically identifiable periclase was formed on calcining. They also claimed to develop ceramic bodies with zero apparent porosity at 1650 °C by proper heat treatment during calcination of the powder.

Aksel et al [63] studied the effect of different parameters such as temperature, time, cooling rate and particle size on the grain growth of sintered magnesite. The effect of impurities on grain growth was also investigated by EDX analysis. Sintering was done at 1700 °C and 1800 °C for different soaking period and the samples were cooled at different cooling rate. It was found that for the samples sintered at 1700 °C for 19 min, cooling rate of 5 °C/min (lowest) assisted grain growth significantly. Further increase in soaking time enhanced the mean grain size but reduced the effect of cooling rate. Rise in sintering temperature up to 1800 °C/19 min with a cooling rate of 25 °C/min resulted in maximum grain growth of ~140 μm for some of the samples.

Influence of CaO, Fe_2O_3, TiO_2, Al_2O_3, SiO_2, di-calcium ferrite and brown millerite on the sintering and dead-burning of magnesia was studied by Kriek et al [64]. Two types of magnesite were used in the study. One is chemically pure magnesium carbonate; another is natural South African magnesite. According to the study, all the additives except CaO, promoted sintering. However, there is an optimum amount above which the additives such

as TiO_2 and Al_2O_3 inhibited sintering process. The optimum values of addition are 1 % and 5 % for TiO_2 and Al_2O_3 respectively.

Daniels et al studied grain growth in magnesium oxide during sintering at temperatures between 1450 °C and 1650 °C and observed normal grain growth with an activation energy of 60 kcal [65]. This value was higher than their expectation for grain boundary diffusion in high purity materials. There was no effect of porosity on the grain growth. However, they opined that the data were not sufficient to come to any strong conclusions concerning this variable.

Layden and Mcouarrie [66] added fourteen metal ions to chemical grade magnesium carbonate and the magnesia obtained after calcining was fired at various temperatures to study the effect of the additives on sintering. Magnesia without additives showed rapid densification at firing temperature near 1200 °C. Most of the additives increased densification while some exhibited no effect on densification. Chromium addition dramatically inhibited sintering in certain percentages. They concluded that most of the additives mainly aided sintering by entering into the magnesia lattice and creating defects, however, vanadium addition promoted sintering by liquid formation.

The effect of addition of transition metal, alkali, alkaline-earth and heavy metal oxides on the sintering of magnesia was studied by Nelson and Cutler [67]. The beneficial effect of zirconium, titanium, silicon, lithium, iron and zinc oxides in promoting high densification on sintering was attributed to the defect structure created by these additions.

Sintering and microstructural growth of magnesia with 0 to10 wt % titania in the temperature range of 1300 °C to 1600 °C was investigated by Lee et al [68]. Addition of titania significantly increased densification and grain growth at comparatively low temperature. This enhancement was attributed to the formation of cation vacancy. The reaction was as follows:

$$TiO_2 \xrightarrow[MgO]{} Ti_{Mg}^{\circ\circ} + V_{Mg}'' + 2O_O^X \qquad \textbf{(Equation 2-3)}$$

They explained that the dissolution of titania in magnesia below its solid solubility limit increased the cation vacancy concentration which helped in densification. Above the solid

solubility limit, excess titania formed Mg_2TiO_4 which did not depress grain growth magnesia.

Mamykin and Drozdova [69] studied the effect of different amount of datolite ($2CaO.B_2O_3.2SiO_2.H_2O$) and boric anhydride on thermal shock factors, thermal shock resistance and refractoriness under load, sintering and recrystallization of magnesia, It was reported that 0.5% datolite and 3% B_2O_3 had the greatest effect on sintering of magnesium oxide.

Chaudhuri et al [70] studied the effect of TiO_2 in anatase form on the grain growth and sintering of two types of Indian natural magnesite. The study revealed that sintering of Salem magnesite started after 1500 °C whereas in case of Almora magnesite perfectly shaped periclase grains were developed at 1500 °C. Sintering was improved in both the cases with the addition of 0.2 mass% of titania. Further they studied the detail microstructure with EDX of sintered natural magnesite of Salem region with titania, zirconia and ilmenite additives [71]. It was observed that zirconia did not react and formed any secondary phase, ilmentite reacted with magnesia and formed magnesioferrite and titania reacted with the impurity and formed calcium titanate. However, they concluded that these mineralisers encouraged grain growth and matrix densification.

Banerjee et al [72] noticed that for magnesite refractories having high silica content, increase in porosity helped in increase in thermal shock resistance whereas the case is reversed in case of low silica content. The explanation behind this behavior was that having more number of pores helped in arresting the crack propagation for high silica containing samples, whereas in low-silica samples, the spalling was caused by a large number of cracks which resulted in loosening of the grains from all sides.

In India, naturally occurring magnesite ore, abundantly available in Salem and Almora region, is the primary source for magnesia. In spite of vast deposit of magnesite, India has to depend largely on imported magnesite for good quality refractory production due to the impurities present in Indian magnesite. In Salem magnesite, the main impurities are SiO_2 and CaO whereas in Almora magnesite, Fe_2O_3 is present as the major impurity. These impurities have detrimental effects on the refractory properties at high temperature as they

can form unwanted low melting phases like monticellite (CMS), merwinite (C_3MS_2) and di-calcium ferrite (C_2F) which deteriorate the high temperature properties of the refractory [73].

Characterization of Indian magnesite in terms of X-ray diffraction, DTA-TG and Infrared Spectroscopy was done by Khandal et al [74, 75] and they found the presence of calcite, dolomite and quartz in it.

Rao et al [76] studied the mineralogical composition of Indian magnesite of Doba area. They found that the magnesite was impure, coarsely crystalline and similar to the Australian magnesite of brunnerite type. They also observed that the magnesite was capable of self-sintering. 2 % titania addition in the form of rutile improved the spalling resistance and Refractoriness under load (RUL). However, 2% ilmenite addition had a negative impact on RUL. Addition of alumina did not improve either spalling resistance or RUL. On the other hand, a small increase in silica content improved RUL.

Studies of Indian magnesite from four different regions were done by Banerjee et al [77]. The raw materials were evaluated in terms of petrography study, DTA and phase analysis. These magnesites were sintered in the temperature range of 1500-1700 °C. They observed that Indian magnesite could be properly dead-burnt around 1650 °C. In general, refractory blocks made by these magnesites performed satisfactorily. In another work Banerjee et al [78] studied the sintering characteristics of Indian magnesite of different regions. They characterized the samples in terms of linear shrinkage, specific gravity, bulk density and apparent porosity. For all the samples they studied, the apparent porosity reduced drastically at around 1400 °C and thereafter the rate of decrease of apparent porosity lowered.

P. Kumar et al [79] studied the densification behavior, mechanical properties and microstructural evolution with temperature of Indian magnesites containing impurities like silica, iron oxide and lime. Sintered Almora magnesite samples showed better high temperature strength than the Salem magnesite ones. However, there was no significant difference in case of room temperature flexural strength.

Effect of yttria on the thermo-mechanical properties of Indian magnesite was studied by P. Kumar et al [80]. They observed that addition of yttria assisted the formation of calcium yttrium silicate and yttrialite phases preventing the formation of low melting monticellite phase. Yttria addition promoted periclase grain growth thereby enhancing the high temperature flexural strength.

Chemical and magnetic properties of Indian magnesites from three different locations namely Salem, Ajmer and Mysore were studied by Banerjee et al [81]. Silica content varied from 0.6 to 8.0 %, lime content varied from 0.1 to 9.7 % and Fe_2O_3 content was from 0.2 to 4.4 %. In Salem magnesite the source of silica was quartz while in case of Almora magnesite it was talc. The magnetic characterization suggested the presence of some ferrous iron in a magnetically dilute system which is supported by the chemical analysis and petrographic results.

2.3 Beneficiation of magnesite

The demand for high purity magnesite has increased significantly in recent years. Therefore, it has become absolute necessity to separate magnesite from associated gangue minerals to obtain good quality magnesite.

Gravity separation and flotation are two mostly used methods for magnesite beneficiation. Gravity separation is used for coarse size (>1 mm) magnesite separation whereas flotation is used for fine magnesite separation when high grade of magnesite concentration is needed [82].

Use of different chemical reagents in mineral processing was extensively reviewed by M. J. Pearse [83]. Various inorganic, organic reagents both natural and synthetic are widely used for froth flotation, solvent extraction and polymer based separation processes. In froth flotation process, the reagents are used in the form of frothers, collectors, depressants and promoters. Acrylic based polymeric reagents are mainly used as agglomerating agent, dispersants, grinding aids, antiscalants, rheology modifiers and tailing stabilizers. Along with these more specialized reagents lime and sulphuric acid are used in large volume in mineral processing.

Santana and Peres [84] used reverse cationic flotation instead of direct anionic flotation to get high purity magnesite. A commercially available mono ether amine was used as collector. Corn starch was used as depressant to achieve a weight recovery level of 92%. Use of depressant lowered the SiO_2 content in the concentrate. Neutral pH and the mixture of amine and fuel oil were suggested to keep a very low level of SiO_2 content in the concentrate.

Interaction of fine particles of the minerals and its effect on the cationic reverse flotation is important in the context of fine ore beneficiation. Yao et al [85] studied the effect of fine particles (< 5 μm) of magnesite and dolomite on the flotation of quartz. Dodecylamine was used as surfactant. It was reported that higher amount of fine magnesite and dolomite drastically reduced the recovery of coarse quartz in the flotation process. Aggregation behavior of the fine particles and attractive interaction forces between magnesite-quartz and dolomite-quartz are responsible for this negative effect on quartz flotation.

Aslani et al [86] studied the effect of reverse flotation on chemical composition, phase assemblage, microstructural evolution physical and mechanical properties of low grade magnesite ore samples. Armoflot 17 and Armoflot 18 were used as collectors in the process. Further, physical and mechanical properties like bulk density, apparent porosity and cold crushing strength were studied for the shaped and unshaped refractory products prepared from processed aggregates. The final product after reverse flotation was found to be acceptable for refractory production.

Gambopoulos and Nestoridis [87] invented a method of removing impurities like silica, iron, lime, alumina from magnesite ore by reverse flotation. They used a mixture of quaternary ammonium compounds and primary amines with impure kerosene in the process. They reported reduction of silica percentage from 12 to 0.08 and iron from 1.4% to 0.08% using this method, while reduction of silica below 1% was difficult by direct flotation.

Enrichment of impure Satkinsk magnesite by flotation was performed by Bron et al [88] using caustic soda, sodium hexametaphosphate, carboxymethyl cellulose, water glass etc.

This method yielded a product in which CaO concentration was reduced by a factor of 3-6 (from 9.1-6.0 % to 1.4-2.8 %) and SiO_2 concentration was reduced to 0.3-0.4 %.

Smertin and Samusenko [89] reported removal of impurities by flotation of magnesite using aliphatic acid collecting agents in alkaline medium with sodium carboxymethyl cellulose and sodium hexametaphosphate as depressors for dolomite, calcium, silicates and quartz.

Viera and Peres [90] studied the effect of different amine collectors for the reverse flotation of quartz. They found that ether di-amine was more effective in case of flotation of medium and coarse quartz, while ether mono amine was a better choice for fine quartz. The optimum pH was 9.0 for both types of amine used.

There are many more researchers who had worked on magnesite beneficiation and removal of quartz from ore. Cronberg et al [91] used primary aliphatic ether amines like 3-isodecoxypropylamine acetate and N-tridecoxypropyl1-1,3-propylene diamine monoacetate as collectors of quartz in froth flotation.

A. Z. Frangiskos [92] invented a method for beneficiation of magnesite ore using gravimetric and magnetic separation procedure. Magnesite ore was at first calcined at a temperature about 500 to 1000 °C to convert it to caustic-calcined magnesite and then conventional gravity separation was followed to separate it from the gangue materials. Alternatively, the gangue was converted to magnetic materials by calcining in reducing atmosphere and separated from the magnesite by magnetic separation.

A. W. Fahrenwald [93] also used froth flotation method to beneficiate magnesite ore for production of high quality magnesite. He used a two stage flotation process for beneficiation of magnesite ore to improve its quality satisfactorily and economically. In the first stage, the siliceous and calcareous gangue material was separated using a non-cationic collector such as methyl amyl alcohol in the froth which left a magnesite enriched concentrate. In the second stage, magnesite was separated using an anionic collector such as oleic acid and a gangue depressant such as sodium disilicate along with another depressor such as tannic acid from this concentrate in the froth. He claimed to reduce the silica content to 1.38% from 3.56% and lime content to 0.15% from 2.36%.

A. J. Weinig's invention too was related to a froth flotation process for separation of constituent minerals of magnesite ores. He used tetra-alkali pyrophosphate and other similar salts of phosphoric acid along with fatty acid collectors and pine oil as frother to improve the recovery of magnesite in the froth and to reduce the amount of contaminant slimes in the froth. Metallic salts like aluminum and ferric salts were used to enhance the action of the collector and to depress the insoluble and lime-containing impurities. They claimed to reduce the CaO content to the extent of 70% by using sodium tetraphosphate [94]. In another patent, Weining used same froth flotation process for the separation of magnesite from the insoluble and lime-containing impurities by using naphthenic acid as frother and collector instead of the fatty acid used earlier as collector for beneficiation of finely ground (-100 mesh) magnesite of Luning, Nevada. This ore had 2.21% insoluble and 4.41% CaO as impurities. The ore was conditioned with ferric chloride, tetrasodium pyrophosphate and naphthenic acid before froth flotation. A recovery in the range of 35-48% with 0.4-0.93% insoluble content and 1.05-1.28% CaO was claimed [95]. Separation of high purity magnesite from dolomite and impure magnesite by froth flotation process was also reported by him using a combination of aluminum sulphate, tetrasodium pyrophosphate, starch and napthenic acid. Starch was used as depressants to reduce the amount of insoluble materials in the forth [96].

Weinig and Mcintosh [97] also patented a economical and efficient process for the treatment of low grade magnesite ores by froth flotation. These ores are primarily brucite-magnesite type and the amount of SiO_2 and CaO were typically 3.0 and 3.5% respectively. A combination of silica froth flotation unit and magnesite froth flotation unit was employed to separate the impurities and to maximize the yield of the magnesite. Magnesite ore was initially milled to -200# and classified using a classifier. Finer material after the classification was subjected to flotation. Combination of cresylic acid and aliphatic ammonium acetate was used as silica collector. Another combination of an amine and primary ammonium acetate was also used as silica collector. Refined tall oil which was mainly a combination of oleic acid, linoleic acid, linolenic acid and rosin acid was used as magnesite collector.

In another work beneficiation of magnesite ores from SiO_2 and CaO containing impurities by forth flotation was studied by T. L. B. Jepsen [98]. Different combinations of Portland cement, heavy metal salt, sulphuric acid, sodium hexametaphosphate, stabilized dolomite, hydraulic lime and sodium silicate were used in premixed condition as depressant for the siliceous and calcareous impurities. It was claimed that the pre-mixed reagents provided better depression of silicates than the individually introduced reagents. In this process it was claimed to obtain magnesite with less than 0.5% silica and 1.60% CaO from a low grade magnesite.

V. P. Mehrotra [99] suggested a new froth flotation agent and an advanced flotation process for beneficiation of silica containing ores in a two stage froth flotation process. They have reported to improve the separation of silica in froth by using silica activating ions (such as Ca^{2+}) and a combination of cationic and anionic collectors from a silica containing ores by an improved flotation process. It was claimed that presence of cationic collectors significantly reduced the amount of anionic collector required to float the silica and also enhanced the recovery of the minerals. As fuel oil was not used in rough flotation, it also reduced the amount of reagent requirements.

The role of different reagents used iron ore beneficiation by flotation to remove quartz was reviewed by Araujo et al. According to them the most widely followed method is reverse cationic flotation with ether amines as the collector of quartz and gelatinized corn starch as the depressant of iron oxide. An alternative option can be the partial substitution of amine by non-polar oils. Cassava starch may be an economically feasible choice over other starches as iron oxide depressant [100].

Tripathy et al investigated the beneficiation of inferior grade dolomite fines to remove siliceous impurity. A detailed study was carried out on direct and reverse flotation of the ore by varying the process parameters. It was observed that silica content could be reduced by both the techniques. Further it was found that while direct flotation resulted in a better control over the product quality, reverse flotation had an advantage on the yield [101].

Heavy medium separation was used to beneficiate raw magnesite ore having particle size > 0.35 mm. However, particles of size < 0.35 mm were rejected from this process. Ignjatović

et al [102] developed a combination of gravity and magnetic separation process for magnesite ore using HGMS (High Gradient Magnetic Separation). They reported a possibility of efficient removal of serpentine & olivine using HGMS and superconducting magnetic separators for fine particles of size < 0.35 mm.

Simonov et al [103] developed a scheme for the beneficiation of impure magnesite in heavy suspensions. It included separate sections in two stages using conical and cylindrical separators for beneficiating different size fraction of ores. They observed that the efficiency of the beneficiation process depended on (a) lump size of the ore, (b) type and productivity of the separators and (c) the structuromechanical properties of the suspension.

Many researchers suggested bacterial leaching to remove silica from magnesite. Mishra et al. [104] studied bacterial leaching of Salem magnesite with gram positive and gram negative strains and reported that gram positives were more effective though they could not understand the mechanism behind the solubilization of siliceous impurities.

Mohanty and Mishra [105] used Bacillus Sp. to solubilize silica from magnesite ore. They reported the optimum conditions for the release of silica from magnesite ore. The optimum temperature was found to be 37 °C and optimum shaking condition was 50-100 rpm. A medium having ammonium sulphate, yeast extract as nitrogen sources, disodium hydrogen phosphate, potassium dihydrogen as phosphate sources and magnesium sulfate, manganese sulfate as divalent cations was found to give the best results. Moreover, an incubation period of 8 days was the most desirable for the maximum silica removal.

Karaoglu et al [106] aimed for a economical and environment friendly method for magnesite enrichment by removing $CaCO_3$. They used Pseudomonas oryzihabitans bacteria for this purpose. Pseudomonas species was reported to effectively dissolve $CaCO_3$ from magnesite ores.

Yanmis et al [107] tried to reduce the quantity of $CaCO_3$ in magnesite ore by using Lactococcus spp. They achieved a reduction of $CaCO_3$ from 2.94 % to 0.57 % using this microorganism. They claimed that this process could be used in industries as the microorganism had no pathogenic properties.

Chattaraj and Chatterjee [108] reported about the beneficiation of off grade magnesite of Salem region, India. They suggested a method consisting of calcinations, hydration and then separation of hydrated magnesia from the unhydrated contaminants by dispersion in water. They studied for the optimum conditions required for the highest yield of good quality magnesia. The non-hydraulic nature of silicates formed during calcinations and physico-chemical properties of freshly formed magnesium hydroxide facilitated the beneficiation of inferior grade magnesite containing approximately 10% silica.

As fired magnesite is difficult to beneficiate because of its fine grained structure and the close association of impurities with periclase, Potapenko et al [109] developed a dry magnetic separation scheme based on their investigation. They beneficiated calcined Satkinsk magnesite by dry magnetic separation in a strong field and thereby increasing the quality of regular metallurgical powders and increasing the yield of granular fractions of 1 to 3 mm.

Urvantsev and Kashcheev [110] studied the enrichment of low grade magnesite by electric separation. They achieved a product having MgO content improved from 95.5 % to 97.3 % with an overall yield of 38 %.

Gavrish et al [111] had recommended chemical method for beneficiation of magnesite. They used hydrochloric acid and ammonium salts for beneficiation. In hydrochloric acid method the natural magnesite was dissolved with hydrochloric acid. Silica and iron sulphide was separated as residue. Other impurities present in the solution were separated as sediment after treatment with ammonia solution or $Mg(OH)_2$ slurry. In this method calcium can also be separated by addition of sulfate ions. In the other hand, basis of the other method is solubility of magnesia in ammonium salt solution. Lightly calcined (600-800 °C) and ground magnesite was treated with ammonium chloride and soluble magnesium chloride was formed. Impurities were separated as undissolved residues.

Kozhevnikov and Chernitskii [112] used photometric concentration method for separating impurities from magnesite ore. The method used the difference in the opticophysical constants of the minerals and rocks. Lumps of ore were fed into a photometric chamber where they were illuminated on a screen of uniform color and the light signal reflected

from them was picked up by a sensor. Later the beneficiated material was separated with a compressed air impulse or jets of water.

Over the past few years, statistical designing of experiment and optimization of process parameters is the subject of study for many researchers. Advantage of using chemometric tools are the reduction in number of experiments thereby reducing the reagent consumption. Moreover, these tools enable the researchers to assess the relevance and statistical significance of the variables. Univariate optimization tool studies the effect of one variable at a time which may lead to erroneous results. Therefore, multivariate optimization is gaining popularity in recent years and Response Surface Methodology (RSM) is one of them. Response Surface Methodology (RSM) is a combination of mathematical and statistical optimization method used to develop empirical models. It is widely used to describe the performance of industrial processes [113], design and development of new products, improvement of existing products [114]. Bezerra et al [115] reviewed the role of RSM in optimizing analytical methods and discussed about different experimental designs. Central composite design (CCD), 2^5 full factorial design, Plackett-Burman methodology, Box-Behnken design are some of the methods which are being used to optimize the flotation process parameters [114, 116]. Box-Behnken is a statistical design based on RSM used for optimizing operational parameters. RSM based on Box-Behnken design has a significant role in industrial research, especially in situations where a large number of operating parameters are involved [117].

2.4 Modification in phase assemblage

2.4.1 Changing C/S ratio

An alternative approach to improve the refractory properties is to change the phase assemblage to reduce the detrimental effects of impurities. The CaO-MgO-SiO_2 system is very much important in metallurgy and ceramics as C/S ratio in magnesia system plays a vital role in determining various properties of samples. Research works have been carried out around the world to change the phase assemblage of sintered magnesite by changing lime/silica ratio to control the detrimental phase formation.

Ferguson and Merwin [118] carried out a series of experiments to get a comprehensive idea about CaO-MgO-SiO_2 system. On the basis of their results they developed a ternary phase diagram for the system. Cristobalite, tridymite, pseudowollastonite, tricalcium-di-silicate, α-calcium orthosilicate, lime, periclase and forsterite were the phases present in the three main binary systems and also had fields in the ternary phase diagram. On the other hand, tricalcium silicate and Clino-enstatite were the binary compounds which did not have any fields in the ternary system while diopside and $2CaO.MgO.2SiO_2$ were the ternary compounds having fields in the ternary system. Additionally there were some phases which had fields in the ternary system but had no constant composition.

Ricker and Osborn [119] studied the CaO-MgO-SiO_2 system and modified the existing ternary phase diagram for this system. They added a field for tricalcium silicate, sketched liquidus isotherms for the lower part of the diagram and showed that substantial solid solution range at high temperatures was present between monticellite and forsterite. However, they could not find any solid solution between monticellite and merwinite.

Hudon et al [120] performed the thermodynamic modeling of CaO-SiO_2-MgO system (Figure 2-3) at 1 GPa and thermodynamic optimization at 1 bar. According to them the optimized model parameters could predict the phase equilibria with accuracy within 50 °C.

Studying the CaO-MgO-SiO_2 phase diagram, R. Staut [121] reported that the silicate phases that formed with C/S ratios between 0 & 1 were forsterite and monticellite, with C/S ratios between 1 & 1.5 were monticellite and merwinite and with C/S ratios between 1.5 & 2 were merwinite and di calcium silicate. He concluded that the occurrence of silicate phases was determined by the C/S ratio, not the amount of CaO present in the system. He also observed a correlation between high temperature strength and lime/silica ratio and found that for higher silica content, hot modulus of rupture value was less for a C/S ratio above 0.4.

Lampropoulou et al [122] also worked in the CaO-MgO-SiO_2 system. However, they reported significant deviations from the expected phase assemblage i.e. the silicate phases coexisting with periclase, differed from the prediction. Very high solubility of CaO in periclase crystals was detected.

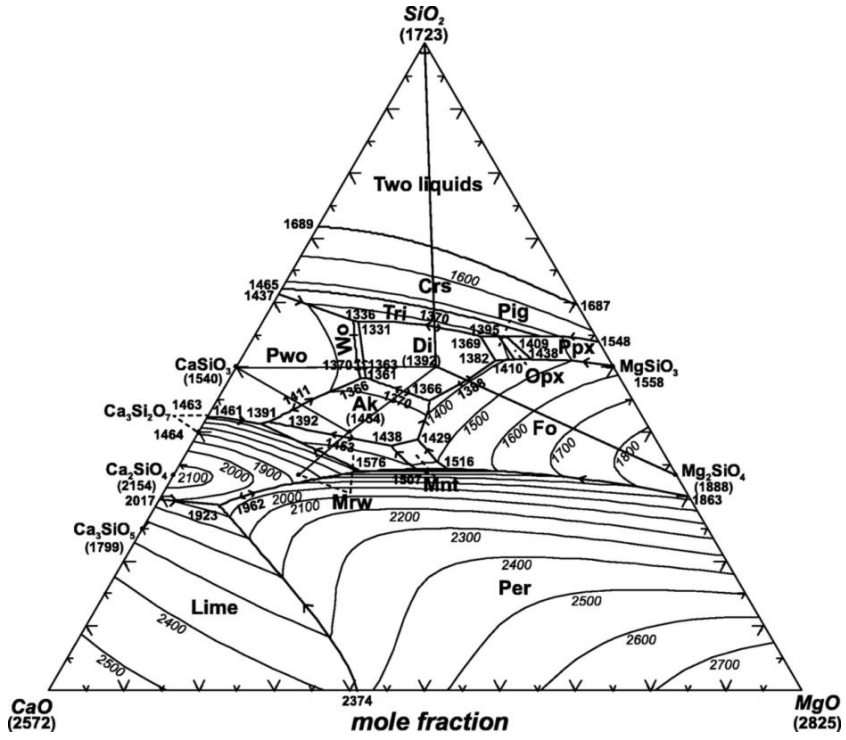

Figure 2-3: CaO-SiO_2-MgO phase diagram

(Where Ak= akermanite; Crs= cristobalite; Di= diopside; Fo= forsterite; Mnt= monticellite; Mrw= merwinite; Opx= orthopyroxene; Per= periclase; Pig= pigeonite; Ppx= protopyroxene; Pwo= pseudowollastonite; Tri= tridymite; Wo= wollastonite) Adopted from Hudon et al [120]

Hatfield et al [123] studied the compatibility relations between solid magnesia containing lime in solution and the silicate phases in the CaO-MgO-SiO_2 system. They suggested that magnesia based refractories should contain a secondary solid phase of high melting point to minimize the penetration of the liquid phase between the periclase grains at high temperatures. This could be done by strategically adjusting the C/S ratio of the system. They suggested maintaining the ratio either low enough to promote the formation of forsterite or high enough to produce dicalcium silicate. Among these two methods, the earlier one is more difficult to practice than the later one because in presence of CaO, the temperature of the MgO-forsterite-liquid boundary falls rapidly.

Rao and Naidu [124] studied refractory bricks having different silica content and C/S ratio. They concluded that high silica content with very high C/S ratio (>2) was tolerable from refractoriness point of view. However, high silica content with low C/S ratio would lead to deterioration of refractoriness due to absorption of lime from the furnace atmosphere. So,

for practical use silica content should be kept as low as possible. From the point of view of lime absorption, C/S ratio should be >2 so that if such absorption happened, it would result in the formation of tricalcium silicate.

2.4.2 Zirconia addition

Impurities and additives play an important role in controlling various physical, mechanical and chemical properties of magnesia based bricks [63]. The presence of minute amount of impurities in a material can have a profound effect on its sintering characteristics [125]. Properties of magnesite refractory can be substantially improved through microstructural modification and through alteration of chemical and physical nature of the bond. However, the most viable process is incorporation of suitable additives which can restrict the formation of low melting phases by changing the reaction pathways and there by forming products having higher melting temperatures. Property enhancement of magnesite is also of prime interest of many researchers. To address the problem of poor thermal shock resistance and high thermal conductivity of magnesia, several researchers have suggested inclusion of different additives, such as SiO_2, Al_2O_3, Cr_2O_3, TiO_2, ZrO_2, $MgCl_2$ and WO_3 [66, 126-134].

Ceramists have long been working on the fabrication of tough and strong ceramics which is otherwise brittle. Tetragonal zirconia or zirconia based ceramics, due to their excellent mechanical properties, have attracted researchers in this matter. The tetragonal to monoclinic phase transformation in zirconia is associated with large volume expansion (~3%) which often causes severe cracking. Martensite transformation in the stress fields of propagating cracks leads to increase in the toughness of two-phase ceramics [135].

Kaberi Das et al [136] studied the sintering behavior and microstructural evolution of Indian magnesite of Almora region with zirconia addition. Zirconia was added in three different amounts of 3, 4.5 and 6 wt% and sintered at temperatures in the range of 1500-1600 °C/2h. They observed magnesio-zirconate phase at the triple point regions of the direct bonded periclase grains. Moreover, the grain morphology changed in presence of zirconia from subrounded/rounded to angular due to the reduction of liquid phase.

Kusiorowski et al [137] added zirconia to improve the properties of magnesia refractory products. The results showed that the addition of 2 wt% zirconia improved the refractory

properties, such as cold crushing strength, corrosion resistance. However, further increase in the amount of zirconia resulted in decrease in cold crushing strength and increase in gas permeability. It was also found that the optimum particle size of zirconia was medium-large or the best refractory properties.

Burhanuddin et al [138] introduced 2 to 6 wt% zirconia to Indian magnesite of Almora region and observed that zirconia reduced the formation of low melting monticellite phase at high temperature. It also improved the flexural strength of the samples. They also observed that the shape of the periclase grains changed from rounded to subrounded due to the presence of zirconia.

2.5 Development of magnesium aluminate spinel

In another approach, Indian impure magnesite is utilized to prepare magnesium aluminate spinel aggregates. Magnesium aluminate spinel ($MgAl_2O_4$) is an important refractory material used in various ferrous and non ferrous industries. Magnesium aluminate spinel is gradually replacing mag-chrome refractories in the areas like transition and burning zones of cement rotary kilns, side walls and bottom of steel teeming ladles and checker work of glass tank of furnace regenerators [139]. Earlier, chrome based spinel refarctories were used primarily for application in steel making vessels and cement rotary kilns [140]. However, chrome bearing materials have the potential to be environmentally hazardous as Cr^{6+} is carcinogenic in nature. Therefore, for the past few years, chrome based spinels are being replaced by magnesium aluminate spinel [141, 142]. Other properties that make Mg-Al spinel an attractive choice as refractory are high melting point (2135 °C), high chemical inertness, high mechanical strength at elevated temperatures, excellent resistance to thermal shock and low thermal expansion coefficient [143-145]. For industrial applications, the expansion related to spinel formation can be beneficial to the healing of thermal stress cracks [146] as well as in improving resistance to slag corrosion for Mg-Al spinel refractories.

The crystal structure of spinel was determined separately by Bragg [147] and Nishikawa [148]. Generally, spinel compounds belong to the space group Fd3m ($F^4_{1/d}\,\bar{3}_{2/m}; O^7_h$;No. 227 in International Tables) [149]. Sickafus et al [150] reviewed the crystal structure of

compounds having the general formula AB_2X_4. These compounds crystallize with the same atomic structure as spinel ($MgAl_2O_4$). Conventional magnesium aluminate spinel (AB_2O_4) has a pseudo-cubic closed packed arrangement of O anions with di valent and tri valent cations occupying tetrahedral and octahedral interstices respectively. Each cubic unit cell of spinel is made of 8 formula units. Total 96 interstices are present between the anions in a cubic unit cell out of which only 24 are occupied by cations. $1/8^{th}$ of the total tetrahedral interstices and ½ of the octahedral interstices are filled up with cations. The rest of the interstices remain vacant. These vacant sites can accommodate other types of divalent and trivalent cations resulting nonstoichiometry and solid solution formation. The cations whose radii are in the range of 0.044 to 0.100 nm can enter into tetrahedral or octahedral sites of the spinel structure [151, 152]. Typical structure of Mg-Al spinel unit cell is depicted in Figure 2-4.

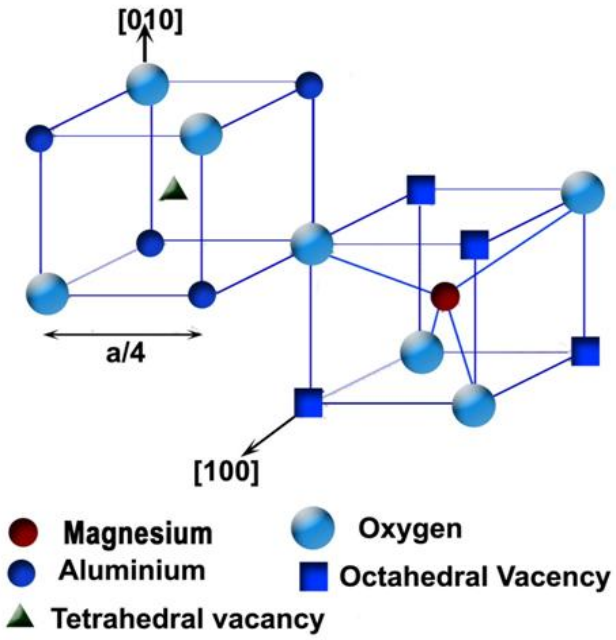

Figure 2-4: Structure of magnesium aluminate spinel [150]

Magnesium aluminate spinel exhibits wide range of MgO/Al_2O_3 stoichiometry as can be understood from the phase diagram. The $MgO\text{-}Al_2O_3$ system was first studied in 1916 by Rankin and Merwin [153]. They reported that MgO and Al_2O_3 formed a single compound

$MgO.Al_2O_3$ having a composition of 28.4% MgO and 71.6% Al_2O_3. This compound congruently melts at 2135±20 °C.

Alper et al [154] studied the MgO-$MgAl_2O_4$ system and determined the solidus, liquidus and sub solidus in this system using X-ray diffraction and optical technique. They determined the melting point of periclase, eutectic composition (MgO 45% and Al_2O_3 55%) and spinel in nitrogen atmosphere and they are 2825 °C, 1995 °C and 2105 °C respectively.

Thermodynamic assessment of MgO-Al_2O_3 system was done by Hallstedt [155] with the CALPHAD technique using a computerized optimization procedure named PARROT. They have also studied the solubility pattern of different components of the MgO-Al_2O_3 system. It was observed that $A1_2O_3$ had very high solubility in spinel at high temperature whereas, MgO showed moderate solubility in spinel (Figure 2-5).

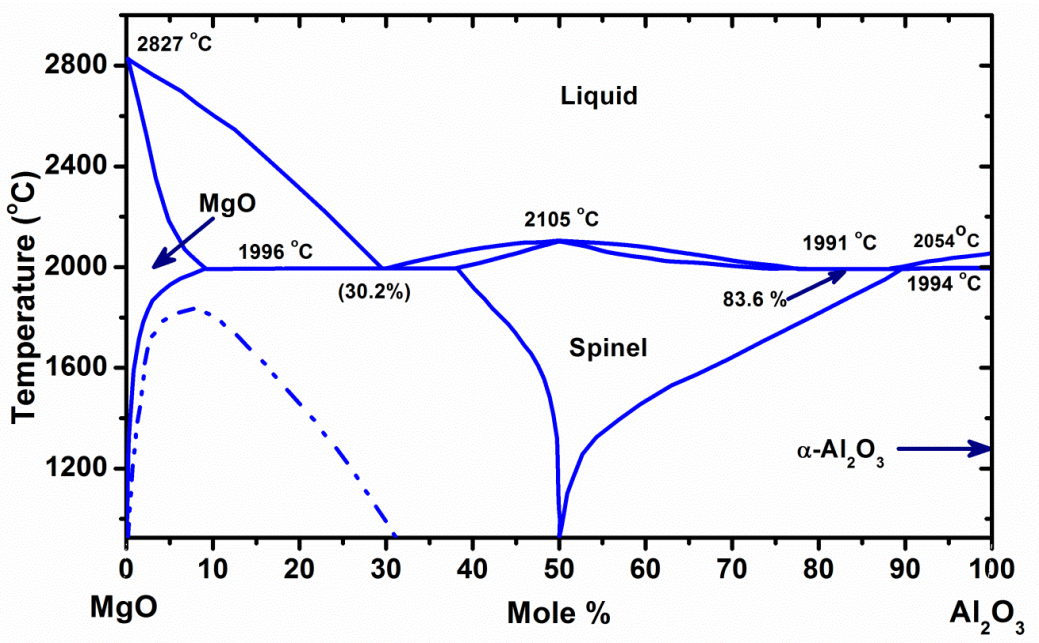

Figure 2-5: Magnesia-alumina phase diagram [155]

Though spinels are known for their desirable refractory properties, they have not yet been widely used commercially due to the difficulty in sintering [156]. 5% volume expansion [157] is associated with formation of spinel from magnesia and alumina which hinders densification in the same firing. Therefore, to overcome this problem, a two stage firing process is practiced [158-161]. In the first stage spinel formation is completed and in the

later one the spinel is densified. In the first stage the raw materials are calcined at >1500 °C to form spinel phase. In the next stage the material is refired at >1650°C to achieve the desired density after fine grinding and compaction. These two successive high temperature firing cycles increase the production cost of dense magnesium aluminate spinel.

Mg-Al spinel was prepared following a conventional double stage firing by Ganesh et al [158]. The used a new type of sintering aid, $AlCl_3$ and studied its effect on densification and formation of spinel. They found that $AlCl_3$ was effective in increasing spinel formation. However, it helped in densification only when the calcined powder contained free MgO and Al_2O_3.

In another study Ganesh et al [159] synthesized different grades of stoichiometric and non-stoichiometric Mg-Al spinel by double-stage firing process using two types of alumina and four types of magnesia raw materials. They observed a strong relation between the formation of spinel and moisture and CaO contents in the precursor oxides. It was also found that excess alumina and magnesia could greatly influence the densification of spinel.

Different types of spinel were synthesized following double stage firing by Ganesh et al [160]. Sintering was carried out in the temperature range of 1500-1800 °C for 1-2.5 h. The effect of different processing parameters, such as average particle size, degree of spinel phase, green density, mass of the powder compact, sintering temperature, holding time at the peak temperature and starting composition on densification was examined in terms of bulk density, apparent porosity, water absorption capacity and microstructural observations.

Ganesh et al [161] reported about synthesis of Mg-Al spinel by solid state reaction of alumina and calcined caustic magnesia at 1400 °C/1h. The surface thus obtained was then coated to protect against hydrolysis. The coated powder was then dispersed in aqueous media. The slurry was then consolidated by different techniques like slip casting, hydrolysis assisted solidification and hydrolysis induced aqueous gelcasting. Spinel samples were also prepared using conventional dry-powder pressing and temperature induced gelatin routes. Hydrolysis induced aqueous gelcasting route was found to be the best among all.

Magnesium aluminate spinel refractory aggregates were successfully synthesized from 16 different combinations of bauxite and magnesia sources by Cunha-Duncan and Bradt [162].

The basis of the synthesis was the alumina-magnesia-silica ternary equilibrium diagram. They observed spinel formation at firing temperature as low as 1000 °C, though the complete reaction took firing for 1 h in air at 1400 °C.

Mohapatra and Sarkar [163] prepared different variety of Mg-Al spinel from commercially available sintered seawater magnesia and α-alumina. The batches were calcined at different temperatures and then were sintered at 1600 °C/4h. They calculated the spinel content in the calcined as well as the sintered samples from the XRD analysis using the following equation:

$$\text{Vol\% of } MgAl_2O_4 = \left\{\frac{\text{height counts of } MgAl_2O_{4\{3\,1\,1\}}}{\left(\Sigma \text{height counts } \left(MgAl_2O_{4\{3\,1\,1\}} + MgO_{\{2\,0\,0\}} + Al_2O_{3\{1\,0\,4\}}\right)\right)}\right\} \times 100$$

(Equation 2-4)

They concluded that by varying calcination temperature, the spinel phase development can be adjusted to obtain better densification and composition in the sintered samples.

Mg-Al spinel was synthesized using a mechanochemical process at room temperature in a single step by Domanski et al [164]. They used a transition alumina (γ-Al_2O_3), bohemite (AlO(OH)) and MgO as the starting materials. The mixtures were milled at room temperature under air atmosphere to form spinel. It was observed that spinel formation occurred faster with γ-Al_2O_3 than with AlO(OH) or α-Al_2O_3. They concluded that the morphological changes due to milling created fresh surfaces that were favorable for spinel formation at an almost constant rate.

Ping et al [165] used self-heat-sustained technique to produce $MgAl_2O_4$ spinel from reagent grade magnesia and metallic alumina powder. Around 92 % densification was achieved in spinel compacts sintered at 1600 °C/4 h.

Mg-Al spinel was formed at 900 °C from MgO and Al_2O_3 after applying high energy ball milling for 12 h to the oxide mixtures [166]. They obtained spinel having 98 % theoretical density by sintering the milled mixture at 1550 °C/2h.

3. Methodology

Indian magnesite of Salem district in Tamilnadu was selected for the present study. At first the magnesite ore was crushed and ground to achieve the desired fineness. Then the powder was characterized in terms of chemical analysis, XRD study, DTA-TG analysis and IR spectroscopy. After that it was milled in an attrition mill. Milled slurry was dried and was passed through 100 mesh. The powder thus achieved was characterized in terms of particle size and specific surface area. In the next step bar samples were prepared from the milled powder through uni-axial followed by iso-static pressing. These bars were sintered and then characterized in terms of bulk density, apparent porosity, specific gravity, phase analysis, flexural strength, thermal shock resistance, microstructural evaluation using FESEM and EDX analysis.

Different methodologies were adopted to improve various properties of refractory aggregates developed from low quality Indian magnesite and they are as follows:

1. Changing lime/silica ratio of the magnesite system
2. Addition of zirconia
3. Preparation of magnesia rich magnesium-aluminate spinel
4. Beneficiation by reverse flotation

3.1 Methodology 1: Controlling the high temperature phase formation by changing the lime/silica ratio

In this approach lime/silica ratio of the magnesite system was changed to 1 and 2 to alter the high temperature phase development. Calcium carbonate was added to Indian raw magnesite in such quantities that after sintering the CaO/SiO_2 ratio is changed into 1 and 2 (two different batches). Bar samples were made using the same mechanism as described in the previous section. These bars were characterized in terms of different properties as mention earlier. The results were compared with the raw batch.

3.2 Methodology 2: Addition of zirconia to modify the high temperature phase formation

In this methodology chemical grade monoclinic zirconia (ZrO_2) was added to Indian magnesite in varying amount. Three different batches were prepared having 1 wt%, 3 wt% and 5 wt% zirconia. Same procedure was followed to prepare the samples of those batches. The results of different characterization were compared with the raw batch.

3.3 Methodology 3: Preparation of magnesium aluminate spinel

Magnesium aluminate spinel was prepared using Indian raw magnesite and calcined alumina. Magnesite and alumina were mixed in 1:1 weight ratio to prepare the batch. Again same route was followed for the preparation of the samples. Magnesium aluminate spinel thus formed was magnesia rich in nature. the samples were evaluated in terms of different properties as stated earlier.

The process flow for methodologies 1, 2 & 3 are shown in Figure 3-1.

3.4 Methodology 4: Beneficiation by reverse flotation and process optimization using RSM

Beneficiation of the raw magnesite was attempted using reverse flotation technique. Pine oil was used as frother, Flotigam EDA, an ether monoamine, was used as collector and sodium hexametaphosphate (SHMP) was used as a depressant of carbonates. Efficiency of the froth flotation process was statistically analyzed by Response Surface Methodology (RSM) using Box-Behnken Design. Experimental design matrix was developed according to the Box-Behnken design. Each froths, collected after flotation, was assessed for complete chemical composition. XRD analysis and quantification of the crystalline phases of the processed magnesite for which maximum silica content was achieved in froth was done. A new experiment was carried out according to the optimized conditions given by the software and chemical analysis of the resultant froth sample was done in order to compare the results with the predicted data. The process flow for methodology 4 is shown in Figure 3-2.

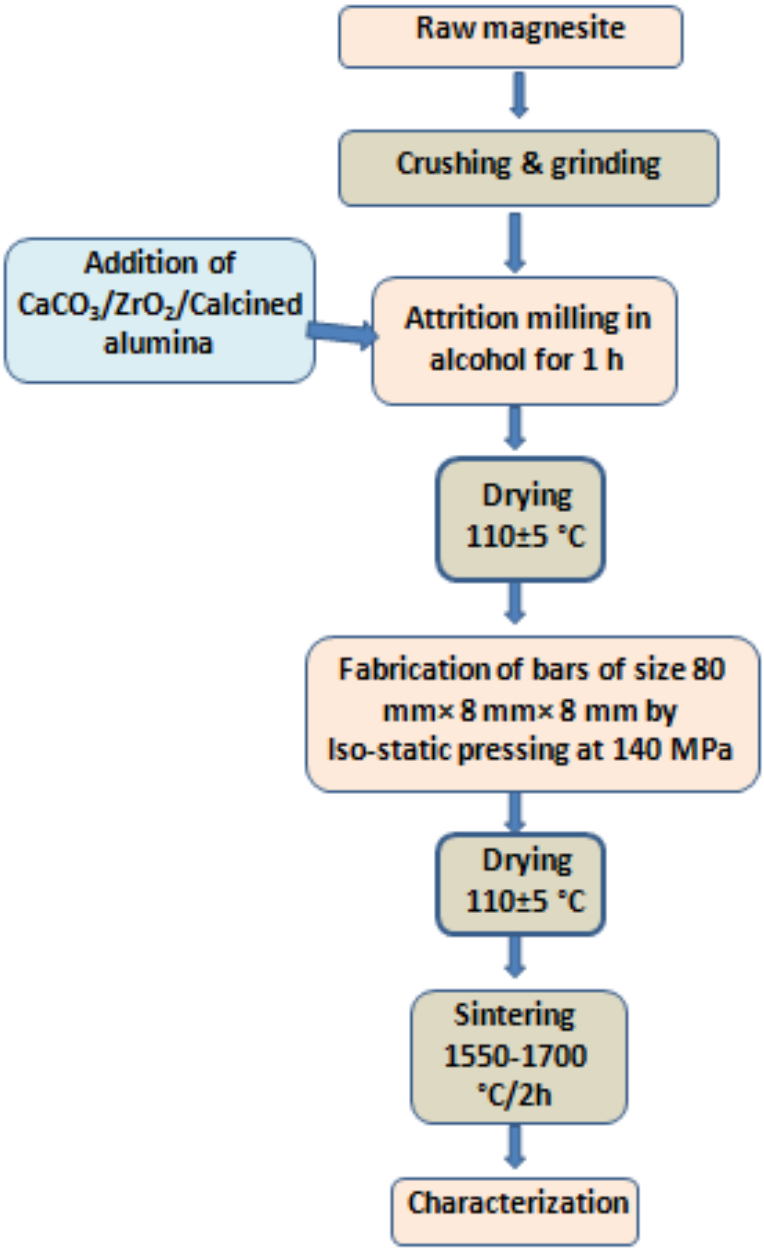

Figure 3-1: Process Flow for methodologies 1, 2 & 3

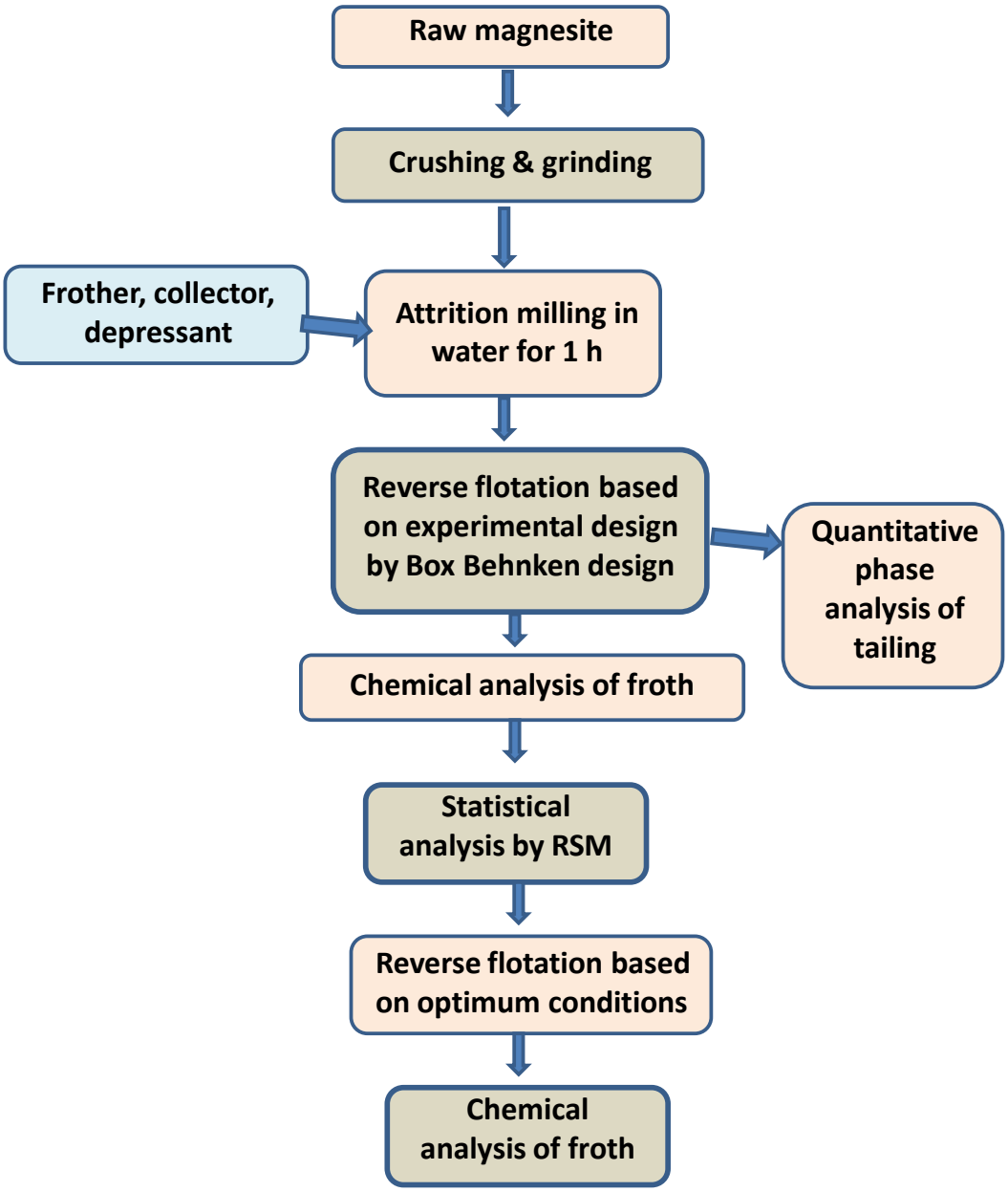

Figure 3-2: Process Flow for methodology 4

4. Experimental

Raw magnesite was supplied by the erstwhile Burn Standard Co. Ltd., presently SAIL Refractory Company Limited, India. It was characterized in terms of different properties stated below. Other raw materials used were calcium carbonate ($CaCO_3$), zirconia and calcined alumina. These were of chemical grade and therefore were not further characterized. In methodology 1, $CaCO_3$ supplied by S.D. Fine Chemical Limited, India was added to the raw magnesite. In another approach chemical grade monoclinic zirconia of Loba Chemie, India was added to the magnesite. In case of magnesium aluminate spinel formation, commercially available calcined alumina (HGRM 30 of Hindalco) was used along with the raw magnesite. Initially raw magnesite lumps were crushed using a crusher (Make: D K Engg. Works, India; Model: 205) and ground to 100 mesh fineness and were characterized in terms of different properties.

4.1 Raw magnesite characterization

4.1.1 Chemical analysis

The chemical analysis of the as received magnesite was done by wet chemical method. 0.25 g of the solid powdered sample was taken into a platinum crucible and the sample was thoroughly mixed with borax-sodium carbonate fusion mixture and fused at around 900 °C for 1 h. After melting, the mass was cooled down and dissolved with nitric acid in order to obtain a clear solution.

Fe_2O_3 and TiO_2 were measured by colorimetric method. Fe_2O_3 was measured by forming Fe-orthopheanthroline color complex and concentration was determined by measuring color intensity at 510 nm. TiO_2 was also measured similarly by forming Ti-hydrogen peroxide color complex and was measured at 410 nm wavelength. MgO, Al_2O_3, CaO were determined by complexometric method using Ethylene diamine tetra acetic acid (EDTA) solution. Na_2O and K_2O were measured by flame photometry using hydrofluoric acid and perchloric acid dissolved in magnesite solution. SiO_2 was measured by gravimetric method.

4.1.2 X-ray diffraction

Identification of crystalline phases was done using X-ray powder diffraction technique using Ni-filtered Cu-Kα radiation. The X-ray diffraction patterns were recorded in X'pert Pro MPD, PANalytical diffractometer (Figure 4-1) within the Braggs angle range of $10°<2\theta<90°$. The test sample was ground, passed through 100 mesh standard B.S. sieve and then finely powdered using an agate mortar pestle.

X-rays are a form of electromagnetic radiation whose frequencies are usually in between the UV and gamma radiation. X-ray diffraction analysis is based on constructive interference of monochromatic X-rays and a crystalline sample. The X-rays are produced by a cathode ray tube and filtered to generate monochromatic radiation. The radiation is then passed through soller slits which collimate the X-ray beam. Finally the beam is directed toward the sample. The diffracted X-rays are detected by a detector and counted. All possible diffraction from different phases and from different planes can be detected by scanning the sample for a range of 2θ angle. Crystalline phases can be identified by determining the 'd' value from 2θ using Bragg's Equation (Equation 4-1). When conditions satisfy Bragg's Equation, the interaction between the incident rays and the sample produces constructive interference. This expression relates the wavelength of the X-rays to the inter-atomic spacing and the diffraction angle.

$$n\lambda = 2d \sin\theta \qquad \textbf{(Equation 4-1)}$$

where,

n= order of diffraction

λ= wavelength of incident ray

d= spacing between the planes in the atomic lattice

θ= angle between the incident ray and the scattering plane (Bragg's angle)

Sharp peaks appear in XRD pattern when constructive interference takes place only after satisfying Bragg's Law. XRD patterns thus obtained were analyzed with the help of X'Pert HighScore Plus software (Make: PANalytical, The Netherlands). Quantification of the phases was done by X'Pert HighScore Plus software using Rietveld refinement method.

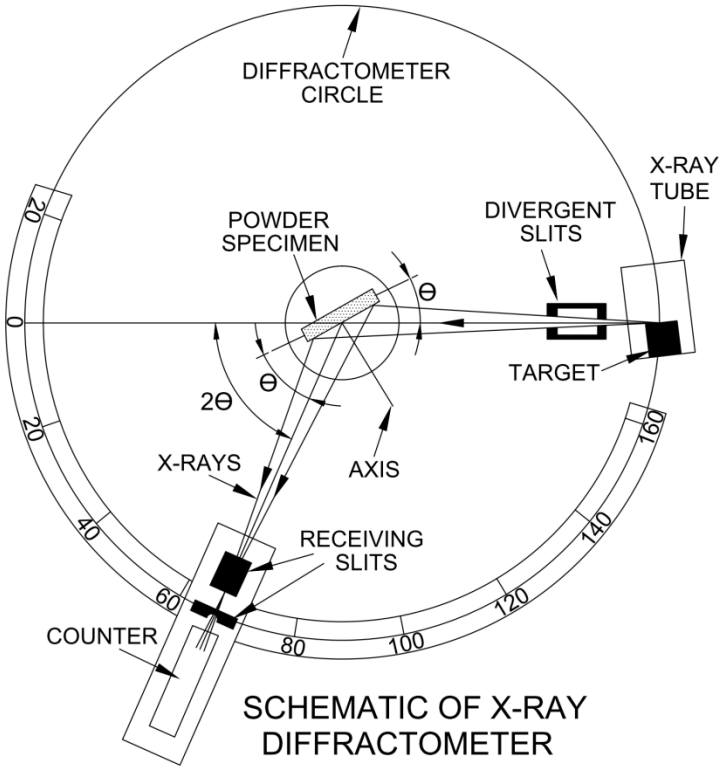

Figure 4-1: Schematic of X-Ray Diffractometer

4.1.3 Infrared spectroscopy

Spectroscopy is a study of the interactions between a sample and energy. Infrared spectroscopy is basically a study of absorption of infrared radiation which causes vibrational transition in the molecules of the sample. In a molecule, atoms are linked by chemical bonds and they vibrate with a typical frequency. The characteristic movement of the atoms is called natural frequency of vibration. When infrared radiation is applied to the sample, it results in vibration between the atoms. If the applied infrared frequency is equal to the natural frequency of vibration, absorption of the infrared radiation takes place and a peak is observed. Different functional groups have different characteristic frequencies. Therefore IR spectroscopy helps in determining the functional groups present in the sample. A small amount of sample (0.2 g) was thoroughly mixed with ground KBr in an agate mortar and a disc (2.5 mm dia) was prepared in vacuum, maintaining a pressing pressure of 3.2 MPa. The infrared spectrograms of these discs were taken by Hitachi spectroscope (270-90) (Figure 4-2). IR transmission spectra were recorded over the wave number range of 400-4000 cm^{-1}.

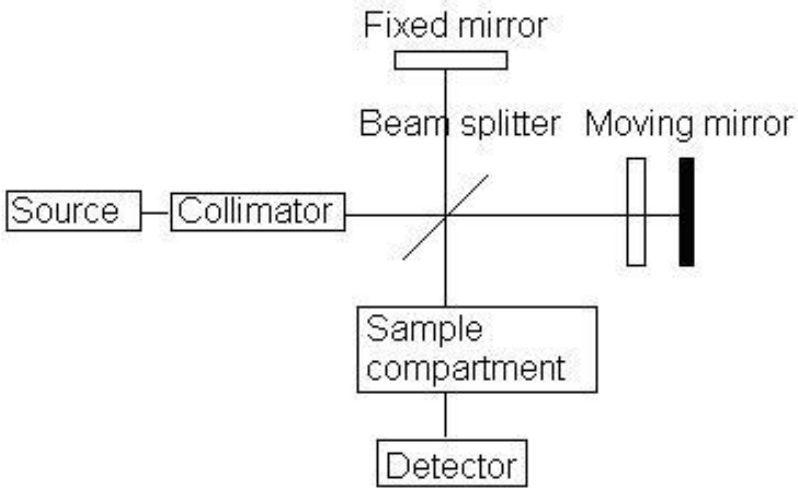

Figure 4-2: Schematic diagram of IR spectroscope

4.1.4 Differential thermal analysis & thermo-gravimetric analysis

Differential thermal analysis (DTA) & thermo-gravimetric analysis (TGA) are the two thermal analysis techniques which depict the changes took place during thermal treatment of a material. TGA measures the change in weight of the sample as a function of temperature under controlled atmosphere. TGA curve (%weight change against temperature) gives information about the thermal stability of the sample and enables the study of any physical or chemical processes which may have caused the variation in weight. On the other hand, in DTA, the sample and an inert material (reference) are subjected to identical thermal condition simultaneously and the difference in temperature of the sample and the reference material is measured. A plot of the temperature difference over the temperature range (DTA curve/ thermogram) results in a series of peaks that shows the temperature at which any changes have occurred. Studying the nature of the peak it can be stated whether the reaction is endothermic or exothermic.

The magnesite, as received, was subjected to differential thermal analysis (DTA) and thermo gravimetric (TG) analysis which were carried out in STA 449F3 thermal analyzer (Netzch, Germany, Figure 4-3). Samples in this study were ground to -200 mesh. The rate of heating was 10°C/min, α-alumina was used as the reference material and the heating was carried out in nitrogen atmosphere.

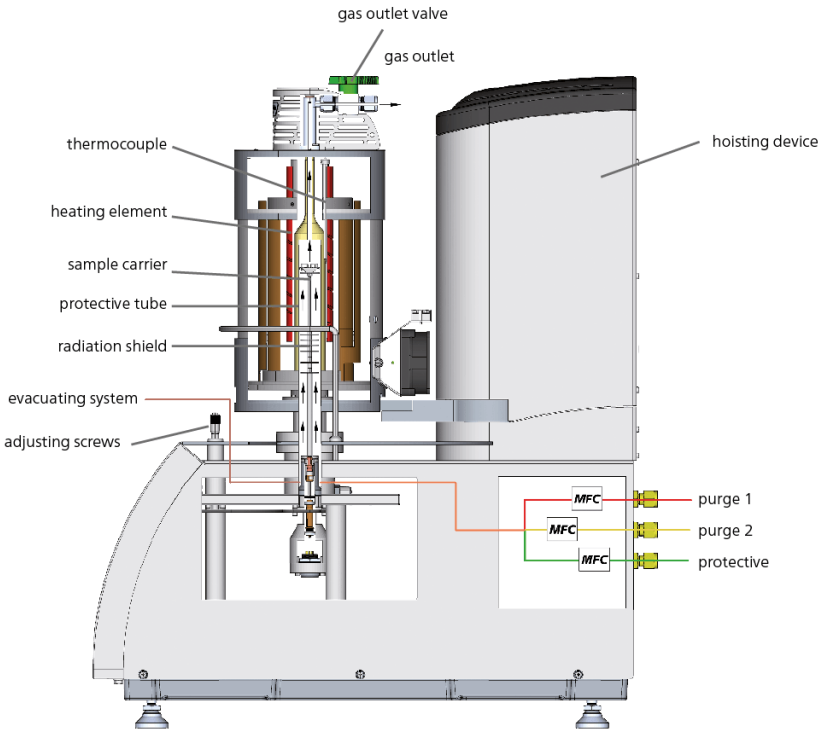

Figure 4-3: Thermal analyzer apparatus

4.1.5 Particle size distribution

Particle size analysis of the milled slurry, froth and tailing was done in a particle size analyser based on laser diffraction principle (Make: Microtrac, USA; Model: S3500). A laser beam is passed through a sample well-dispersed in liquid and scattered. Particle size is measured by detecting the scattered light thus produced. Scattered light is measured at different angles and data is collected continuously. Small particles scatter light at larger angles than large particles. The collected data is analyzed by an algorithm to determine the particle size distribution. The resultant data is presented as cumulative mass% distribution in terms of equivalent spherical diameter. The samples are required to be well dispersed in a liquid of known density and viscosity. The liquid must be carefully selected so that the powdered sample is completely dispersed in that. In the current study, distilled water is used as the dispersing liquid.

4.1.6 Surface area measurement

The specific surface area of the milled powder is determined by standard multi point BET (Brunauer, Emmett and Teller) method using a surface area analyzer, Nova Station D (Quantachrome Instruments, USA). This method is based on weak and reversible (physical) adsorption of gas onto the solid surface. Different surface textural properties such as specific surface area, pore volume, pore size and shape can be measured by this method. 3-5 g of dried sample was taken in the sample cell and degassed at 110±5 °C in vacuum upto 3 mbar. The sample tube was then closed and cooled to room temperature and placed in a liquid nitrogen bath. In the next step Grade I nitrogen gas was passed over the sample so that it was adsorbed on the surface of the sample at the liquid nitrogen temperature (-196 °C). The amount of gas adsorbed by the sample to develop a monolayer on the surface was determined by the instrument and the total surface area was displayed by digital indicator. The BET adsorption equation (Equation 4-2) is as follows:

$$\frac{P}{V(P_s - P)} = \frac{1}{V_m C} + \frac{C-1}{V_m C} \times \frac{P}{P_s} \qquad \textbf{(Equation 4-2)}$$

where,

P = Partial vapour pressure of adsorbate nitrogen gas

P_s = Saturation pressure of adsorbate nitrogen gas

V= Volume of gas adsorbed at STP

V_m = Volume of gas adsorbed at STP to produce an apparent monolayer on the sample surface

C= Constant

Equation 4-2 gives a straight line with slope (C-1)/V_mC and intercept 1/V_mC. V_m is calculated from these values. Finally specific surface area is calculated using Equation 4-3:

$$S = \frac{V_m \times N \times a}{m \times 22400} \qquad \textbf{(Equation 4-3)}$$

where,

N= Avogadro constant (6.023×10^{23} mol^{-1})

a = Effective cross-sectional area of 1 adsorbate molecule (in mm^2)

m = Mass of test sample (in g)

22400 = volume occupied by 1 mole of the adsorbate gas at STP (in ml)

4.2 Sample preparation

4.2.1 Batch composition

Different batches having different compositions for all four methodologies were formulated and the details are given in Table 4-1

Table 1-1: Methodology wise batch code and composition

Batch	Batch Code	Batch Composition
As received batch	M0	100% magnesite
With different C/S ratio (Methodology 1)	M0	100% magnesite (C/S ratio 0.58)
	M1	Magnesite + $CaCO_3$ (C/S ratio 1:1)
	M2	Magnesite + $CaCO_3$ (C/S ratio 2:1)
With addition of ZrO_2 (Methodology 2)	MZ0	100% magnesite
	MZ1	99 wt% Magnesite + 1 wt% ZrO_2
	MZ3	97 wt% Magnesite + 3 wt% ZrO_2
	MZ5	95 wt% Magnesite + 5 wt% ZrO_2
Spinel composition (Methodology 3)	MS	Magnesite + calcined alumina (1:1 wt ratio)
Beneficiation of magnesite (Methodology 4)	PM	Processed magnesite after beneficiation

Sintered aggregates developed from Indian raw magnesite were evaluated in terms of different properties. Effect of different methodologies on densification, mechanical, thermo-mechanical strength, phase assemblage and microstructural evolution was studied thereafter using all the aforementioned batches.

4.2.2 Powder preparation

Raw materials in appropriate proportion were subjected to attrition milling (Union Process Attritor, USA) for 1 h in alcohol medium. Milling of the batches was carried out in a zirconia pot with zirconia balls. After milling, the slurry thus obtained was dried initially in air and then at 110±5 °C in an oven. The dried agglomerate were then crushed and passed through 100 mesh sieve to get the desired powder.

4.2.3 Fabrication of bars

5 w/v % PVA solution was added to each powdered batch in an amount of 5 v/wt % as green binder. After thorough mixing, each batch was sieved through BSS 60 standard sieve to ensure uniform mixing of the binder with the material. Bars of 80 mm × 8 mm × 8 mm were uniaxially pressed using a Carver Laboratory Press (capacity 30 T) at 100 MPa pressure. To obtain uniform packing density, bars were then iso-statically pressed. The uniaxially pressed bars and pellets were put inside flexible rubber moulds and entrapped air was removed by vacuum. Those rubber moulds in sealed condition were then put into a cylindrical oil chamber of laboratory model cold iso-static press (ABB Autoclave Engineers, USA) in suspended condition. In this condition, a pressure of 140 MPa was applied for 1 min. The green samples thus produced were air dried for 24 h and then oven dried at 110±5 °C for another 24 h.

4.2.4 Sintering

All the samples after drying at 110±5 °C were sintered in an electrical furnace in the temperature range of 1550 °C to 1700 °C at a temperature interval of 50 °C and soaking period of 2 h at the peak temperatures. The temperature during firing was raised at the rate of 5 °C/min upto 1000 °C and thereafter 3 °C/min upto the final temperature. Firing was done in an electric chamber furnace with $MoSi_2$ as heating element in normal atmospheric condition.

4.3 Characterization of sintered aggregates

The sintered aggregates were characterized in terms of the following properties:

1. Linear shrinkage on firing
2. Bulk density and apparent porosity
3. True density
4. Phase analysis by XRD study
6. Modulus of rupture at ambient and elevated temperature
7. Thermal shock resistance
8. Microstructural analysis by field emission scanning electron microscope (FESEM) and energy dispersive X-ray analysis (EDX)

4.3.1 Linear shrinkage on firing

To measure linear shrinkage, the length of the green bar samples were measured before firing. Final length of the bars after sintering at different temperatures was also measured and the difference between the initial length and final length was calculated. Percentage linear shrinkage is then evaluated using the following equation:

$$\% \text{ Linear shrinkage} = \Delta L/L_0 \times 100 \qquad \textbf{(Equation 4-4)}$$

where,

L_0 = Initial length of the bar, mm

$\Delta L = L_0 - L$, mm

L = Length of the bar after firing, mm

4.3.2 Bulk density and apparent porosity

Bulk density (BD) and apparent porosity (AP) were measured by liquid displacement method using Archimedes' principle. Sintered samples were weighed in dry state (W_d) and then kept in kerosene under vacuum for 2 h to ensure complete filling up of the open pores by kerosene. After 2 h, the weight of the samples, suspended in kerosene was taken and noted as W_{sus}. The sample was then weighed in fully soaked condition (W_s). Bulk density and apparent porosity were calculated using the following formulas:

$$\text{Bulk Density (g/cc)} = \frac{W_d}{W_s - W_{sus}} \times \rho \qquad \textbf{(Equation 4-5)}$$

where,

ρ = Density of kerosene

$$\text{Apparent Porosity (\%)} = \frac{W_s - W_d}{W_s - W_{sus}} \times 100 \qquad \textbf{(Equation 4-6)}$$

4.3.3 True density

True density of the powdered sample was measured using a specific gravity bottle of 10 cc volume. The test sample was ground in such a manner that it passed through 60 mesh BS sieve but did not pass thorough 100 mesh BS sieve. After grinding, the sample was subjected to magnetic separation of iron particles.

The specific gravity bottle was weighed (W_1) after complete drying in an oven at 110±5 °C. Then the sample was taken in the bottle and it was weighed again (W_2). Next kerosene was introduced into the bottle and the bottle was evacuated upto a pressure of 4 mm Hg and it was then kept at this pressure for 2 h for complete removal of entrapped air. The bottle completely filled with kerosene and weighed (W_3). The bottle was then emptied, thoroughly cleaned and dried. Finally the bottle was completely filled with kerosene and weighed (W_4). The relative density was measured by dividing the bulk density by the true density.

$$\text{True density of the sample} = \frac{W_2 - W_1}{(W_4 - W_1) - (W_3 - W_2)} \times \rho \qquad \textbf{(Equation 4-7)}$$

where,

ρ = Specific gravity of the kerosene at room temperature, in g/cm^3

4.3.4 Phase analysis by XRD

Phase identification and analysis was done following the same procedure as stated earlier.

4.3.5 Flexural strength at ambient temperature

Flexural strength at ambient temperature was measured by three point bending test [ASTM C1161-13] using Instron-1185 universal testing machine. The span length was 40 mm and the cross head speed was maintained at 0.5 mm min^{-1}. The modulus of rupture (MOR) or the flexural strength was calculated using the following equation and result values are in MPa.

$$\text{MOR} = \frac{3\,WL}{2\,BD^2} \qquad \textbf{(Equation 4-8)}$$

where,

W = breaking load, kg

L = length of the bearing span, mm

B = breadth of the sample at the breaking point, mm

D = depth of the sample at the breaking point, mm

4.3.6 Flexural strength at elevated temperature

The high temperature modulus of rupture strength was measured at 1300 °C by an instrument developed at Central Glass and Ceramic Research Institute, Kolkata, India. The test was carried out by three point bending method [ASTM C1211-13] on a span of 45 mm. The rate of temperature rise was maintained at 5 °C/min and samples were allowed a soaking period of 30 min at test temperature. The result was calculated using the same equation as described in the previous section.

4.3.7 Thermal shock resistance

When a ceramic material experiences rapid fluctuation of temperature, a stress is developed within the body which may cause failure of the material. Thermal shock resistance refers to a material's ability to withstand rapid changes in temperature. Thermal shock resistance can be measured using different methods depending on the field of application [167-170]. Here, it was determined by measuring the retained flexural strength after multiple thermal shock cycle as adopted by Peretz and Bradt [168].

Thermal shock resistance of the sintered samples was measured using the following test method. The sintered rectangular bars were heated upto 1200 °C in an electric furnace with a soaking period of 30 minutes. Then they were air-quenched in room temperature (without any draught in the surroundings) for 10 minutes and again put into furnace for 10 minutes. This cycle was continued up to ten times and the samples of fourth and tenth cycle were tested for retained flexural strength by standard three point bending method using an Instron-1185 universal testing machine. The span length and crosshead speed were same as mentioned earlier.

4.3.8 Microstructure analysis

Microstructural evolution of the samples was studied by Field Emission Scanning Electron Microscope (FESEM) and Energy Dispersive X-ray (EDX) analysis. Polished and thermally etched samples were used for microstructure analysis. Scanning electron microscope is used to observe the morphology of a sample at higher magnification and resolution as compared to an optical microscope. An accelerated beam of mono-energetic electrons is focused on a solid surface and is scanned over the specimen surface on a small

area. Multiple signals such as secondary electron (SE), back scattered electron (BSE), characteristics X-rays, cathode luminescence (CL) etc are generated and the appropriate ones are collected to create the image. In SEM, interaction volume extends from 100 nm to 5 μm and signals are generated as a result of interaction of the electron beam with the atoms at different levels. Secondary electrons are generated from a location very close to the sample surface and provide information about the sample topography. Back scattered electrons are generated from inner location of the sample and strongly related with the atomic number of the element. It provides information about element distribution in the sample. Characteristic X-Rays are emitted when electron beam removes an electron from inner shell and this is used to determine the composition and relative abundance of the elements.

The surface to be studied was ground with the help of a series of diamond grinding pad from 125 to 9 μm on a manual polishing machine. The sample was then polished in a manual polishing machine with 6, 3 and 1 μm diamond suspension to get mirror finished surface. Thermal etching of the sample was done by heating the sample at 1400 °C for 30 min and by removing the sample at different temperatures according to the nature of the sample. Polished surface was then analyzed by FESEM (Make: Zeiss, Germany). The etched sample was mounted on a metal stub using a conducting tape. Polished surface of the sample was coated with carbon under vacuum to make the surface conducting. Secondary electron image as well as back scattered image of the samples were taken. EDX analysis was carried out with an additional EDX attachment. Elemental mapping of the samples was also carried out with the help of the same machine to see the distribution of the elements throughout the matrix.

4.4 Beneficiation through froth flotation

Flotation is a separation process which is based on the difference in physicochemical properties of the interfaces. It can take place at liquid-liquid, liquid-gas and liquid-solid and solid-gas interface. Froth flotation occurs on a gas-liquid interface. Among all the flotation techniques, froth flotation is the only one used for industrial application.

4.4.1 Froth flotation principles

Froth flotation is a separation process of materials depending on their hydrophobicity. Hydrophobicity is increased by the addition of surfactants and wetting agents so that the hydrophobic materials get selectively attached to the surface of air bubbles rising through suspension. As a result, they are either concentrated or separated from the suspension in the form of froth.

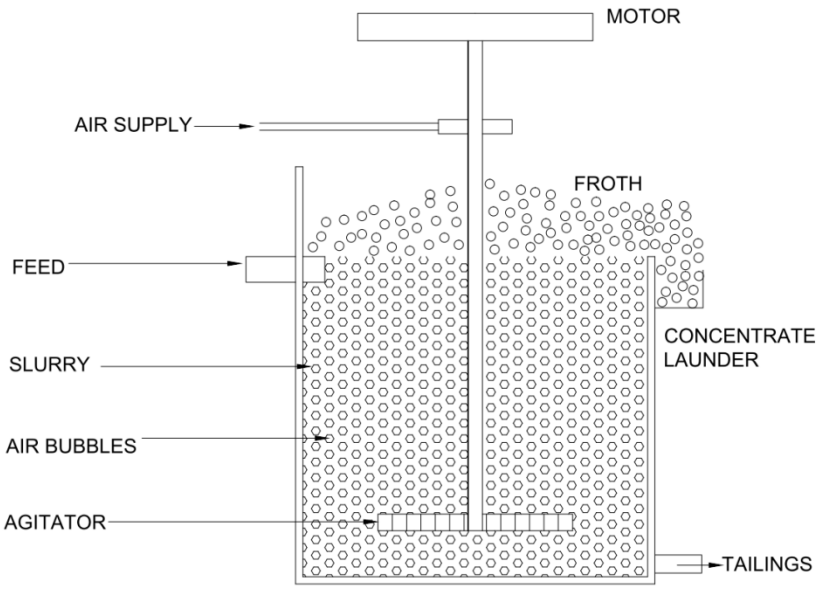

Figure 4-4: Schematic diagram of froth flotation cell

The feed to the flotation cell (Figure 4-4) is a suspension usually consisting of 1:3 solid to water by weight. The mixture of the particles is conditioned using different reagents before feeding into the flotation cell. After conditioning the pulp is placed into the flotation cell and it is then agitated using impellers. Air is fed near the impeller to form gas bubbles. These bubbles collide with the hydrophobic particles, adhere to them and rise to the surface to form froth. The froth is then removed by skimming like a concentrate or a froth product. The hydrophilic particles on the other hand are removed from the cell as tailings.

The hydrophobic or hydrophilic nature of the surface can be modified using suitable surfactants. A surfactant that is used to make the surface hydrophobic is called a collector. A collector must have at least one non-polar group which imparts hydrophobicity to the particles. Due to the chemical, electrical or physical attraction between the polar groups and

the surface sites, the collectors adsorb onto the particles having the non polar groups directed towards the bulk solution which as a result induces hydrophobicity to the particles. On the other hand, frothers are compounds that stabilize the air bubbles so that they remain well-dispersed in the pulp and form a steady froth layer which can be removed before the air bubbles burst. Attachment of the bubbles to the surface is determined by Young's equation (Equation 4-9).

$$\gamma_{sg} = \gamma_{sl} + \gamma_{lg} \cdot \cos\theta \qquad \textbf{(Equation 4-9)}$$

where, γ_{sg}, γ_{sl}, γ_{lg} are the surface energy of the solid/gas, solid/liquid, liquid/gas interfaces respectively and θ is the contact angle formed between solid, liquid and gas phases. If the contact angle is too small then the bubbles will not attach to the surface. So, large contact angle is needed for stronger bubble attachment. Generally, a contact angle of 90° is sufficient for effective froth flotation.

4.4.2 Flotation experiment

Experimental design matrix was developed according to the Box-Behnken design. Different batches of raw magnesite with varying amount of frother, collector and depressant were attrition milled in a zirconia lined attrition mill (Make: Union Process, USA; Model: 01HD) in water medium for 1 h. The resulting slurry was then poured into the flotation cell (Make: Denver Lab, USA; Model: F-41-A). Pine oil was used as frother, Flotigam EDA as collector and sodium hexametaphosphate (SHMP) as a depressant of carbonates.

4.5 Process optimization by Response Surface Methodology

Statistical designing of experiments and optimization of process parameters are nowadays very much popular among researchers. Traditionally optimization has been done by studying the effect of one factor at a time on one experimental response. However, the major disadvantage of this method is that it does not take into account the interactive effect of all the variables. Another disadvantage of this method is that it requires a large number of experimental outputs in order to optimize and validate the functional relationship between the dependant variable with several independent variables. To overcome these problems multivariate statistical techniques have been used in recent times. Response Surface Methodology (RSM) is one of these techniques. Response Surface Methodology

was developed by Box and his group in 1951. This technique is a combination of mathematical and statistical techniques based on the fit of a polynomial equation to the experimental data. It is used to identify the relationship between the response and the independent variables. It shows the effect of each of the independent variables alone or in various combinations, on a certain process. The relation between the response and the input variables is shown in Equation 4-10 below:

$$\eta = f(x_1, x_2, x_3, \ldots, x_n) + \varepsilon \qquad \textbf{(Equation 4-10)}$$

where,

η is the response,

f is the function of response,

$x_1, x_2, x_3, \ldots, x_n$ are the independent variables,

n is the number of independent variables and ε is the statistical error.

Before applying RSM one must select an experimental design. For linear function data set, experimental designs for first order models like factorial design can be used. However, when the data set cannot be described by linear function, experimental designs for quadratic response surfaces should be used. Box-Behnken, Central composite and Doehlert designs are some of the examples of such type of experimental design.

4.5.1 Box-Behnken Design

Box-Behnken designs (BBD) are developed by George E. P. Box and Donald Behnken in 1960. Experiments are run at different factor values called the 'levels'. Box-Behnken design is a type of experimental design having three levels to run an experiment. The number of runs required for a BBD is defined in Equation 4-11.

$$N = 2k(k-1) + C_0 \qquad \textbf{(Equation 4-11)}$$

where,

N is the number of runs,

k is the number of factors

C_0 is the number of central points.

BBD is more efficient than other experimental designs like the Central Composite Design and three-level full factorial designs. Its advantage over other designs is that it does not contain combinations where all the factors are at their extreme conditions simultaneously thereby avoiding any unsatisfactory results which might have occurred at those conditions [171].

Efficiency of the froth flotation process was statistically analyzed in terms of increase in silica content (in wt %) in froth by Response Surface Methodology (RSM) using a suitable Box-Behnken Design. The flotation process was carried out under different air pressures ranging in between 0.5-3.5 mm water, collector/frother ratio ranging in between 1-2 and amount of depressant in between 1-2 g per 4 kg of slurry. Each froths, collected after flotation, was assessed for complete chemical composition. Significance of the variables was analysed by ANOVA (analysis of variance). Statistical analysis of the data was carried out by Design Expert, version 10.0.3 (Make: Stat-Ease Inc., USA) software.

4.6 Phase analysis

Quantification of the crystalline phases of the processed magnesite for which maximum silica content was achieved in froth was done using the same procedure as stated earlier.

5. Results & Discussion

5.1 Raw material characterization

Characterization of the raw material is important because it serves as the basis of any research. The starting material of this research was natural magnesite ore. Therefore it was important to characterize the magnesite in terms of different techniques to ascertain its purity.

5.1.1 Chemical analysis

Chemical analysis results of raw magnesite are tabularized in Table 5-1. It contains 90 % magnesia (loss free basis) as the major component. Silica content in the sample is 4.8 % and lime content is 2.79 % making these the major impurities. The loss on ignition (L.O.I.) of the sample is 49.52 %.

Table 5-1: Chemical analysis results of raw magnesite

Constituents	Wt%	Wt% (loss free basis)
SiO_2	2.44	4.80
Al_2O_3	0.17	0.34
Fe_2O_3	0.24	0.48
TiO_2	0.02	0.04
CaO	1.41	2.79
MgO	45.68	90.49
Na_2O	0.08	0.16
K_2O	0.05	0.10
L.O.I.	49.52	-

5.1.2 Phase analysis

XRD pattern of raw magnesite is shown in Figure 5-1. The main crystalline phase is magnesite along with dolomite and quartz as minor phases. Quantification of the phases reveals that the amount of magnesite in the sample is 94 %, that of dolomite is 3.7 % and

amount of quartz is 2.3 %. XRD analysis results are in good agreement with the chemical analysis report ascertaining the presence of silica and lime as main impurities [172, 173].

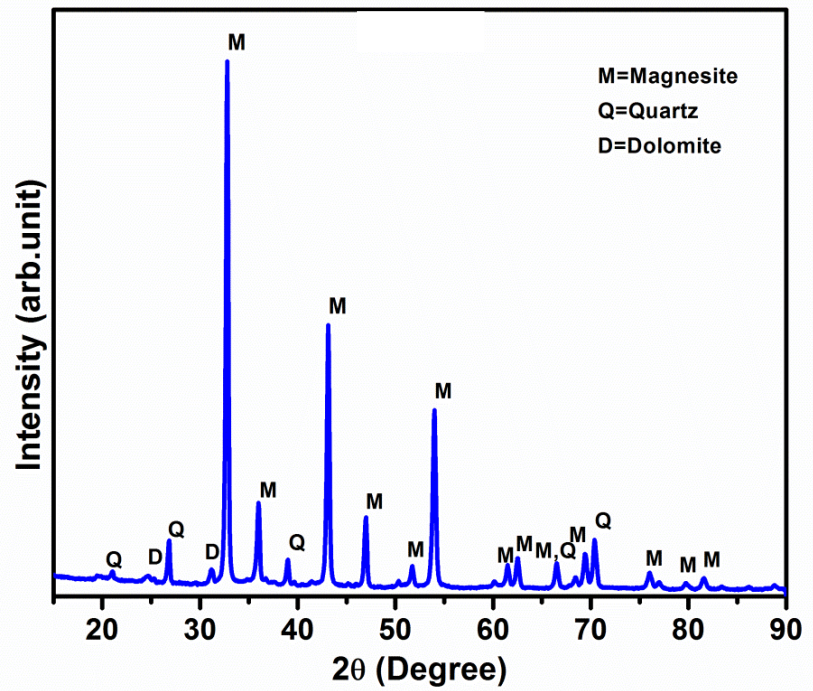

Figure 5-1: XRD pattern of as received magnesite [172]

5.1.3 Thermal decomposition behavior

Thermal decomposition study of raw magnesite is done using differential thermal analysis (DTA) and thermo-gravimetric analysis (TG) (Figure 5-2). Three distinct endothermic peaks can be observed from the DTA curve. The first peak at around 630 °C corresponds to the decomposition of magnesite ($MgCO_3 \xrightarrow{\Delta} MgO + CO_2$). The second peak at around 730 °C is due to the decomposition of magnesite present in dolomite. Dolomitic magnesite needs some extra energy to break the structure of 1:1 compound at first. Therefore, the endothermic peak due to the decomposition of dolomitic magnesite is at 100 °C higher temperature than normal magnesite. The third endothermic peak which is at 803 °C corresponds to the decomposition of calcite present in dolomite.

TG curve shows that there is a major weight loss of 44.14 % at around 630 °C which is associated with the decomposition of magnesite into MgO and CO_2. The next weight loss is at 730 °C due to the decomposition of magnesite present in dolomite [172].

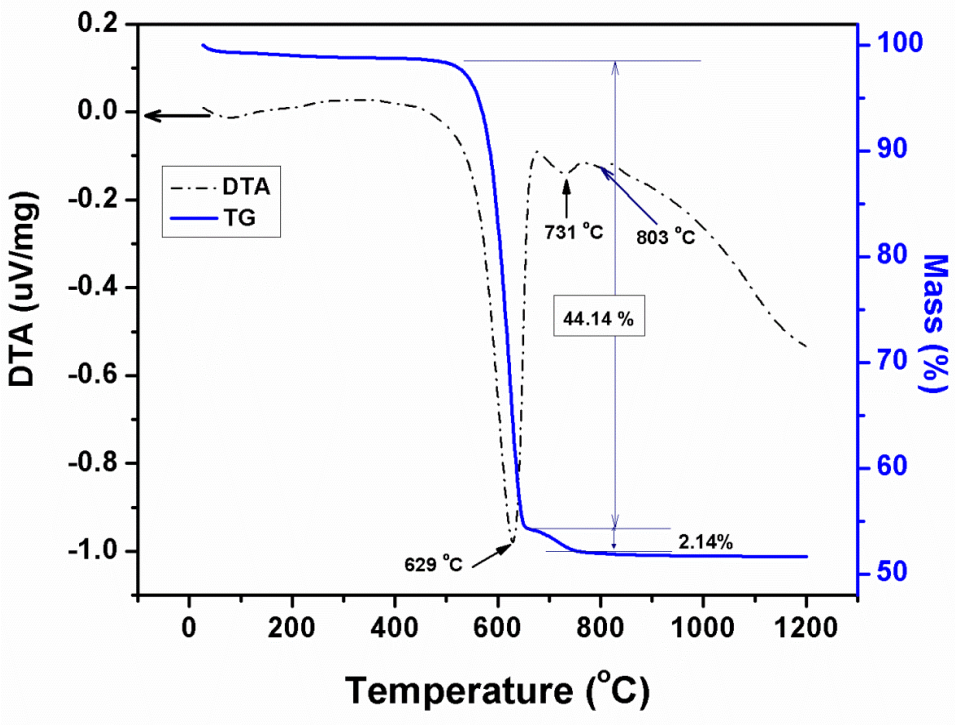

Figure 5-2: TG-DTA thermogram of as received magnesite [172]

5.1.4 Infrared spectroscopy

IR spectra of raw magnesite are shown in Figure 5-3. It shows stray bands at 1450 cm^{-1}, 900 cm^{-1} and 775 cm^{-1} which corresponds to magnesite mineral. These are the characteristic absorption bands of carbonate group of magnesite and are different from all other carbonate minerals. The band at 1450 cm^{-1} represents asymmetric stretching which signifies the combination of transverse and longitudinal components of this vibration. Other two bands represent bonding vibration arising from the out of plane bending mode and in plane bending mode of the carbonate ion [174].

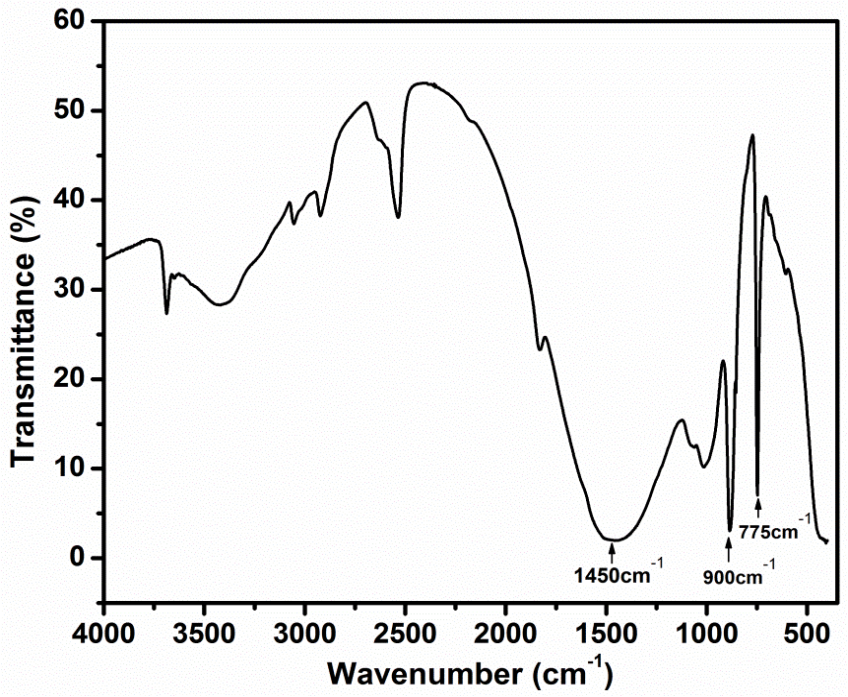

Figure 5-3: Infrared spectroscopy of as received magnesite [174]

5.1.5 Particle size analysis

Particle size distribution of the raw material is important as it determines the microstructure which eventually controls the final properties after sintering. The particle size distribution is reported as individual size distribution and cumulative mass % finer than a given size. The distribution is uni-modal and the D_{50} value of the milled slurry is 2.706 μm. All the particles are in the range starting from 0.486 to 44.00 μm. K_G value of the distribution is 1.46 which means the distribution is leptokurtic [173].

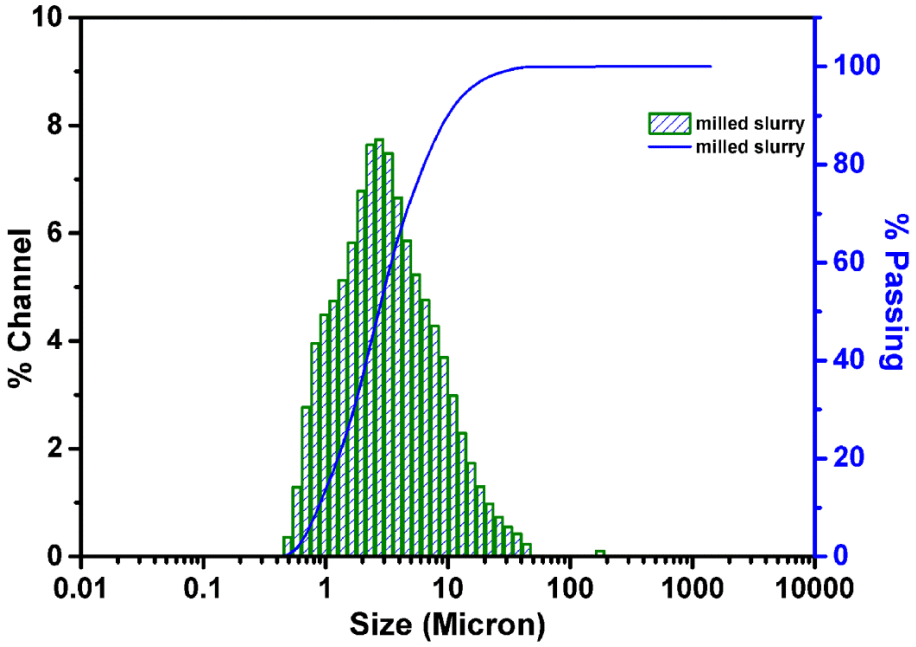

Figure 5-4: Particle size distribution of milled slurry [173]

5.1.6 Surface area analysis

Attrition milling is done to ensure homogenous mixing of the material as well as to increase the surface area. Raw magnesite was attrition milled for this purpose. The specific surface area was found to be 15.769 m^2/g.

5.2 Characterization of sintered aggregates

5.2.1 Densification behavior

Densification plays an important role in fabrication of ceramic materials. It is determined by measuring bulk density (BD) and apparent porosity (AP). Figure 5-5 shows the densification behavior of magnesite samples with increasing sintering temperature. It is observed that BD increases and AP decreases with sintering temperature. It is evident from the densification plot that rate of densification is low upto 1400 °C. After 1400 °C, densification is quite rapid and apparent porosity becomes very low at 1550 °C. Therefore the temperature range was chosen from 1550-1700 °C. Samples sintered in the temperature range of 1550-1700 °C have very low AP which may be due to the presence of low melting phase. There is not much variation in both BD and AP in the temperature range of 1550-1700 °C. However, at 1700 °C a slight decrease in BD can be observed. AP is also the

lowest at this temperature. Lower BD with lower AP indicates the formation of low density liquid phase at 1700 °C.

Figure 5-6 depicts the change in linear change and percentage densification of magnesite samples with sintering temperature. There is not much change in linear shrinkage over the sintering temperature range of 1550-1700 °C as the reduction in porosity level is not much and the densification is very high for all the samples. Highest linear shrinkage is found at 1550 °C due to the rapid densification during the early stage of sintering that leads to coalescence of small particles into large ones and results in grain growth and reduction of small pores [174].

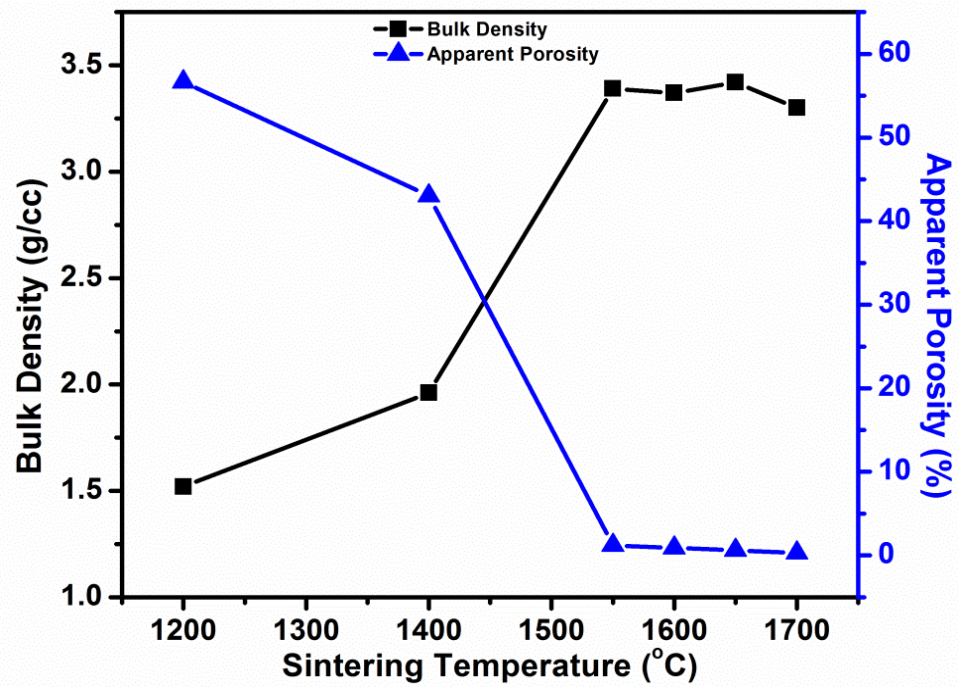

Figure 5-5: Variation in bulk density and apparent porosity of magnesite samples (M0) as a function of sintering temperature

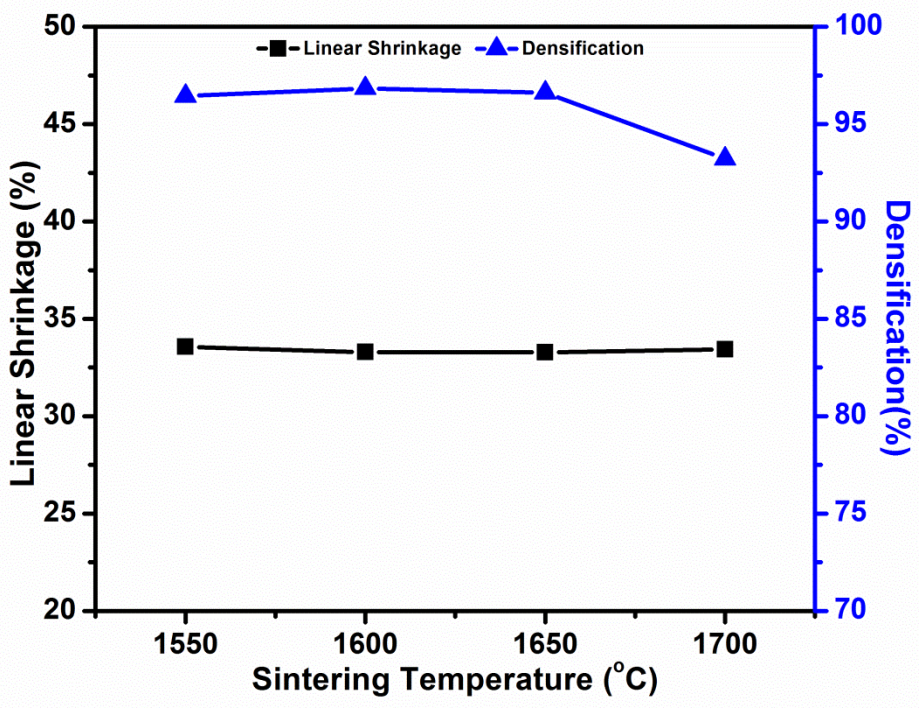

Figure 5-6: Variation in linear shrinkage and percentage densification of magnesite samples (M0) as a function of sintering temperature

5.2.2 Phase analysis

High temperature phase development of magnesite samples at different sintering temperatures is depicted in Figure 5-7. Periclase is the main crystalline phase along with forsterite and monticellite as secondary phases as can be observed from that figure. The presence of silica and lime in the raw magnesite results in forming a low melting phase when sintered at high temperature. This low melting phase containing magnesia, silica and lime is called monticellite or calcium magnesium silicate ($CaMgSiO_4$) (Melting point 1503 °C). Forsterite or Mg_2SiO_4 on the other hand is a desirable phase having a melting point of 1890 °C. Quantification of the crystalline phases reveals that considerable amount of monticellite is present in the samples (Table 5-2).

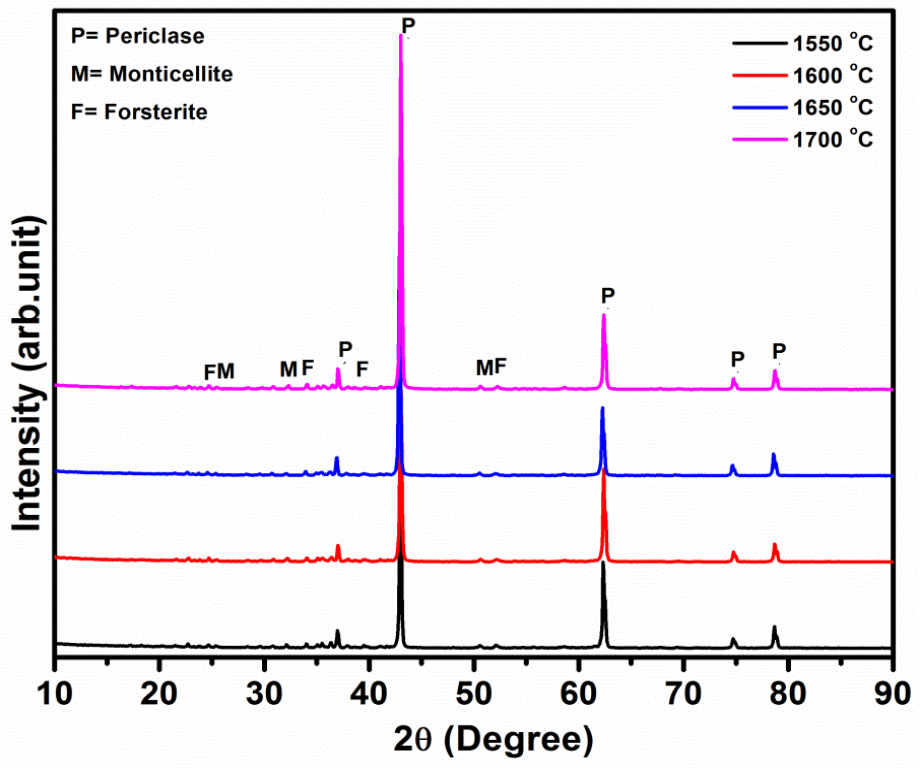

Figure 5-7: XRD pattern of magnesite samples (M0) sintered in the temperature range of 1550-1700 °C

Table 5-2: Quantification of the crystalline phases of magnesite sample (M0)

Sintering temperature (°C)	Crystalline phase		
	Periclase	Forsterite	Monticellite
1550	83.3	10.8	5.9
1600	82.3	11.4	6.7
1650	79.1	13.7	7.2
1700	77.3	14.9	7.8

5.2.3 Mechanical/thermo-mechanical properties

Flexural strength was measured at room temperature as well as high temperature (1300 °C) (Figure 5-8). It is observed that room temperature flexural strength gradually decreases with sintering temperature. High values of CMOR may be attributed to very low AP of the samples. On the other hand high temperature flexural strength is quite low in the temperature range of 1550-1700 °C. HMOR values vary in the range of 40.57 MPa to 47.09 MPa. The highest HMOR is achieved at 1600 °C [174].

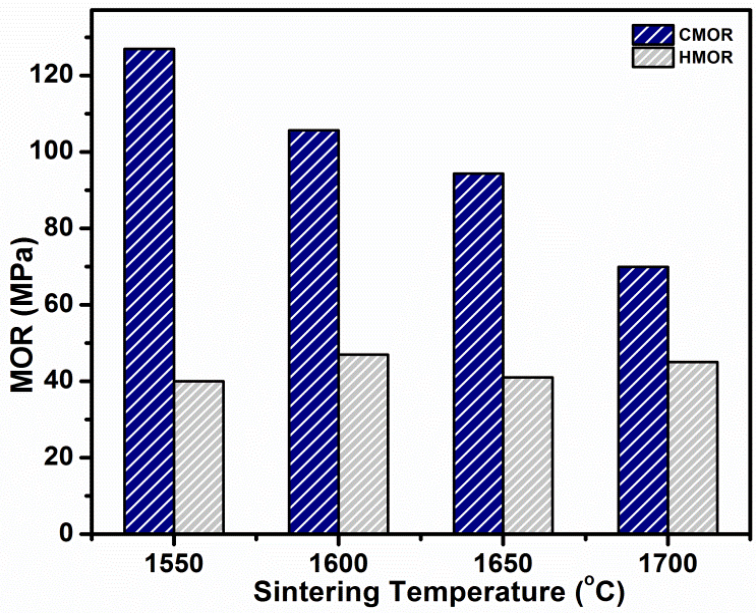

Figure 5-8: Variation in CMOR and HMOR (at 1300 °C) of magnesite samples (M0) as a function of sintering temperature

Thermal shock resistance of the magnesia samples sintered at different temperatures is depicted in Figure 5-9. It is evident from the graph that retained flexural strength gradually decreases with thermal cycle. Samples sintered at 1550 °C show better thermal shock resistance than the other samples which may be because of the presence of lesser amount of monticellite phase at that temperature.

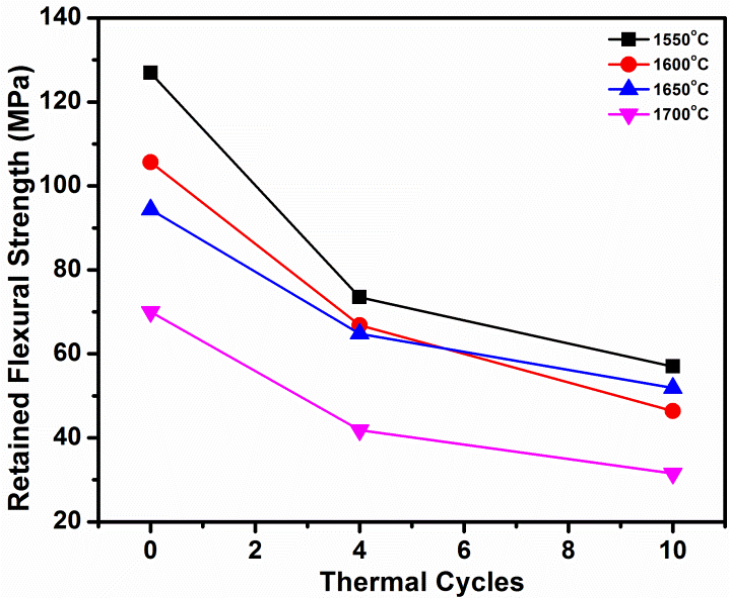

Figure 5-9: Retained flexural strength of magnesite samples (M0) with thermal cycles

5.2.4 Microstructure analysis

FESEM images of magnesite samples sintered at different temperatures are shown in Figure 5-10 (a-d). Substantial amount of liquid phase can be observed in the FESEM images. The main periclase grains are rounded to subrounded in shape. Some smaller grains are also observed all over the matrix. Those grains are later predicted to be forsterite. Another irregular shaped phase along the grain boundaries can be seen in the FESEM images. This phase is monticellite as indicated by EDX analysis.

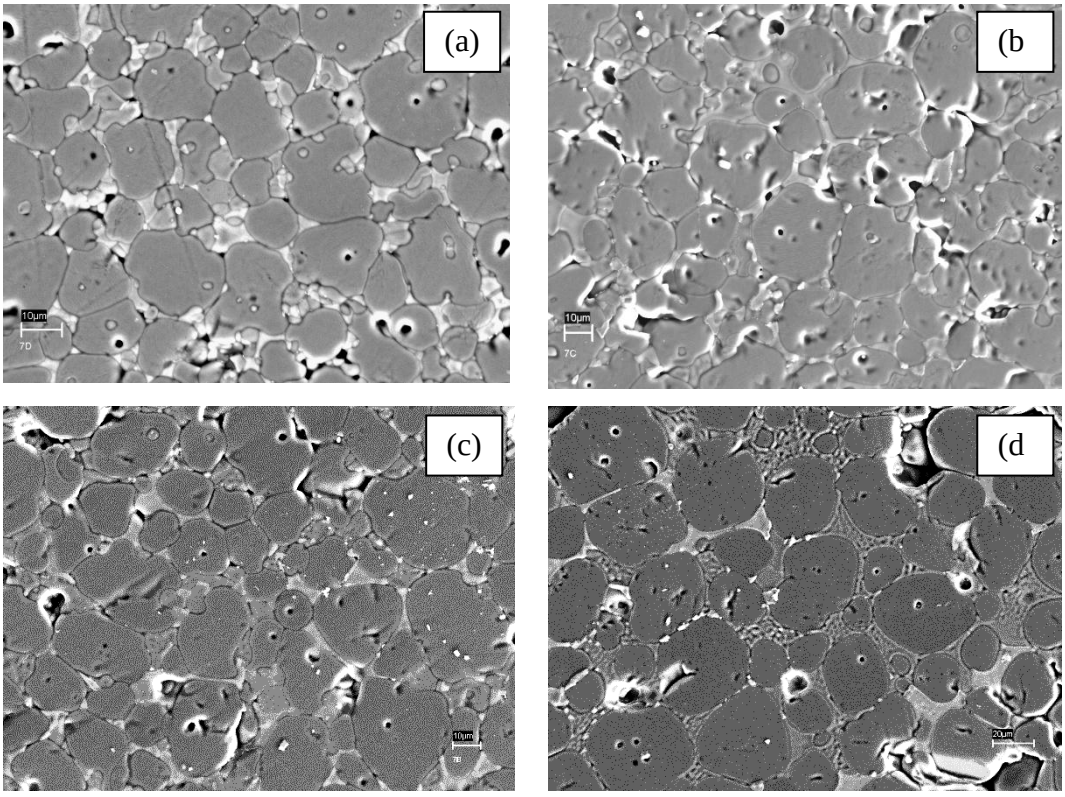

Figure 5-10: FESEM images of magnesite samples (M0) sintered at (a) 1550 °C, (b) 1600 °C, (c) 1650 °C and (d) 1700 °C

Elemental mapping of magnesite sample sintered at 1550 °C is depicted in Figure 5-11. Magnesia grains are present throughout the matrix. Lime is present along the periclase grain boundaries and forms the light colored monticellite phase. Forsterite is mainly present in the intergranular positions. However, silica can be observed in intragranular positions of periclase grains. That predicts the presence of forsterite grains inside periclase grains.

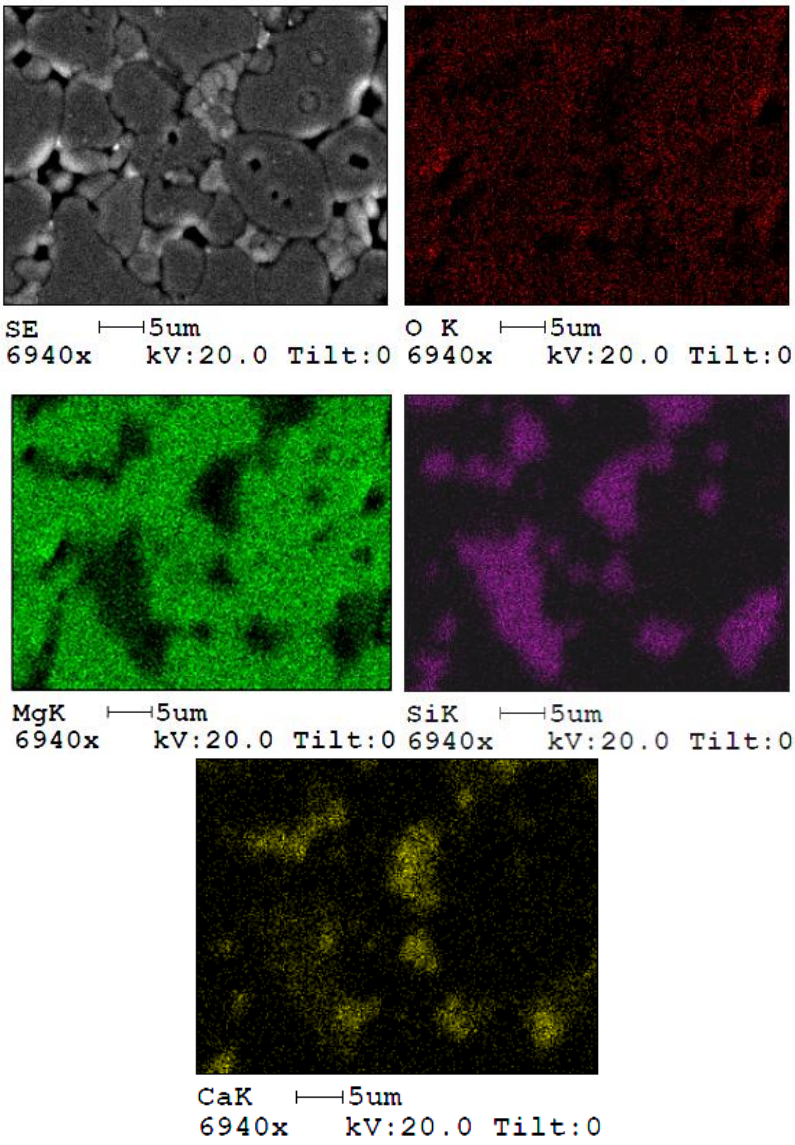

Figure 5-11: Elemental mapping of magnesite sample (M0) sintered at 1550 °C

Line scan of magnesite sample sintered at 1600 °C is shown in Figure 5-12. Quite a high amount of monticellite phase can be observed in the image. Some forsterite grains are also found just beside the periclase grains.

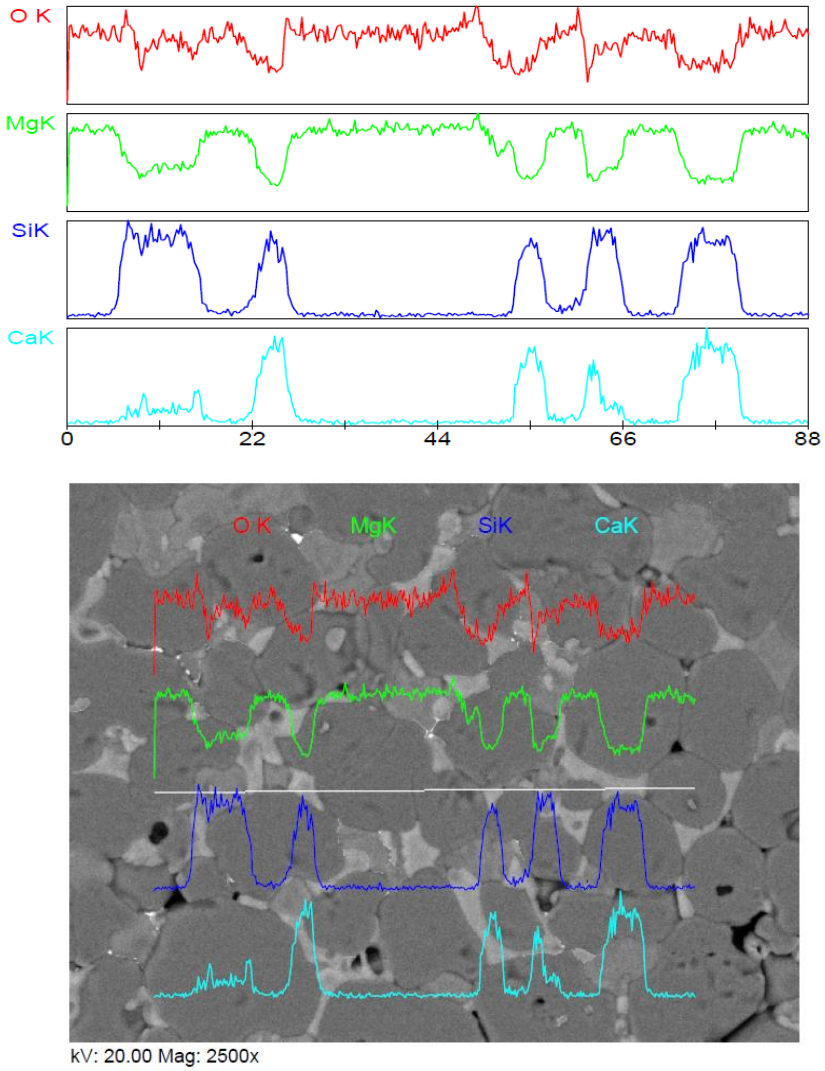

Figure 5-12: Line scan of magnesite sample (M0) sintered at 1600 °C

From the line scan image of magnesite sample sintered at 1650 °C (Figure 5-13) it can be said that the matrix is consisted of mainly magnesia grains and monticellite phase along the grain boundaries. Forsterite grains cannot be observed in this particular image. This means at higher temperature more amount of monticellite is present.

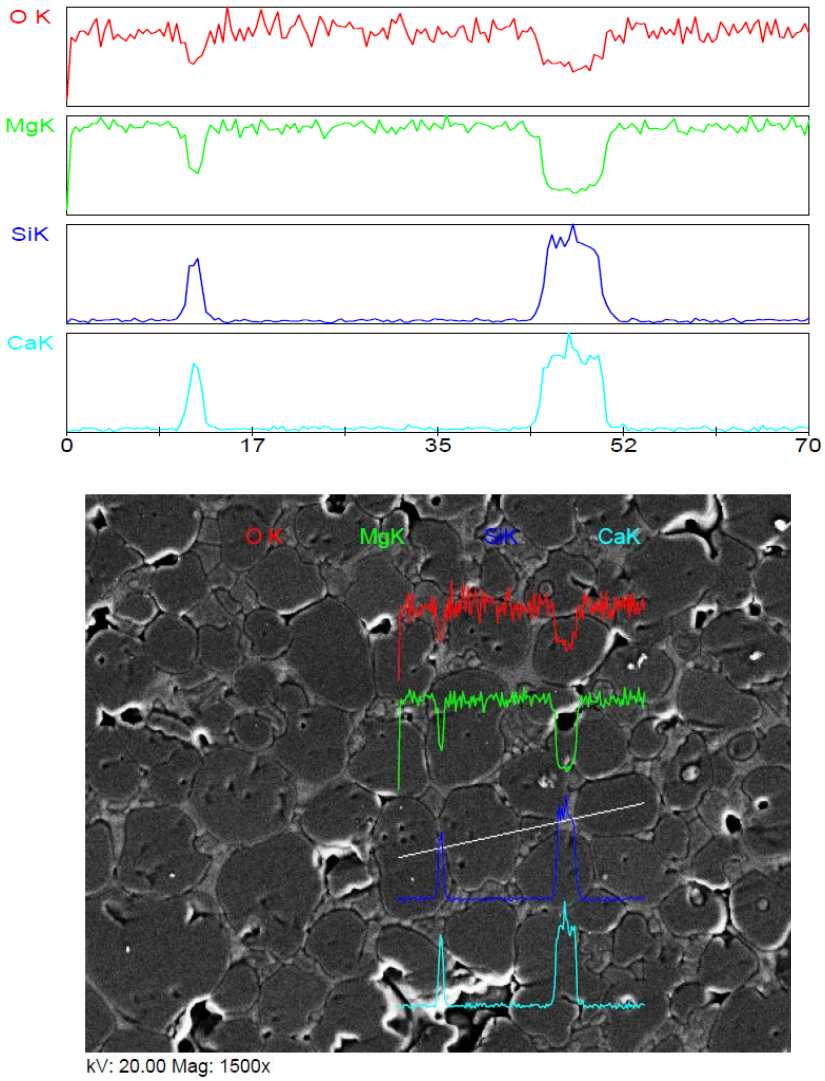

Figure 5-13: Line scan of magnesite sample (M0) sintered at 1650 °C

Figure 5-14 depicts the elemental distribution in the magnesite sample sintered at 1700 °C. Here, the microstructure consists of a textured phase where silica concentration is higher and lime is not present. This textured phase is predicted to be forsterite. On the other hand, monticellite is observed as the irregular shaped phase present along the grain boundaries as seen in the previous EDX analysis images.

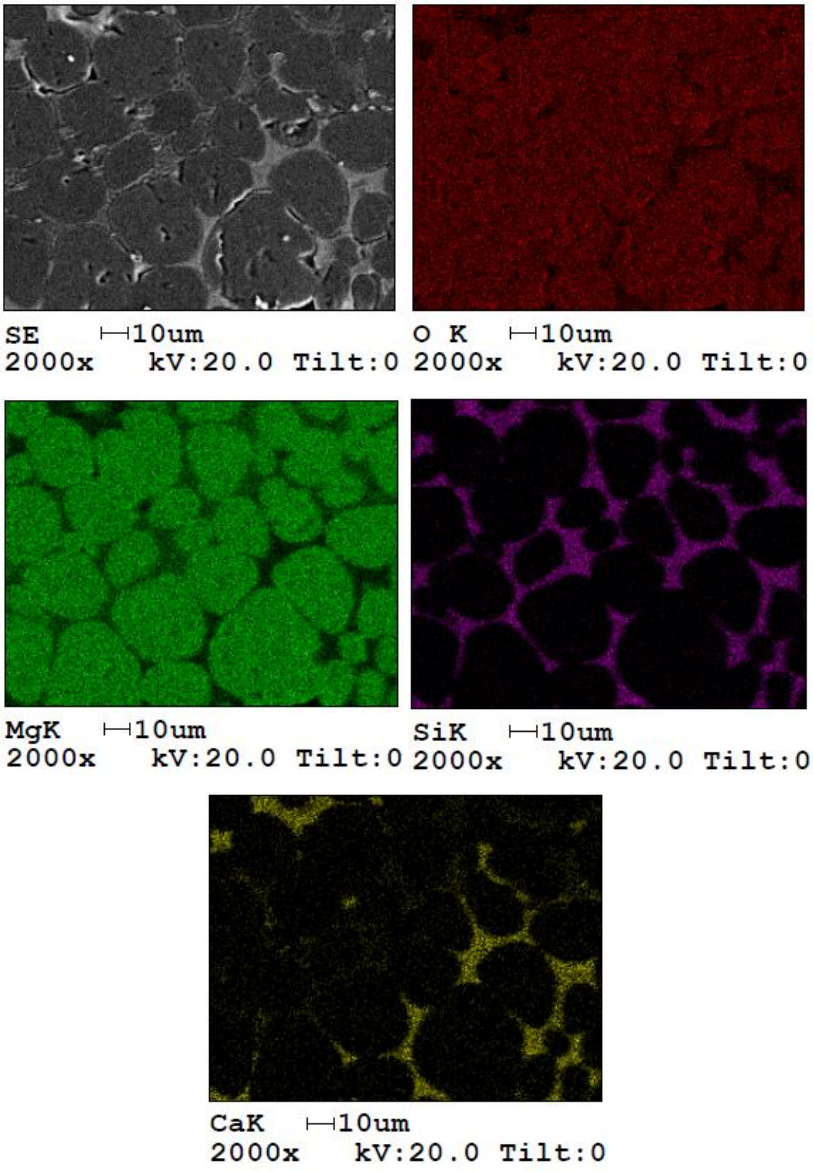

Figure 5-14: Elemental mapping of magnesite sample (M0) sintered at 1700 °C

Methodology 1

(Controlling the high temperature phase formation by changing the lime/silica ratio)

- ***Chandrima Ghosh, A. Ghosh, H. S. Tripathi, J. Ghosh, M. K. Haldar, Ceramics International 40 (2014) 16791-98 [174]***

- ***M. K. Haldar, Chandrima Ghosh, A. Ghosh, Journal of Material Science & Chemical Engineering 2 (2014) 1-8 [175]***

5.3 Methodology 1

5.3.1 Densification behavior

Effect of sintering temperature on bulk density and apparent porosity of M1 and M2 samples is depicted in Figure 5-15. It is observed that bulk density slightly increases upto 1650 °C with increasing temperature for both the samples. At 1700 °C there is a small decrease in BD along with a slight increase in AP for M1 samples. AP is <1 % for all the M1 samples irrespective of the sintering temperature. This low apparent porosity may be due to the presence of siliceous liquid phase in M1 samples. M1 samples have AP even lower than M0 samples because in case of M0 samples, high melting forsterite phase is present along with monticellite. However, M1 samples contain only monticellite as secondary phase as confirmed by the XRD analysis. However, M2 samples show higher AP than M1 as the amount of liquid phase is reduced when the C/S ratio is 2:1. At 1550 °C M2 samples have the highest AP of 4.3 % which further reduces with sintering temperature due to densification. Later XRD analysis proves that M2 samples contain C_2S phase which is high melting in nature along with some amount of merwinite. Therefore, it can be said that change in phase assemblage have increased the AP of the M2 samples [174, 175].

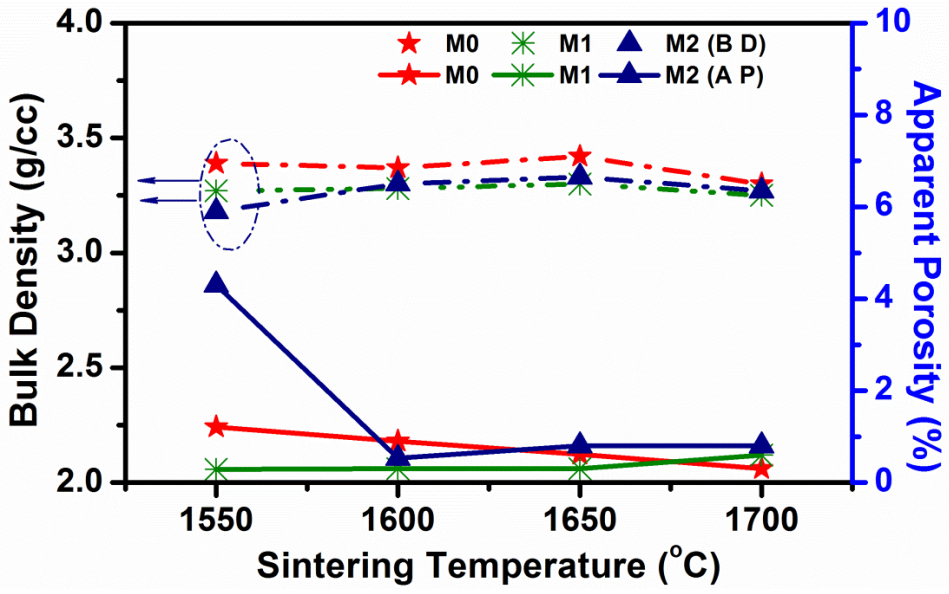

Figure 5-15: Variation in bulk density and apparent porosity of M0 (as received), M1 (C/S ratio 1:1) and M2 (C/S ratio 2:1) samples as a function of sintering temperature

5.3.2 Phase analysis

Figure 5-16 and Figure 5-17 show the XRD pattern of M1 & M2 samples sintered at different temperatures respectively. In case of both M1 and M2 samples, periclase is the major crystalline phase; however, the minor phases are different for M1 and M2 batch samples. In M1 samples, the only minor phase present is monticellite whereas M2 samples contain dicalcium silicate (C_2S) and merwinite as minor phases. C_2S is the phase that we have aimed for because it has a very high melting point (~2100 °C). From the CaO-MgO-SiO_2 phase diagram it is evident that the formation of silicate phase changes depending on the CaO/SiO_2 ratio. When the ratio is in between 0 and 1, monticellite and forsterite phases are formed. Between C/S ratio 1.5 and 2, dicalcium silicate and merwinite phases are formed. Therefore it can be concluded that the findings of this research are in good agreement with other research works.

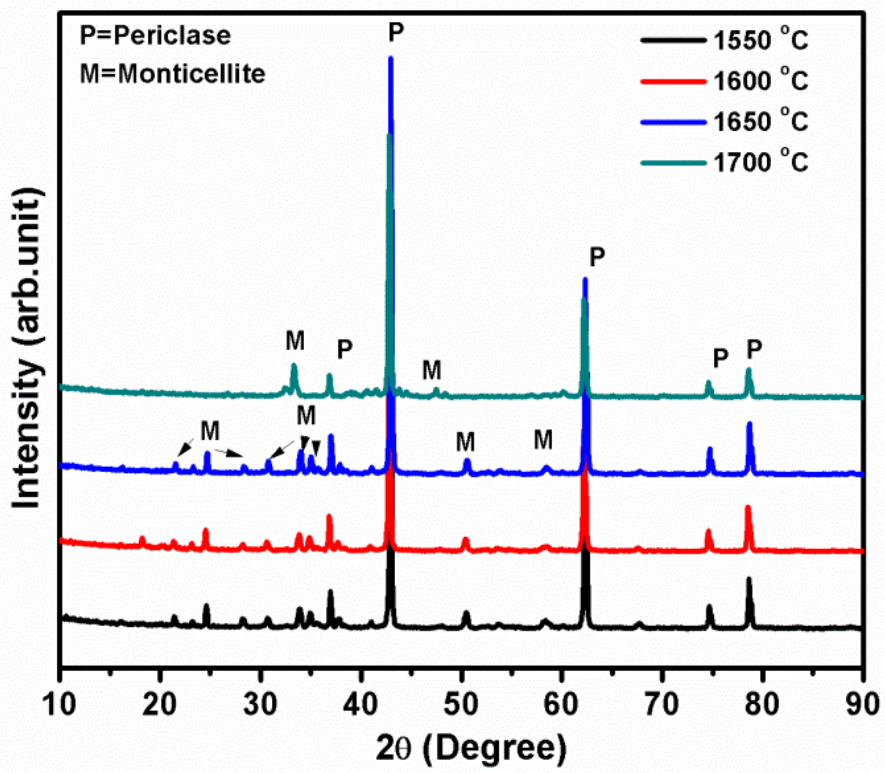

Figure 5-16: XRD pattern of M1 samples (C/S ratio 1:1) sintered in the temperature range of 1550-1700 °C

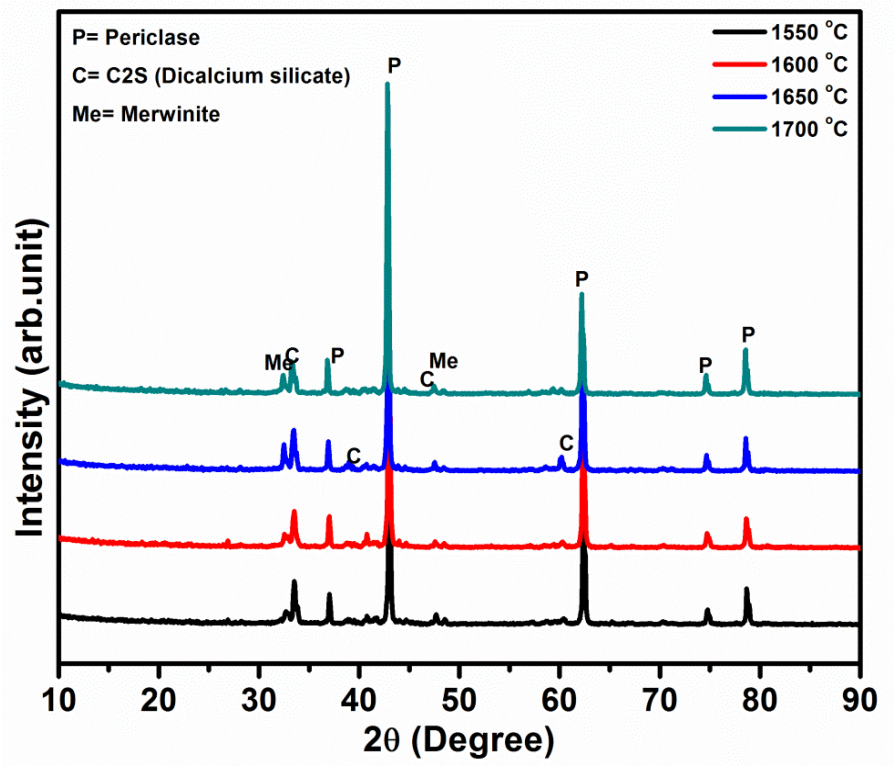

Figure 5-17: XRD pattern of M2 samples (C/S ratio 2:1) sintered in the temperature range of 1550-1700 °C

Quantification of the crystalline phases present in M1 and M2 samples was done by Rietveld refinement method and the results are shown in Table 5-3 and Table 5-4 respectively. Quantification of the crystalline phases developed in the temperature range of 1550-1700 °C in case of M1 samples displays that changing the C/S ratio into 1:1 has an adverse effect on the high temperature phase development as very high amount of monticellite is found in these samples.

Table 5-3: Quantification of the crystalline phases of M1 samples (C/S ratio 1:1) sintered at different temperatures

Sintering temperature (°C)	Crystalline phases (%)	
	Periclase	Monticellite
1550	79.3	20.7
1600	75.7	24.3
1650	74.6	25.4
1700	71.6	28.4

Table 5-4 shows that change in the C/S ratio into 2:1 has a positive effect on high temperature phase assemblage. In case of M2 samples, C_2S phase (desirable) is found along with some amount of merwinite [175]. It is also observed that amount of C_2S phase increases with sintering temperature upto 1650 °C. However, periclase content is low in these samples due to the reduction in initial magnesite content with addition of $CaCO_3$.

Table 5-4: Quantification of the crystalline phases of M2 samples (C/S ratio 2:1) sintered at different temperatures

Sintering temperature (°C)	Crystalline phases (%)	
	Periclase	C_2S
1550	65.9	12.6
1600	71.8	14.8
1650	74.6	15.1
1700	76.4	12.2

5.3.3 Mechanical/thermo-mechanical properties

Figure 5-18 shows the effect of sintering temperature on flexural strength of M1 samples both at room temperature and at 1300 °C. The highest CMOR and HMOR are achieved at 1550 °C. Further increase in the sintering temperature reduces the flexural strength except for samples sintered at 1650 °C.

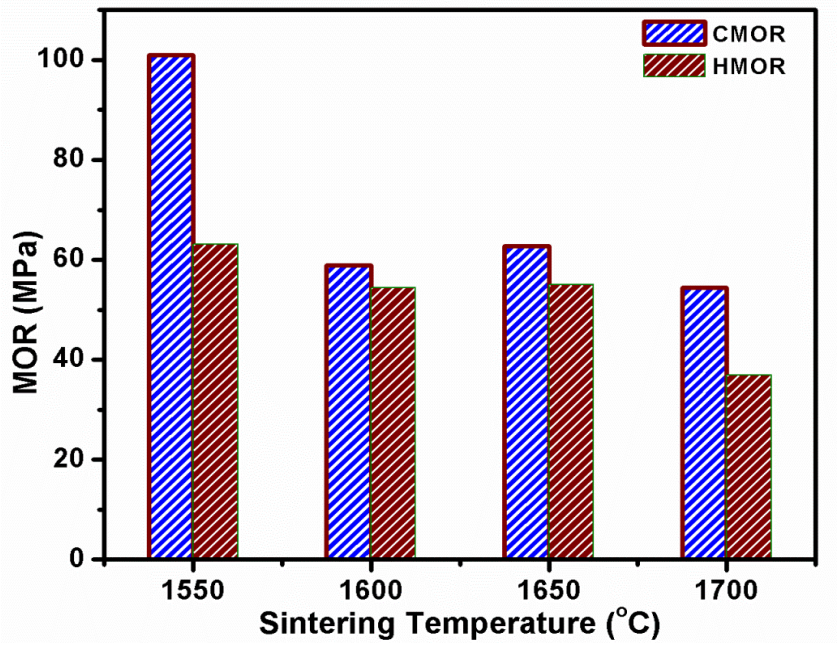

Figure 5-18: Variation in CMOR and HMOR (at 1300 °C) of M1 samples as a function of sintering temperature

In case of M2 samples, flexural strength gradually increases with sintering temperature upto 1650 °C and then decreases at 1700 °C (Figure 5-19). Samples sintered at 1650 °C also perform better than the samples sintered at other temperatures in HMOR test. This is possibly because of the presence of higher amount of C_2S phase at 1650 °C as found in XRD phase quantification.

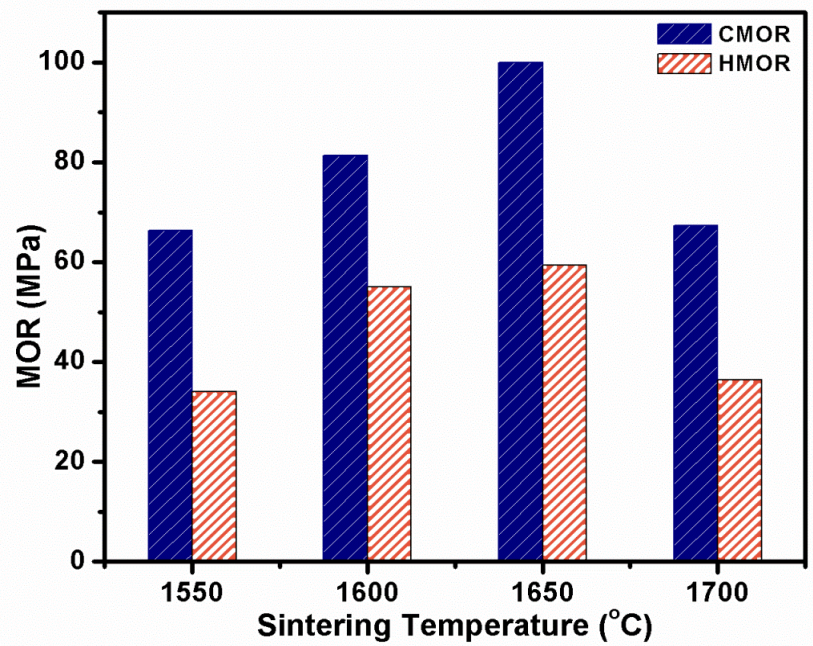

Figure 5-19: Variation in CMOR and HMOR (at 1300 °C) of M2 samples (C/S ratio 2:1) as a function of sintering temperature

Figure 5-20 shows the retained flexural strength after thermal shock for M1 samples. Flexural strength gradually decreases from 0 to 10th cycle for all the samples except for the samples sintered at 1600 °C, where there is a slight increase in strength from 0 to 4th cycle of thermal shock. Samples sintered at 1550 °C show better resistance to thermal shock than the other batches.

The pattern of retained flexural strength is similar in case of M2 samples also (Figure 5-21). Here too retained flexural strength gradually decreases with thermal cycle except for samples sintered at 1550 °C. M2 samples sintered at 1550 °C gained some amount of strength after 4th cycle of thermal shock. These cases of initial strengthening during thermal shock in case of both M1 and M2 samples may be attributed to tempering [176-178].

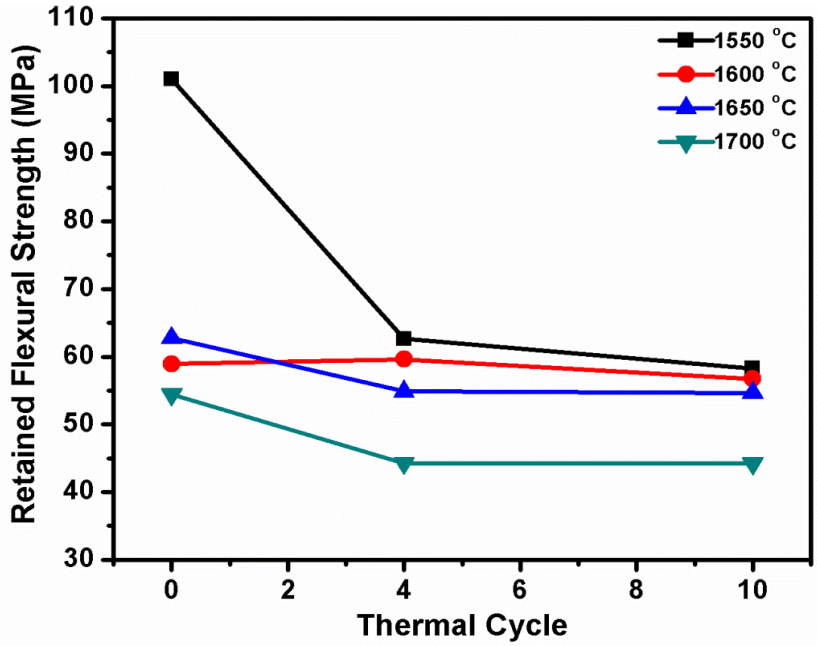

Figure 5-20: Retained flexural strength of M1 samples (C/S ratio 1:1) with thermal cycle

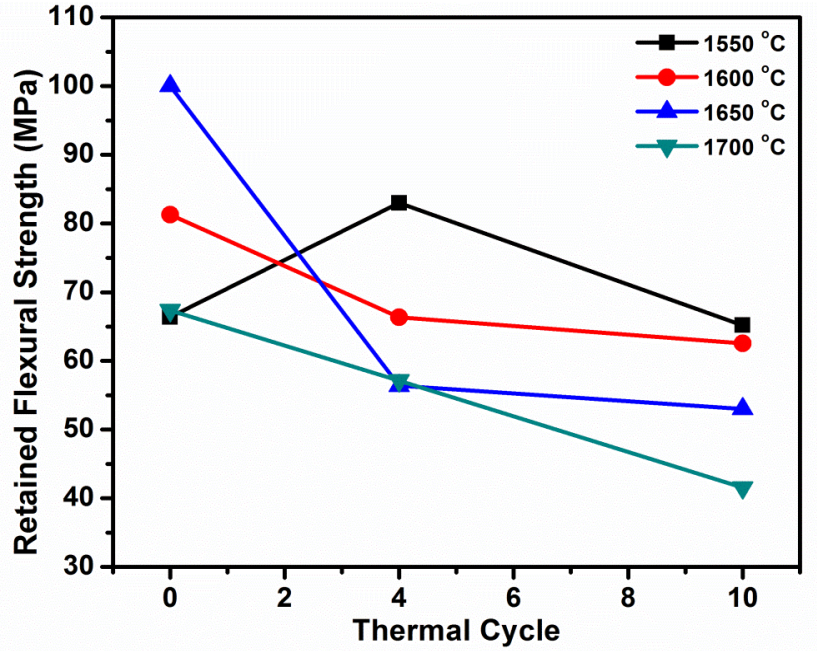

Figure 5-21: Retained flexural strength of M2 samples (C/S ratio 2:1) with thermal cycle

5.3.4 Microstructure analysis

Figure 5-22 and Figure 5-23 show the FESEM images of M1 and M2 samples sintered at different temperatures. In case of M1 samples, two distinct types of phases could be seen from the FESEM images; the dark periclase grains and the surrounding liquid siliceous phase. Periclase are round in shape because the matrix consists of substantial amount of liquid phase. The presence of high amount of liquid phase results in quite high grain growth as can be observed form the FESEM images.

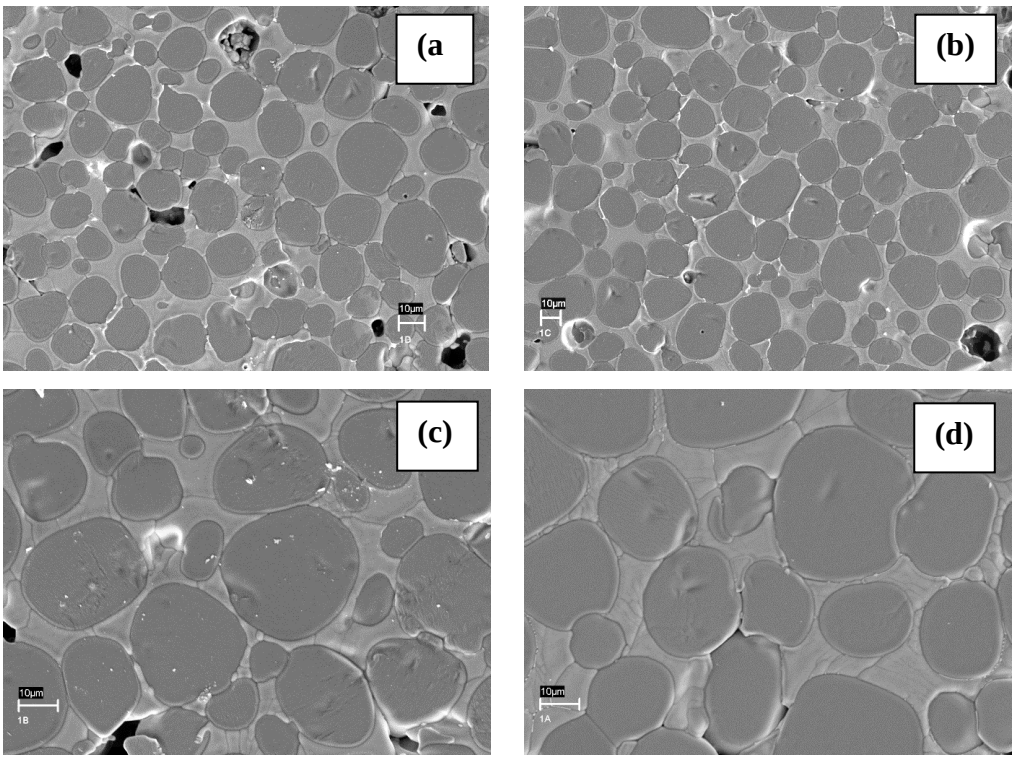

Figure 5-22: FESEM images of M1 samples (C/S ratio 1:1) sintered at (a) 1550 °C, (b) 1600 °C, (c) 1650 °C and (d) 1700 °C

Microstructure of M2 samples reveals that it consists of periclase grains with two bonding phases (Figure 5-23). Periclase grains are less rounded in shape as compared to M1 batch because of the presence of lower amount of liquid phase. Better grain to grain contact is observed in case of samples sintered at 1550 °C. Grain growth is not as pronounced as M1 batch.

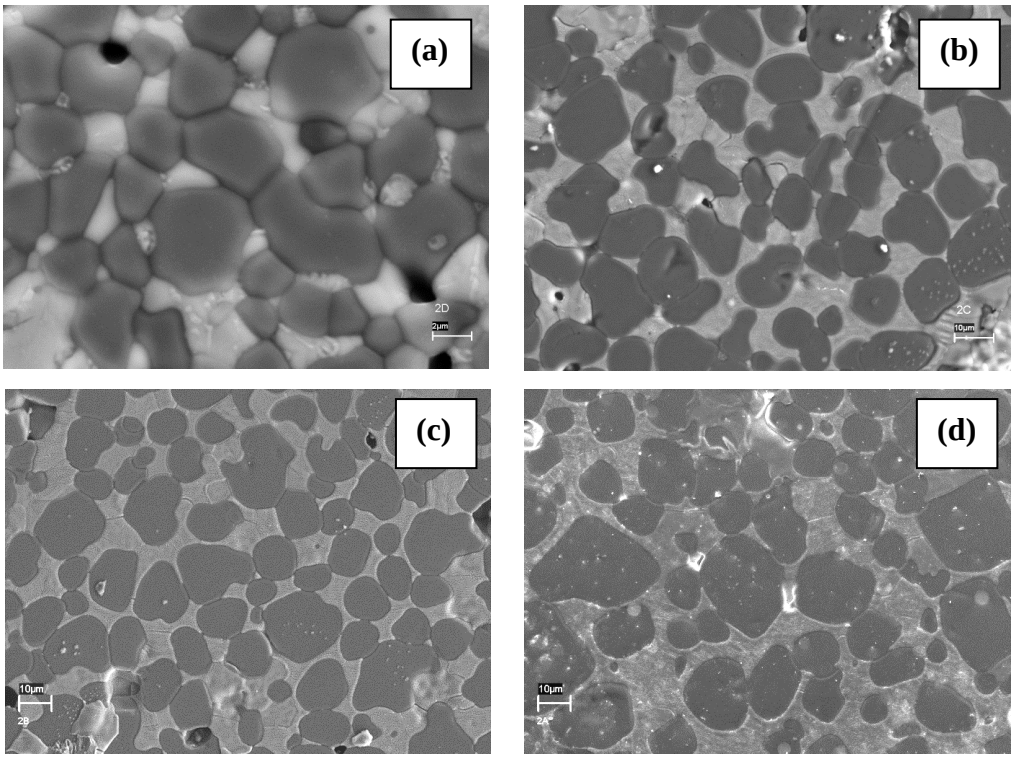

Figure 5-23: FESEM images of M2 samples (C/S ratio 2:1) sintered at (a) 1550 °C, (b) 1600 °C, (c) 1650 °C and (d) 1700 °C

Figure 5-24 shows the elemental distribution in the matrix of M1 sample sintered at 1550 °C. Presence of lime and silica is observed in the matrix along the grain boundaries. Similar results are found in EDX study of M1 samples sintered at 1600 °C (Figure 5-25), 1650 °C (Figure 5-26) and 1700 °C (Figure 5-27). The findings corroborate the findings of XRD analysis where monticellite was the only secondary phase found along with periclase. Therefore, it can be concluded that in the temperature range of 1550-1700 °C, periclase and monticellite phase are developed in M1 samples. The microstructure consists of rounded grains which are periclase and the matrix phase which is the low melting siliceous phase monticellite.

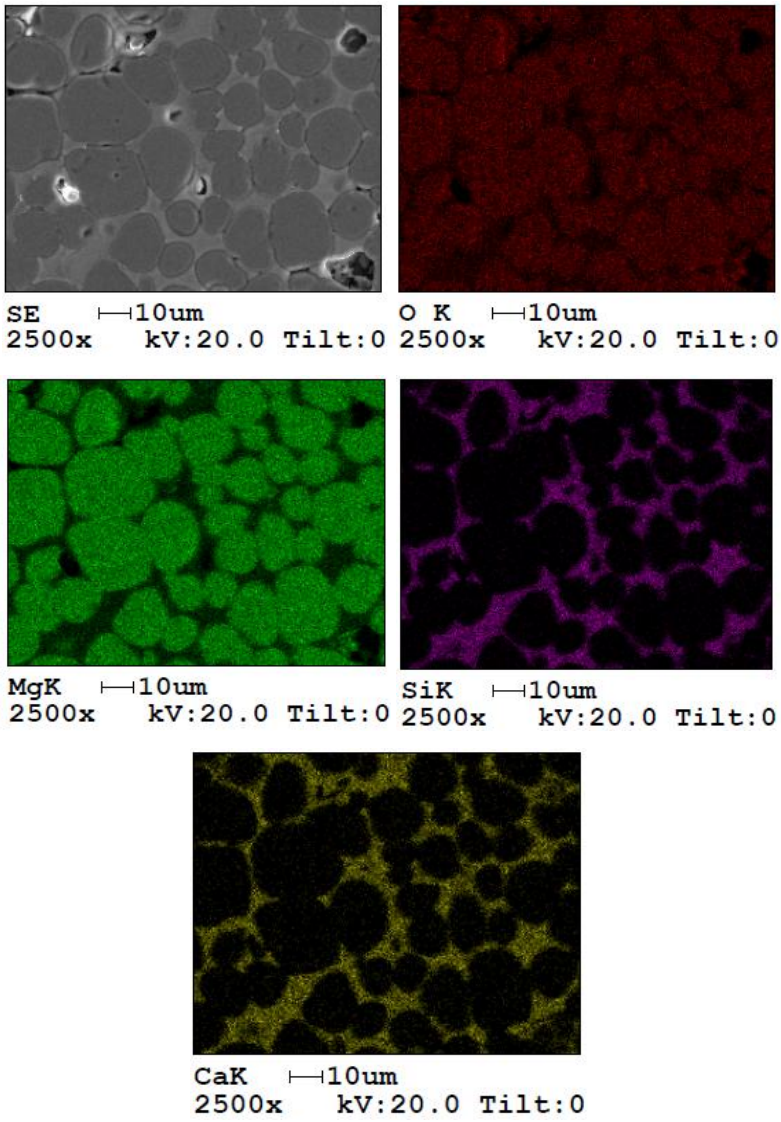

Figure 5-24: Elemental mapping of M1 sample (C/S ratio 1:1) sintered at 1550 °C

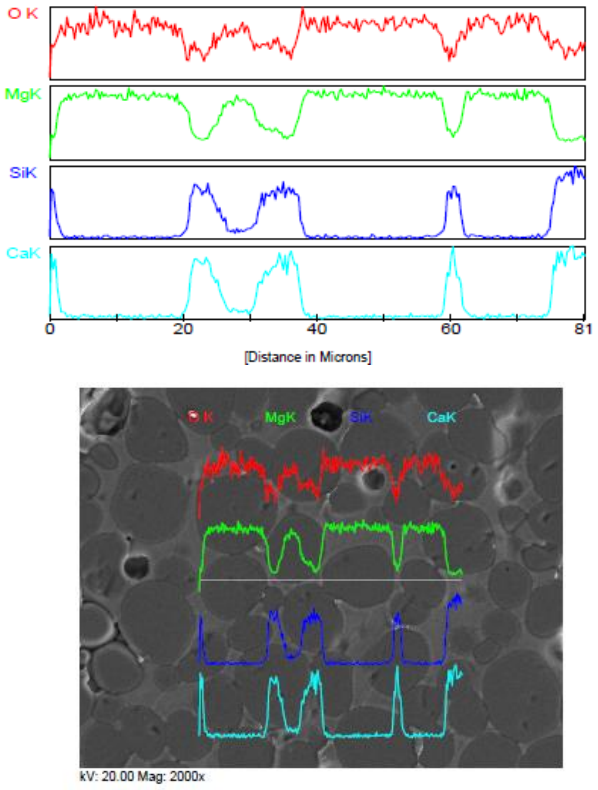

Figure 5-25: Line scan of M1 sample (C/S ratio 1:1) sintered at 1600 °C

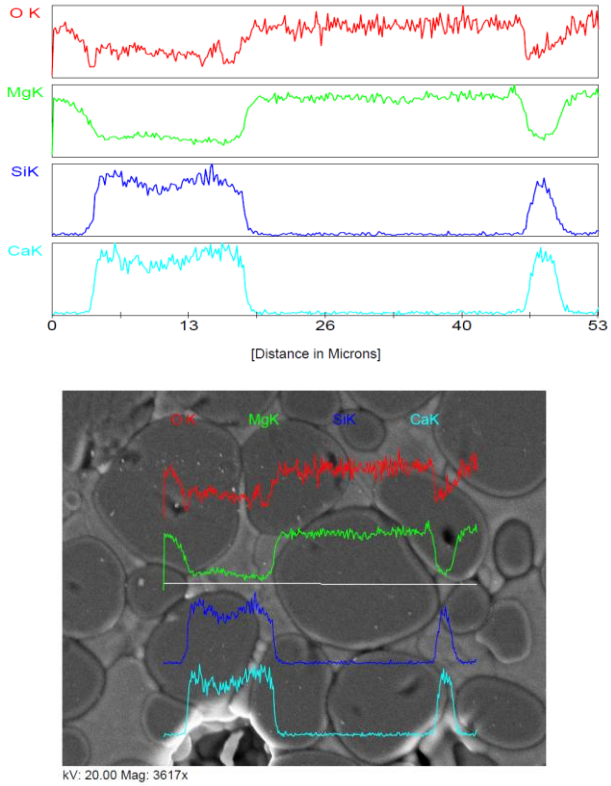

Figure 5-26: Line scan of M1 sample (C/S ratio 1:1) sintered at 1650 °C

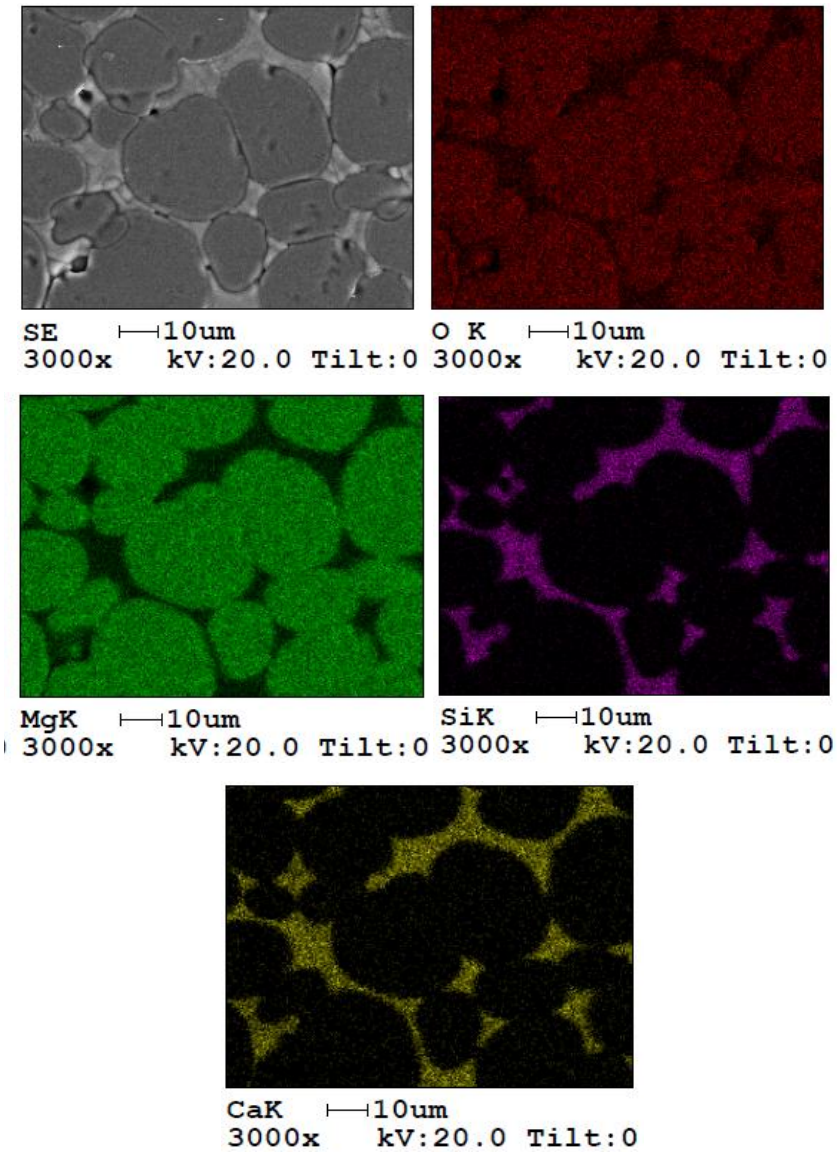

Figure 5-27: Elemental mapping of M1 sample (C/S ratio 1:1) sintered at 1700 °C

EDX analysis of M2 samples sintered at different temperatures are shown in Figure 5-28 (1550 °C), Figure 5-29 (1600 °C), Figure 5-30 (1650 °C) and Figure 5-31(1700 °C). As earlier confirmed by the XRD study, it contains two types of siliceous phases in the matrix (Figure 5-28); one containing lime, silica and magnesia (merwinite) and another containing only lime and silica (C_2S). However, it is observed that with increasing sintering temperature the amount of lime and silica containing phase is incresaed in the microstructre. Elemental distribution shows only silica and lime in the matrix phase (Figure 5-29). Line scan image (Figure 5-30) depicts that the matrix is mainly consisted of lime and silica containg phase with a little amount of a second phase which contains magnesia, lime and silica. Line scan analysis of M2 sample sintered at 1700 °C (Figure 5-31) exhibits slightly higher amount of merwinite along with C_2S and periclase.

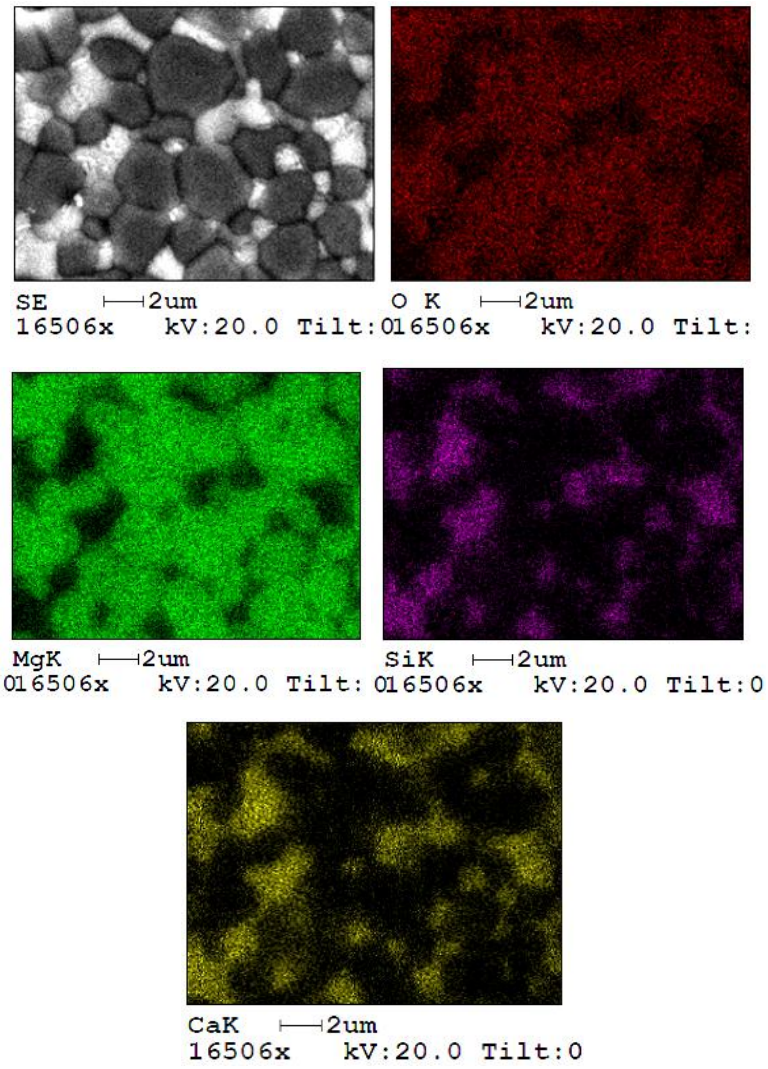

Figure 5-28: Elemental mapping of M2 sample (C/S ratio 2:1) sintered at 1550 °C

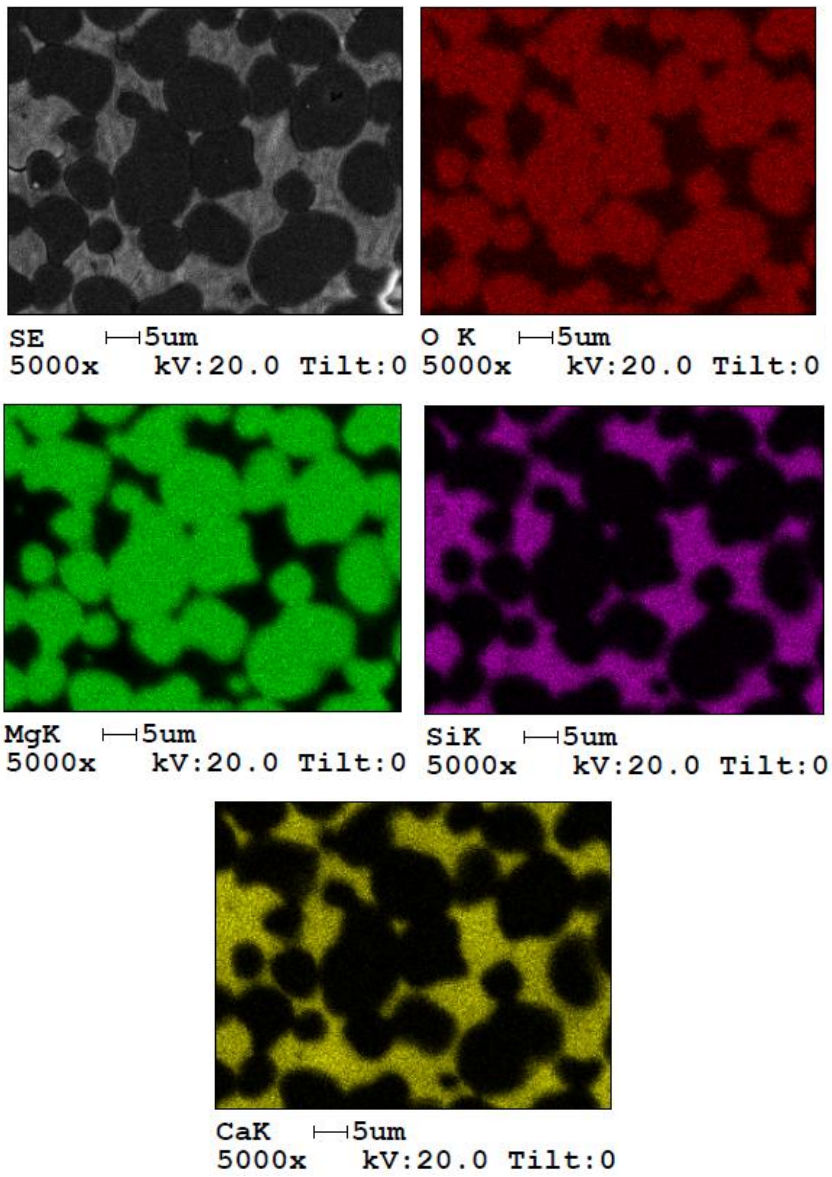

Figure 5-29: Elemental mapping of M2 sample (C/S ratio 2:1) sintered at 1600 °C

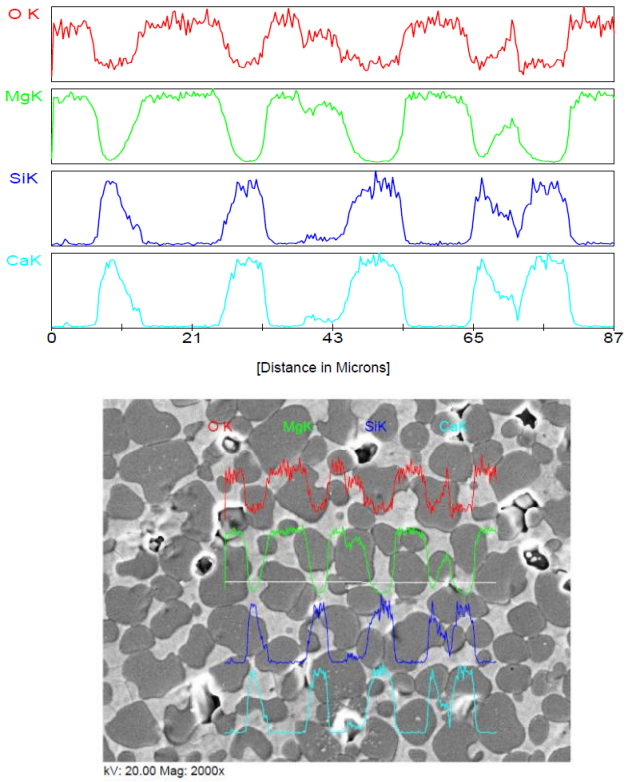

Figure 5-30: Line scan of M2 sample (C/S ratio 2:1) sintered at 1650 °C

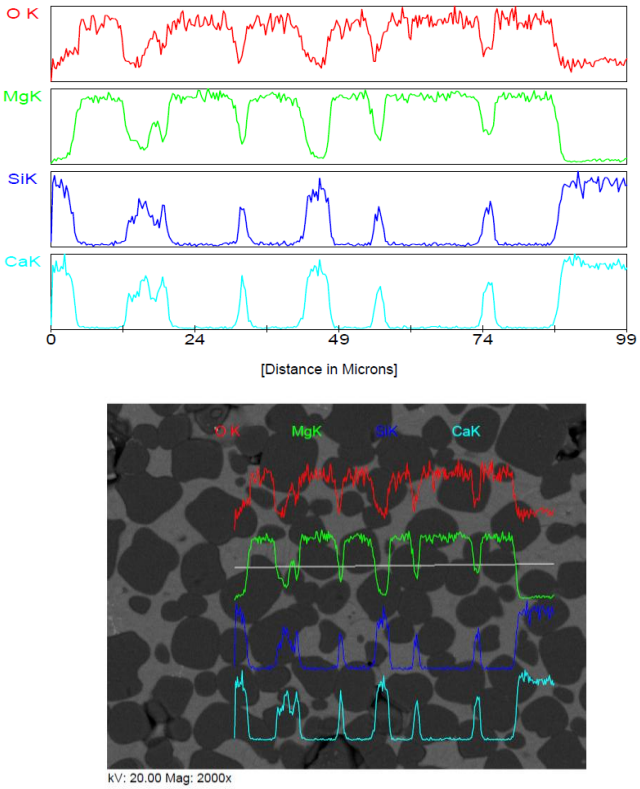

Figure 5-31: Line scan of M2 sample (C/S ratio 2:1) sintered at 1700 °C

5.3.5 Summary

- $CaCO_3$ is added to Indian natural magnesite to change the C/S ratio thereby modifying the high temperature phase assemblage to improve the thermo-mechanical properties.
- It is observed that high temperature phase formation is altered with changing C/S ratio.
- The samples having C/S ratio 1:1, contain high amount of monticellite phase which deteriorate the thermo-mechanical properties.
- C/S ratio of 2:1 has a positive impact on high temperature phase development as C_2S phase is found in good quantity in XRD analysis.
- Presence of C_2S phase improves the high temperature properties of the samples.

Methodology 2

(Controlling the high temperature phase formation by adding zirconia)

- ***Chandrima Ghosh, S. Sinhamahapatra, H. S. Tripathi, International Journal of Applied Ceramic Technology 16 (2019) 410-417) [172]***

5.4 Methodology 2

5.4.1 Densification behavior

Variation in apparent porosity and bulk density of different batches sintered at different temperatures is shown in Figure 5-32 and Figure 5-33 respectively. It is observed that apparent porosity of the samples without zirconia (MZ0) gradually decreases with increase in sintering temperature. MZ0 samples have very low apparent porosity throughout the entire sintering temperature range of 1550-1700 °C. Addition of zirconia increases the apparent porosity of the samples. In contrary to MZ0 sample, apparent porosity of zirconia containing samples increases with increase in sintering temperature. Lower apparent porosity of MZ0 samples may be attributed to the presence of higher amount of low melting phases in the sample at high temperatures. On the other hand, higher apparent porosity of the zirconia containing samples may be due to the fact that zirconia addition reduces the amount of low melting phase which is otherwise present in the sintered samples. Zirconia may react with some of the impurities present in the magnesite and forms new phases or it may utilize these impurities for its stabilization and thereby restricts the amount of low meting phases in the samples. This can be confirmed by the phase analysis of these samples by XRD. Also zirconia being a refractory material hinders the densification of the sample.

It is also observed that bulk density of the samples increases after adding zirconia which may be attributed to the higher density of zirconia (5.83 g/cc). Slight reduction in the bulk density for MZ1 and MZ3 samples with increasing sintering temperature is observed which is due to higher apparent porosity of the samples at high temperatures. MZ5 samples have almost constant bulk density throughout the sintering temperature range. In this case, higher density of zirconia circumvents the effect of higher apparent porosity of the samples.

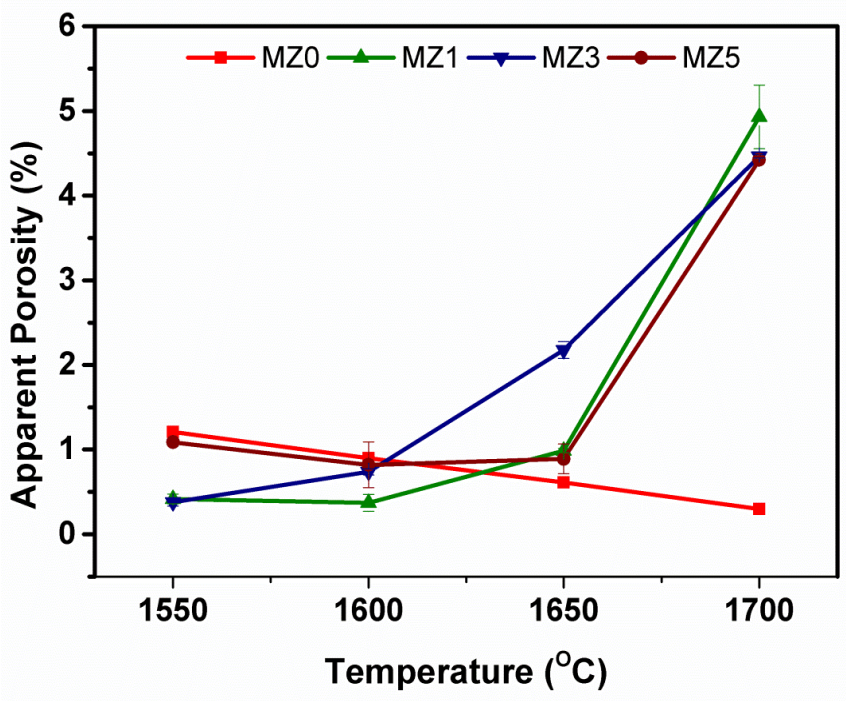

Figure 5-32: Variation in apparent porosity of the samples with sintering temperature and zirconia content

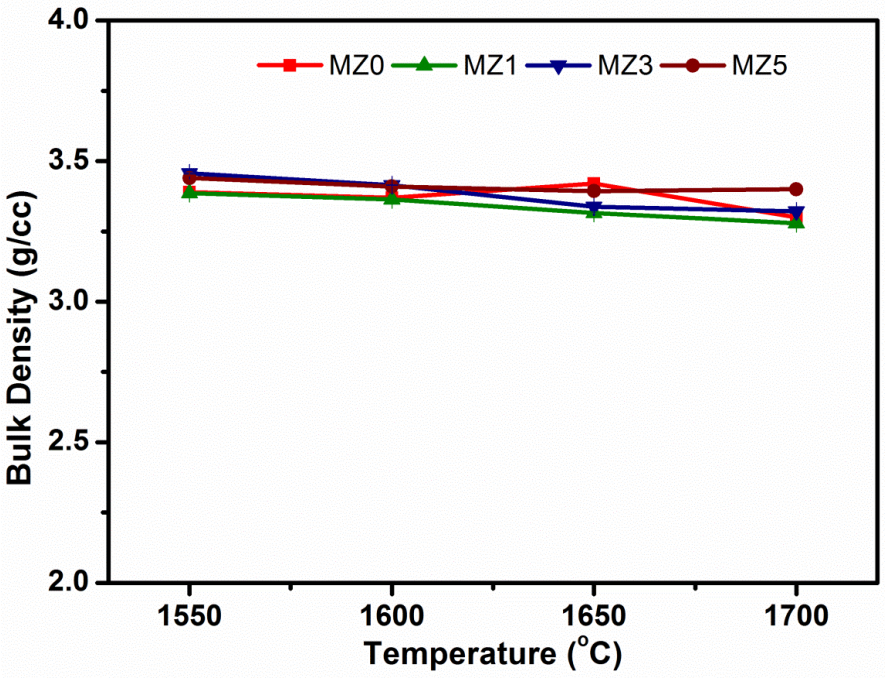

Figure 5-33: Variation in bulk density of the samples with sintering temperature and zirconia content

5.4.2 Phase analysis

XRD patterns of the samples sintered at 1600 °C having different zirconia content are depicted in Figure 5-34. It is observed that the main crystalline phase is periclase with zirconia (tetragonal), forsterite and monticellite as secondary phases. It is evident from the phase identification study that zirconia does not react with silica or lime rather it transforms into tetragonal zirconia from monoclinic in presence of magnesia and lime. Tetragonal form of zirconia is not generally stable at room temperature unless it uses some stabilizers like lime or magnesia which helps in tetragonal phase stabilization of zirconia at room temperature.

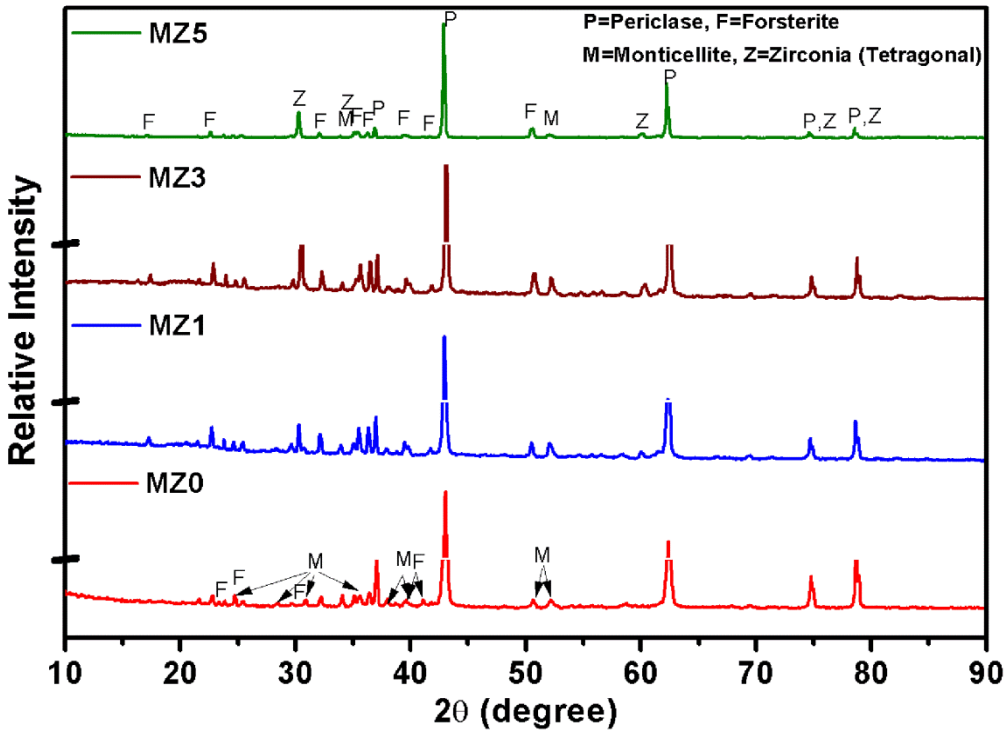

Figure 5-34: Phase development of samples sintered at 1600 °C with different zirconia content [172]

Quantification result of the crystalline phases is presented in Table 5-5. It is clear from the data that amount of monticellite is reduced with zirconia addition. Initially in the as received samples the amount of monticellite was 6.7 % which is reduced to 5.7 % in MZ1, 4.8 % in MZ3 and 3.6 % in case of MZ5 samples. It is also observed that the amount of periclase is reduced after zirconia addition. Moreover the amount of forsterite phase is increased in zirconia containing samples. However, in case of MZ5 samples, there is an

increase in the amount of periclase phase which may be due to the fact that the amount of forsterite is reduced in MZ5. Therefore, from the XRD study it can be concluded that monoclinic zirconia addition to Indian low grade magnesite reduces the amount of low melting monticellite phase formation as monoclinic zirconia uses lime to stabilize its tetragonal form at room temperature.

Table 5-5: Quantification of the crystalline phases of the samples sintered at 1600 °C with varying amount of zirconia

Samples	Amount of Crystalline Phases (%)			
	Periclase (P)	Monticellite (M)	Forsterite (F)	Tetragonal Zirconia (Z)
MZ0	82.3	6.7	11.4	0
MZ1	57.6	5.7	35.4	1.2
MZ3	57.9	4.8	33.8	3.5
MZ5	67.6	3.6	23.6	5.2

5.4.3 Mechanical/thermo-mechanical properties

Effect of zirconia content on room temperature flexural strength of the samples sintered at 1550 °C and 1600 °C is shown in Figure 5-35 and Figure 5-36 respectively. It is observed that in case of samples sintered at 1550 °C, flexural strength remains almost unchanged after 1 wt% zirconia addition. Further 3 wt% zirconia addition results in decrease in the room temperature flexural strength (CMOR). This may be due to the reduction in monticellite content in MZ3 which is a load bearing phase present in higher amount in MZ0 and MZ1 samples. Flexural strength again increases with 5 wt% zirconia addition. This is because zirconia is a load bearing material itself; therefore further increase in the amount of zirconia increases the flexural strength [172].

In case of all the samples sintered at 1600 °C, flexural strength is lower than that of 1550 °C. This decrease in strength may be attributed to increase in the grain size of the samples. Grain growth results in decrease in the amount of grain boundaries. In case of room temperature flexural strength, the applied load is distributed through grain boundaries. Therefore, CMOR value decreases with increasing grain size. It is also observed that with gradual increase in zirconia content, flexural strength decreases. However, again in case of MZ5 samples, there is an increase in strength as seen earlier in case of the samples sintered at 1550 °C. The reason behind this phenomenon is the same as stated earlier.

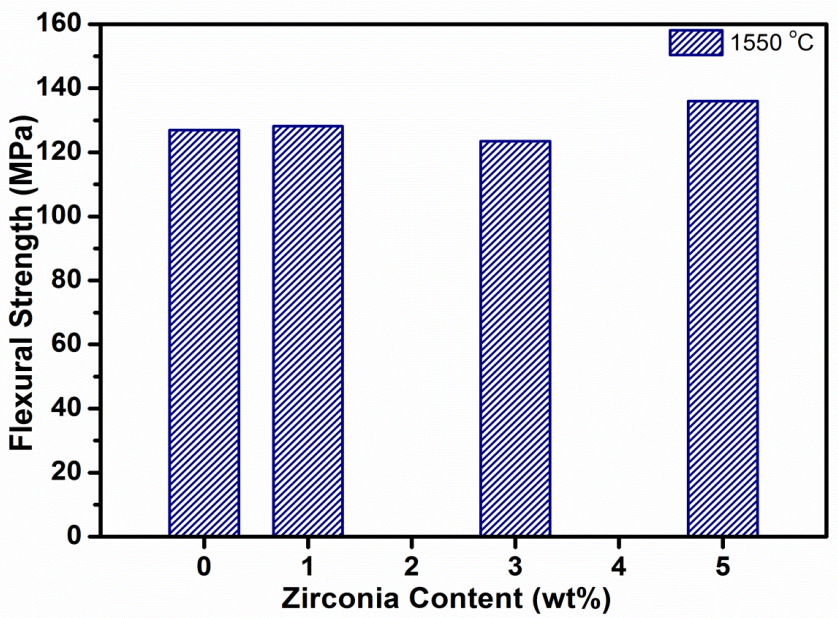

Figure 5-35: Variation in flexural strength at room temperature with zirconia content of the samples sintered at 1550 °C

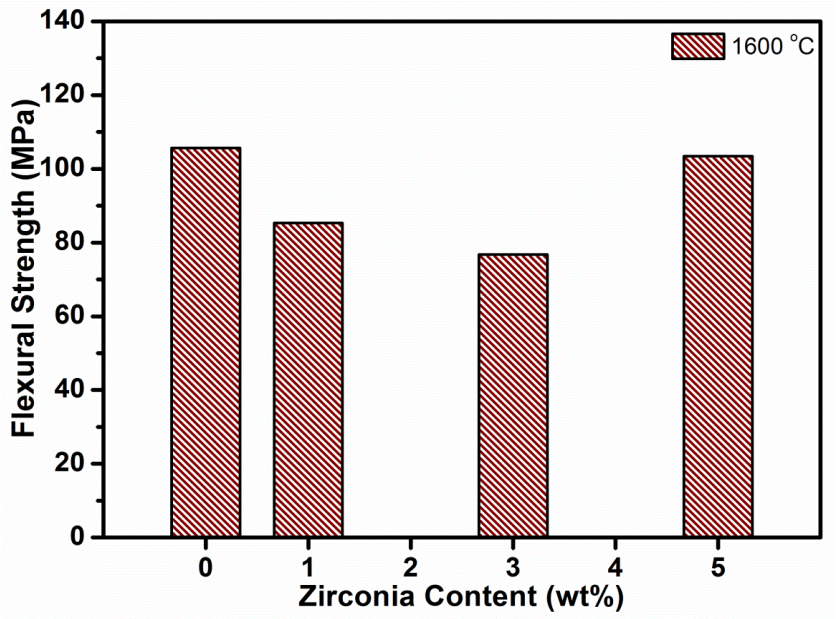

Figure 5-36: Variation in flexural strength at room temperature with zirconia content of the samples sintered at 1600 °C

Thermal shock resistance of the samples sintered at 1550 °C and 1600 °C is depicted in Figure 5-37 and Figure 5-38 respectively. In case of the samples sintered at 1550 °C MZ5 batch samples show the highest retained flexural strength after thermal shock whereas, the samples of MZ1 and MZ3 batch performed poorly in the thermal shock resistance test after

4th cycle of thermal shock. However, again after 10th cycle, they regained some amount of strength which may be attributed to tempering.

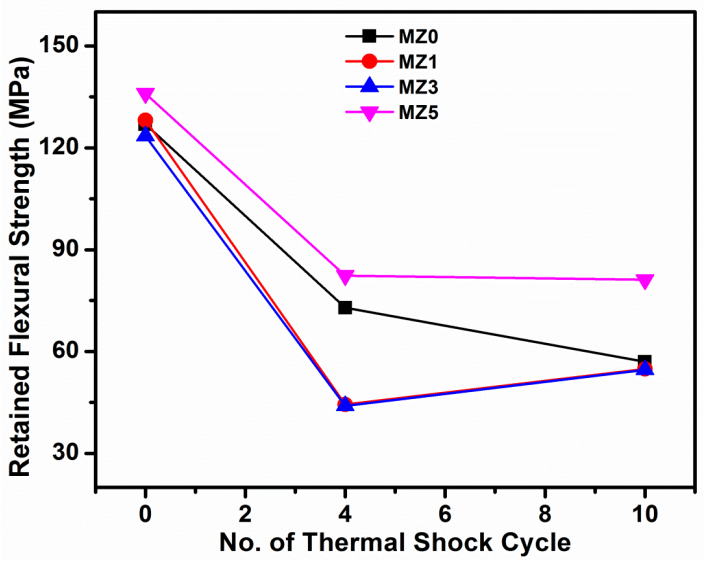

Figure 5-37: Retained flexural strength of the samples sintered at 1550 °C with varying amount of zirconia after different thermal shock cycles

In case of the samples sintered at 1600 °C, it is observed that MZ1 and MZ3 samples mostly keep their flexural strength even after 10th cycle of thermal shock. However, MZ5 samples lose their strength after 10th cycle of thermal shock. This may be because of the generation of higher amount of micro cracks in these samples as they contain higher amount of zirconia.

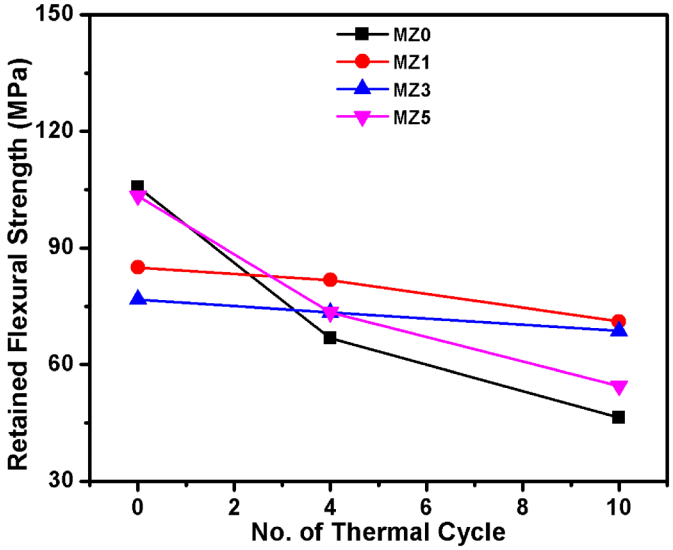

Figure 5-38: Retained flexural strength of the samples sintered at 1600 °C with varying amount of zirconia after different thermal shock cycles [172]

5.4.4 Microstructure analysis

FESEM images of thermally etched samples sintered at 1550 °C and 1600 °C are shown in Figure 5-39 (a-d) and Figure 5-40 (a-d) respectively. In case of the samples sintered at 1550 °C it is observed that grain size is much smaller for zirconia containing batches than the MZ0 batch. MZ0 batch contains higher amount of low melting phase which may be the main cause of bigger grain size of MZ0 than zirconia containing samples. Zirconia addition reduces the formation of low melting monticellite phase in the samples. As a result the expansion of periclase grains are restricted. With increasing amount of zirconia, monticellite phase formation is reduced. Hence, grain size of the samples gradually decreases with increasing amount of zirconia. Better grain to grain contact is observed with increasing zirconia content.

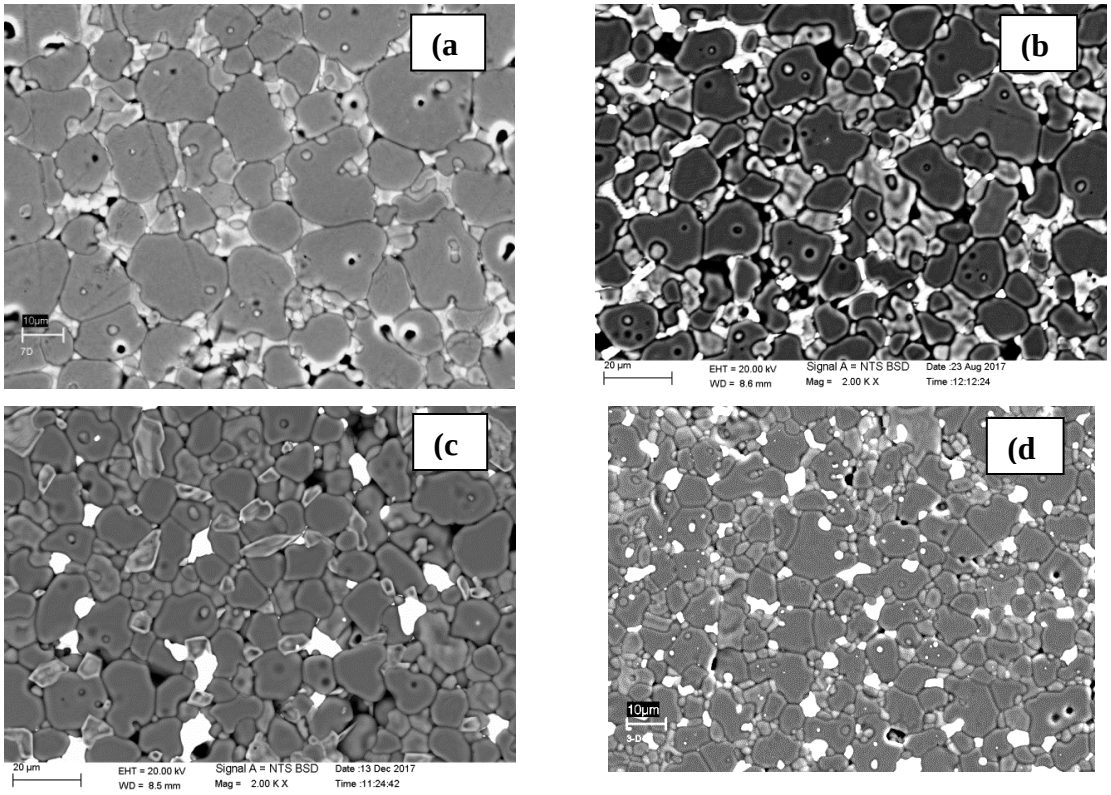

Figure 5-39: FESEM images of (a) MZ0, (b) MZ1, (c) MZ3 and (d) MZ5 samples sintered at 1550 °C

Figure 5-40 (a-d) shows the FESEM images of samples sintered at 1600 °C. It is observed that in case of samples sintered at 1600 °C, microstructural development is same as at 1550 °C. Large, dark periclase grains are present in all the samples along with small grey colored

grains of forsterite. Irregular shaped monticellite phase is present in MZ0 along the grain boundaries. Zirconia is present as bright white colored phase throughout the matrix in intergranular as well as intragranular positions.

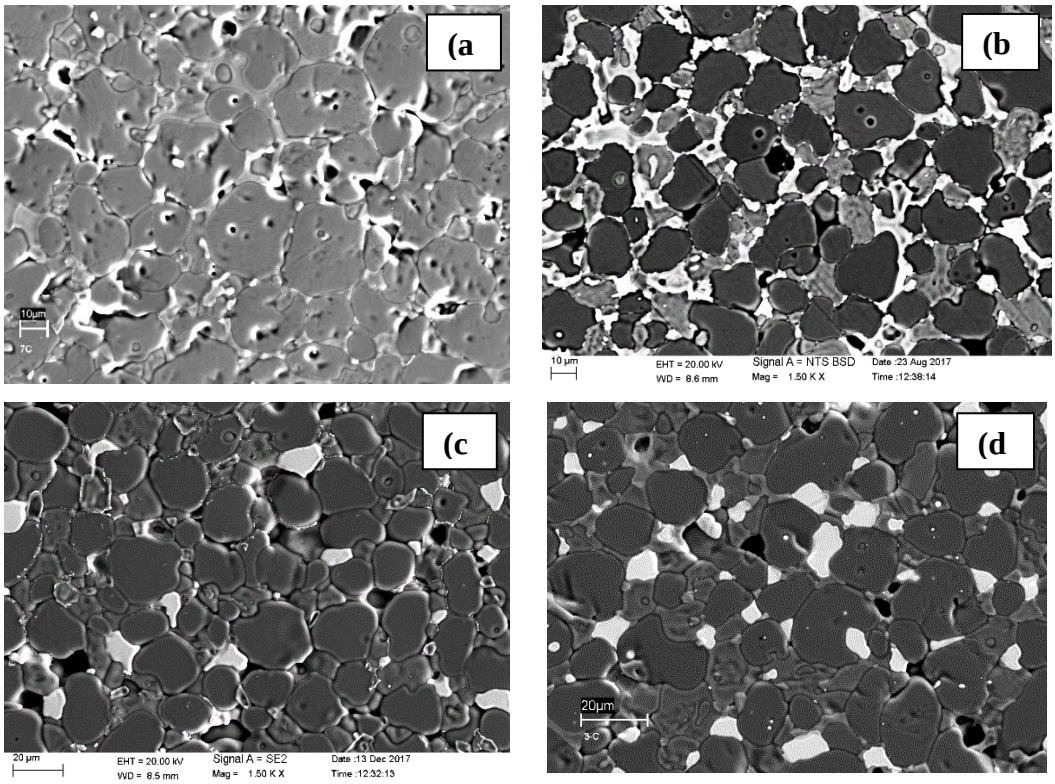

Figure 5-40: FESEM images of (a) MZ0, (b) MZ1, (c) MZ3 and (d) MZ5 samples sintered at 1600 °C

Comparative study of the average grain size of the samples sintered at 1550 °C and 1600 °C is depicted in Figure 5-41. It is evident from grain size analysis that grain growth occurs with increasing sintering temperature for all the samples. Zirconia containing samples have smaller grain size than MZ0 samples. Moreover, increase in zirconia content results in decrease in grain size due to the same reason as stated earlier. According to Hall-Petch equation grain size has an inverse effect on strength. That is the reason behind the lower CMOR value achieved in case of the samples sintered at 1600 °C where grain growth has occurred.

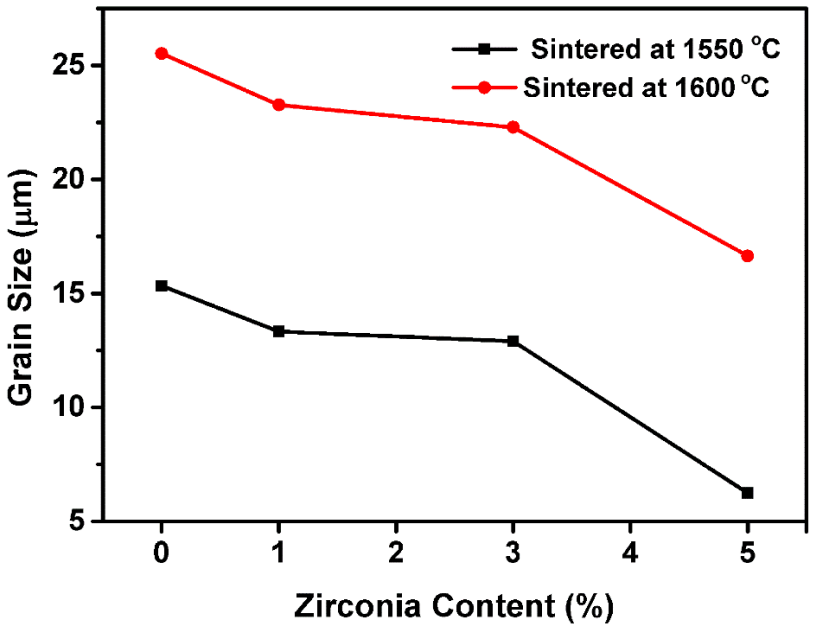

Figure 5-41: Average grain size of the samples sintered at 1550 °C and 1600 °C [172]

Details of the grain size analysis of the samples sintered at 1550 °C and 1600 °C are given in Table 5-6.

Table 5-6: Details of microstructural analysis of MZ0, MZ1, MZ3 and MZ5 samples sintered at 1550 °C and 1600 °C

Batch code	Sintering temperature (°C)	Mean Feret dia	Standard deviation
MZ0	1550	15.34582	5.28654
	1600	25.52971	9.82527
MZ1	1550	13.32467	5.49013
	1600	23.26995	7.34831
MZ3	1550	12.89552	4.57025
	1600	22.29195	6.76403
MZ5	1550	6.23642	3.94308
	1600	16.64748	6.4103

Figure 5-42 depicts the elemental distribution of MZ1 samples sintered at 1550 °C. Elemental mapping of the sample clearly shows that dark black grains are periclase, lighter grains are forsterite, whitish phase is monticellite and bright white phase is zirconia. Zirconia is mainly present in the intergranular positions and monticellite phase is present along the grain boundaries. Presence of lime can be observed inside zirconia grains.

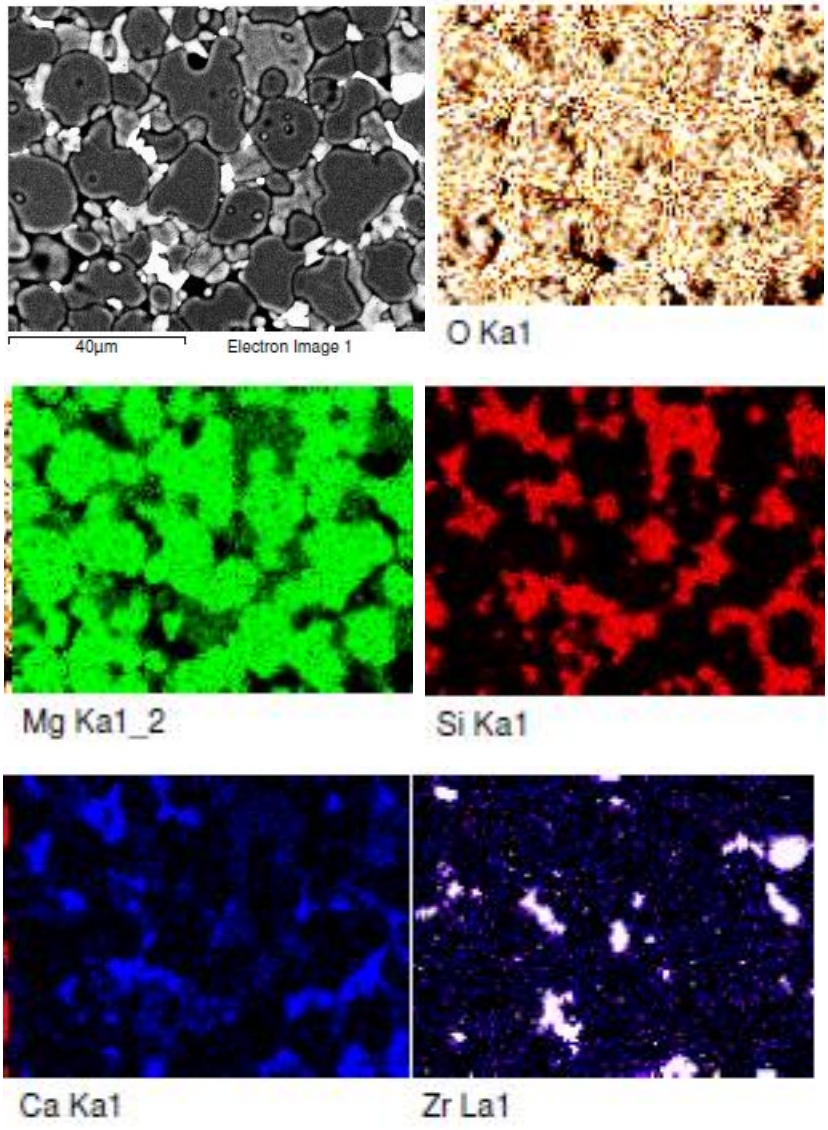

Figure 5-42: Elemental mapping of MZ1 sample sintered at 1550 °C

EDX analysis of MZ3 sample sintered at 1550 °C is shown in Figure 5-43, Figure 5-44 and Figure 5-45. Spot analysis of bright white phase predicts that the phase is zirconia. Presence of little amount of lime can be observed inside zirconia grain (Figure 5-43).

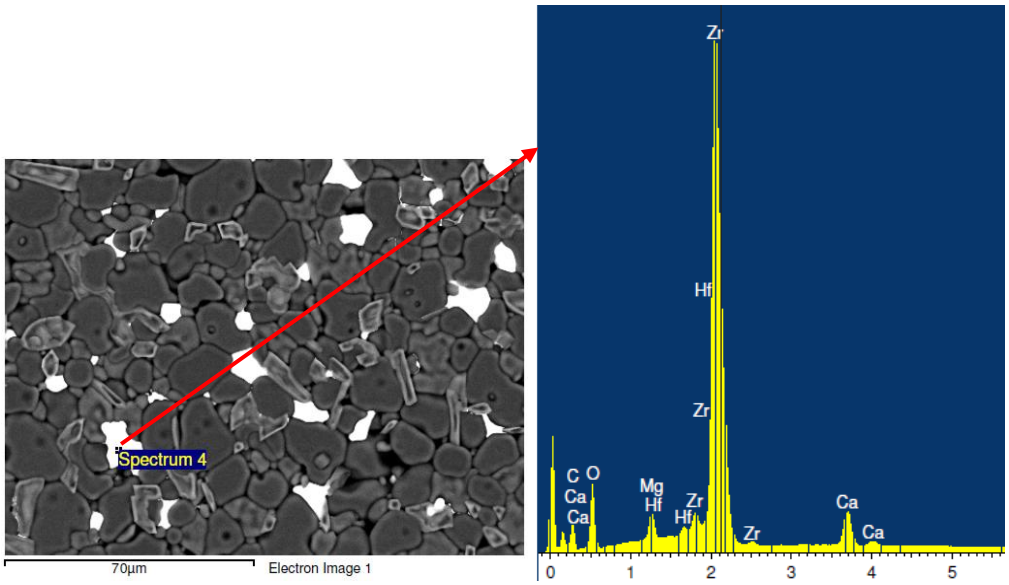

Figure 5-43: Point analysis of MZ3 sample sintered at 1550 °C

Figure 5-44 shows the spot analysis of a grey grain where presence of magnesia and silica is high. Hence it can be predicted as forsterite grain.

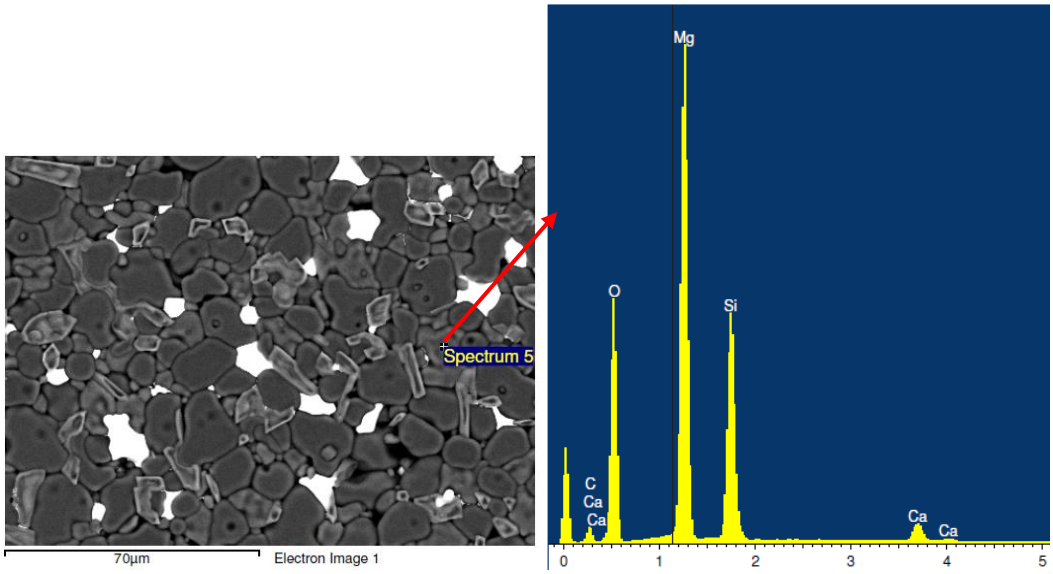

Figure 5-44: Point analysis of MZ3 sample sintered at 1550 °C

Spot analysis of light grey colored, irregular shaped phase is shown in Figure 5-45. From the EDX spectra it can be assumed that this phase is monticellite.

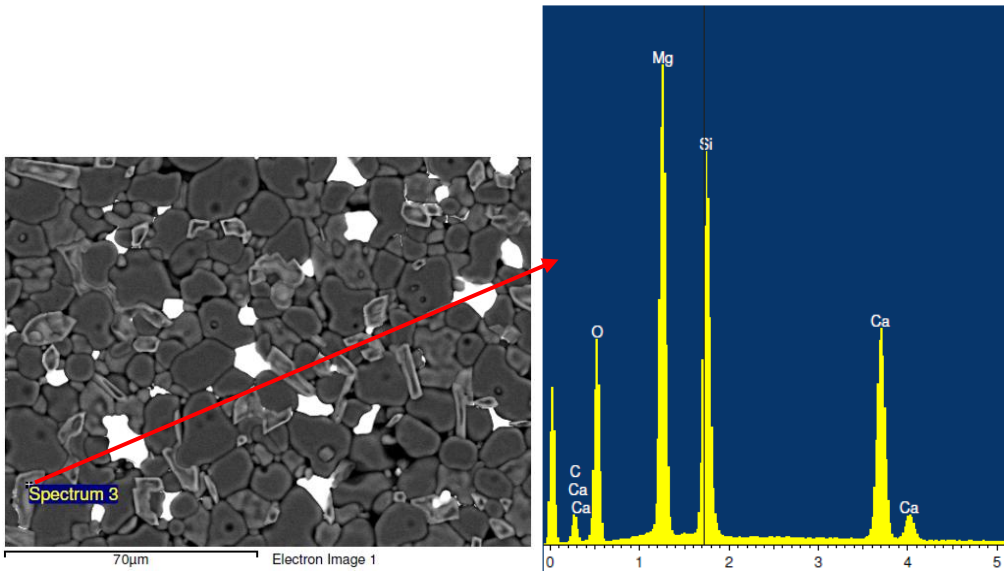

Figure 5-45: Point analysis of MZ3 sample sintered at 1550 °C

Figure 5-46 depicts the spot analysis of MZ3 sample sintered at 1600 °C. Four types of phases can easily be seen from this image. Point analysis of zirconia revels that lime is present inside of the zirconia grain.

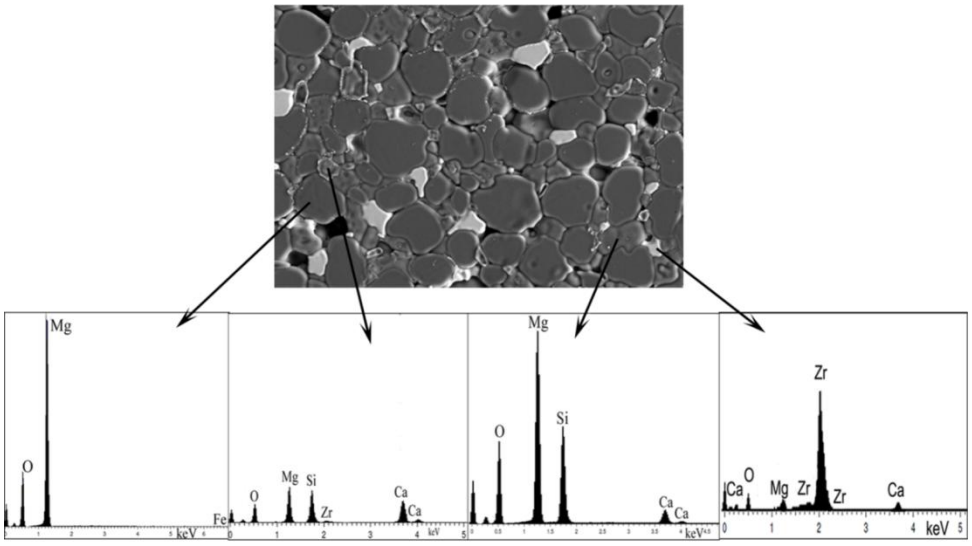

Figure 5-46: Point analysis of MZ3 sample sintered at 1600 °C [172]

Line scan analysis of MZ5 sample sintered at 1550 °C is shown in Figure 5-47. Presence of lime can be observed inside the zirconia grain present in the intragranular position.

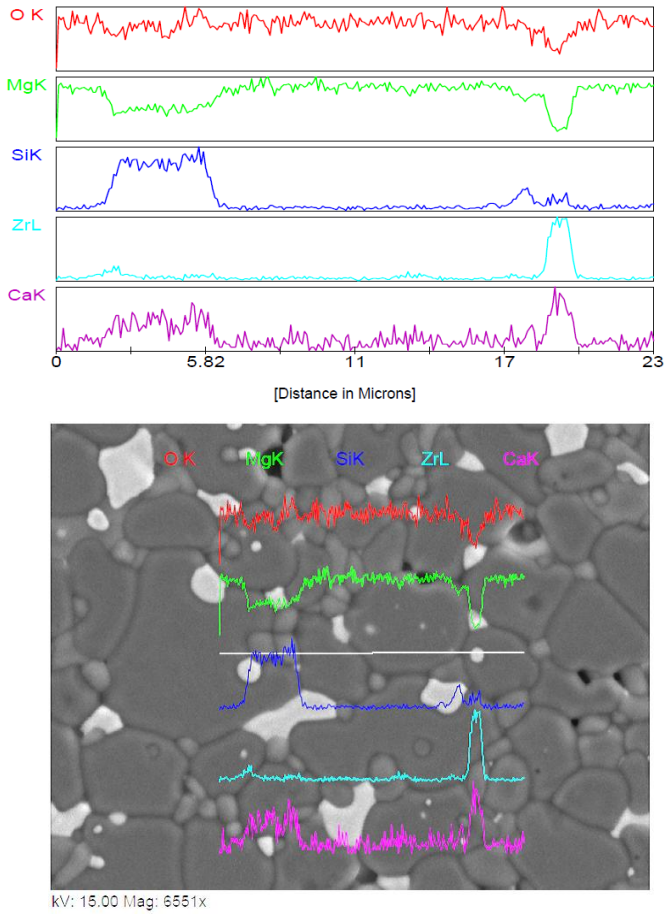

Figure 5-47: Line scan of MZ5 sample sintered at 1550 °C

5.4.5 Summary

- Monoclinic zirconia is added to Indian magnesite in varying amount to modify the high temperature phase formation.
- XRD analysis confirms that zirconia does not react with any impurity and transforms into tetragonal form
- Presence of CaO is found inside zirconia grains. This could mean that zirconia utilizes CaO to stabilize its tetragonal form which is otherwise not stable at room temperature.

- As CaO is used by zirconia, monticellite phase formation is reduced as confirmed by the XRD phase quantification results. Amount of monticellite phase reduces to 3.6 % from 6.7 % with increasing amount of zirconia.
- Samples sintered at 1550 °C show better CMOR than the samples sintered at 1600 °C due to the inverse effect of grain growth on flexural strength.
- Samples containing 1 & 3 wt% zirconia and sintered at 1600 °C show better thermal shock resistance than samples having 0 and 5 wt% zirconia.
- 5 wt% zirconia containing samples sintered at 1600 °C may contain higher amount of microcracks which deteriorate its thermal shock resistance.

Methodology 3

(Preparation of Magnesium aluminate spinel)

- ***Chandrima Ghosh, A. Ghosh, M. K. Haldar, Material Characterization 99 (2015) 84-91 [179]***

5.5 Methodology 3

5.5.1 Densification behavior

Densification behavior of the magnesium aluminate spinel (MS) samples over the sintering temperature range was studied in terms of bulk density, apparent porosity, specific gravity, relative density and linear as well as volume shrinkage. Variation in bulk density and apparent porosity of the samples is depicted in Figure 5-48. It is observed that bulk density increases and apparent porosity decreases up to 1600 °C. After that the trend is reversed and bulk density decreases and apparent porosity increases that is because initially sintering is predominant but after 1600 °C spinelization plays the lead role which is associated with 5-7 % volume expansion. This volume expansion results in increase in the apparent porosity of the samples. Variation in linear and volume shrinkage of the sample sintered at different temperatures is presented in Figure 5-49. In both the cases the pattern of shrinkage is similar. After an initial increase of shrinkage from 1550 °C to 1600 °C, it decreases at 1650 °C and remains almost unchanged till 1700° C. Figure 5-50 shows the variation in true density and densification (%) of the samples as a function of sintering temperature. The plot shows that densification increases in the beginning upto 1600 °C owing to sintering. However, after 1600 °C spinelization is dominant and it results in decreasing densification. It is also observed that true density varies in the range of 3.52-3.56 g/cc in the said sintering temperature range. Variation in closed porosity and total porosity of the samples with increasing sintering temperature is presented in Figure 5-51. Closed porosity is very low in the beginning of sintering process. After initial stage of sintering, closed porosity increases and remains almost unchanged upto 1650 °C. However, there is a decrease in closed porosity level from 1650 °C to 1700 °C. In case of total porosity, after initial reduction from 1550 °C to 1600 °C, it remains almost unchanged upto 1700 °C.

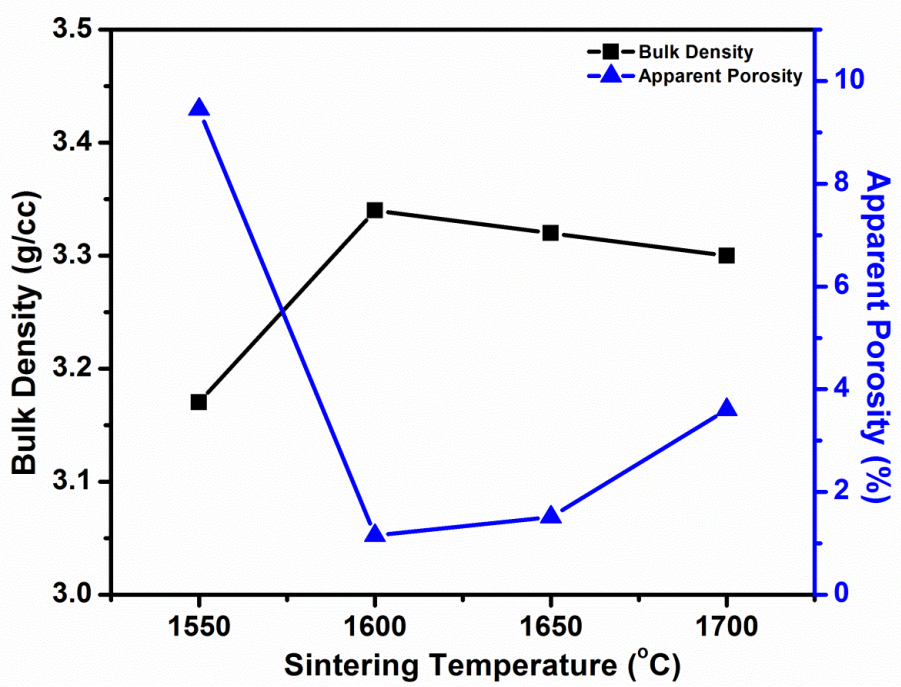

Figure 5-48: Variation in bulk density and apparent porosity of magnesium aluminate spinel samples as a function of sintering temperature

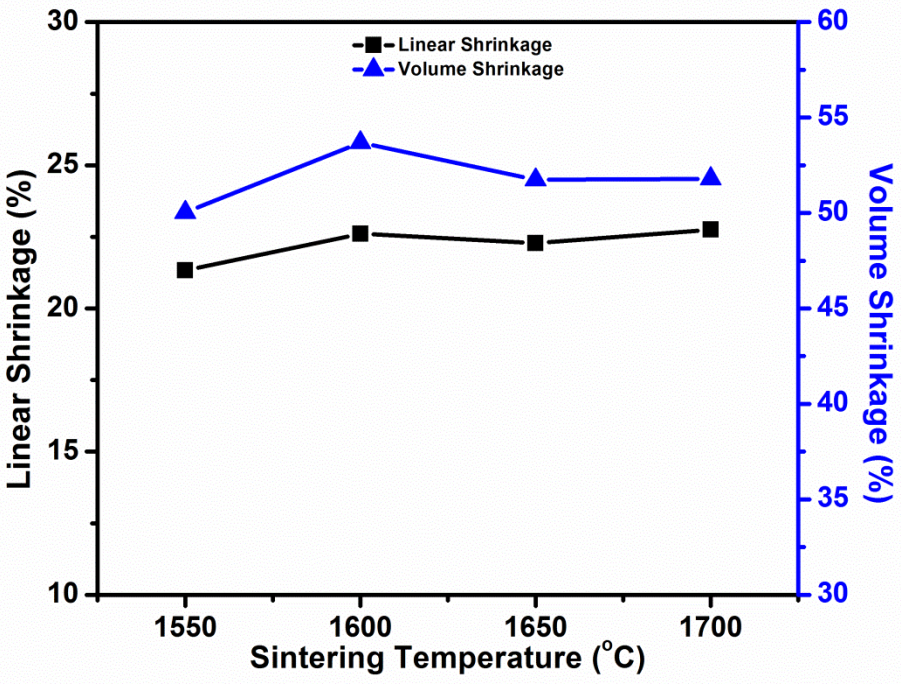

Figure 5-49: Variation in linear shrinkage and volume shrinkage of magnesium aluminate spinel samples as a function of sintering temperature

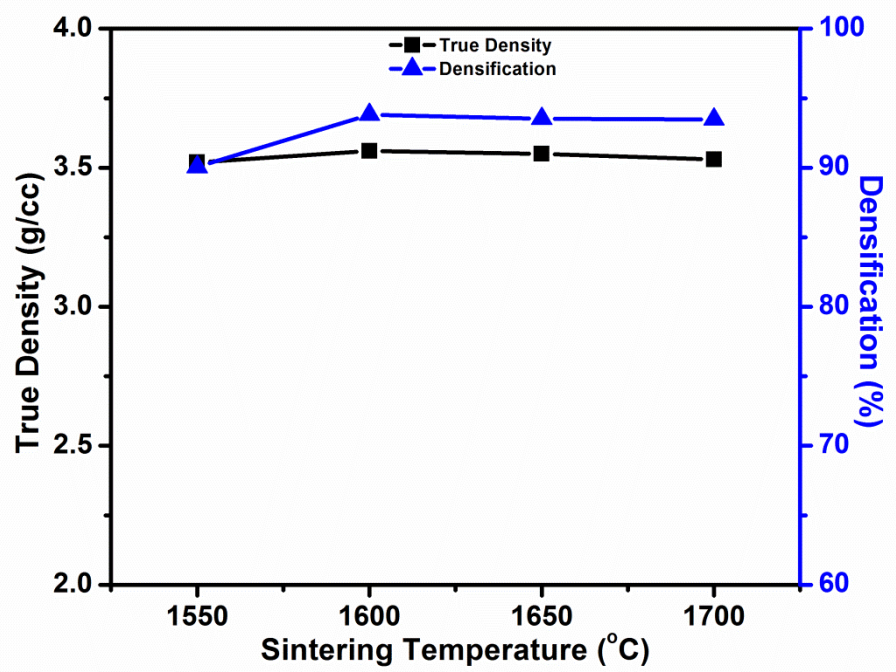

Figure 5-50: Variation in true density and densification (%) of magnesium aluminate spinel samples as a function of sintering temperature

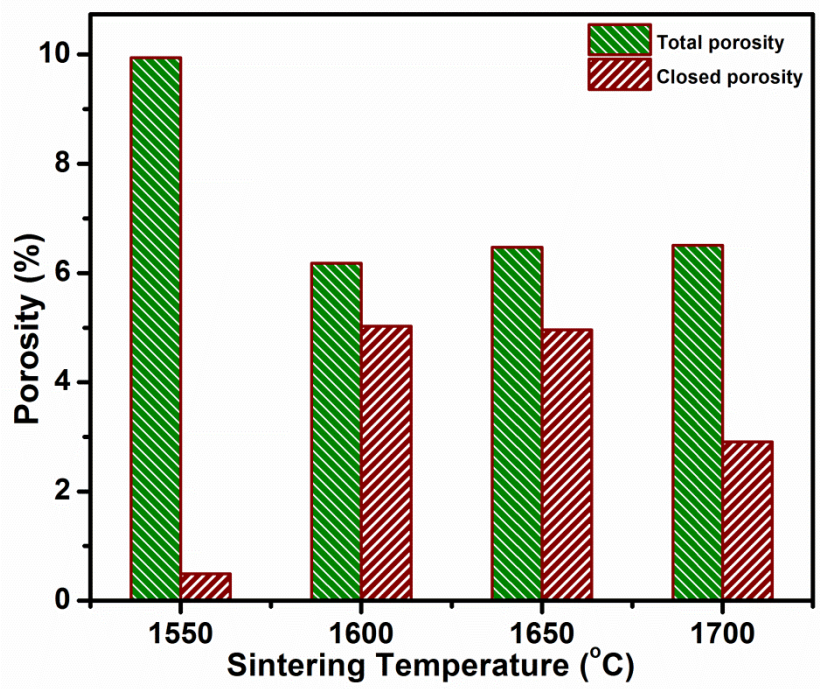

Figure 5-51: Variation in total porosity and closed porosity of magnesium aluminate spinel as a function of sintering temperature

5.5.2 Phase analysis

Figure 5-52 shows the XRD pattern of MS samples sintered at different temperatures. It is observed that spinel is the main crystalline phase developed at the high temperatures. As the composition is magnesia rich, excess magnesia is present in the system which is present as periclase and also it is utilized to form forsterite and monticellite. Quantification data of spinel phase is presented in Table 5-7. The results show that spinel content increases from 90.9 % to 95 % with sintering temperature from 1550-1700 °C. This increase in spinel content justifies the densification result.

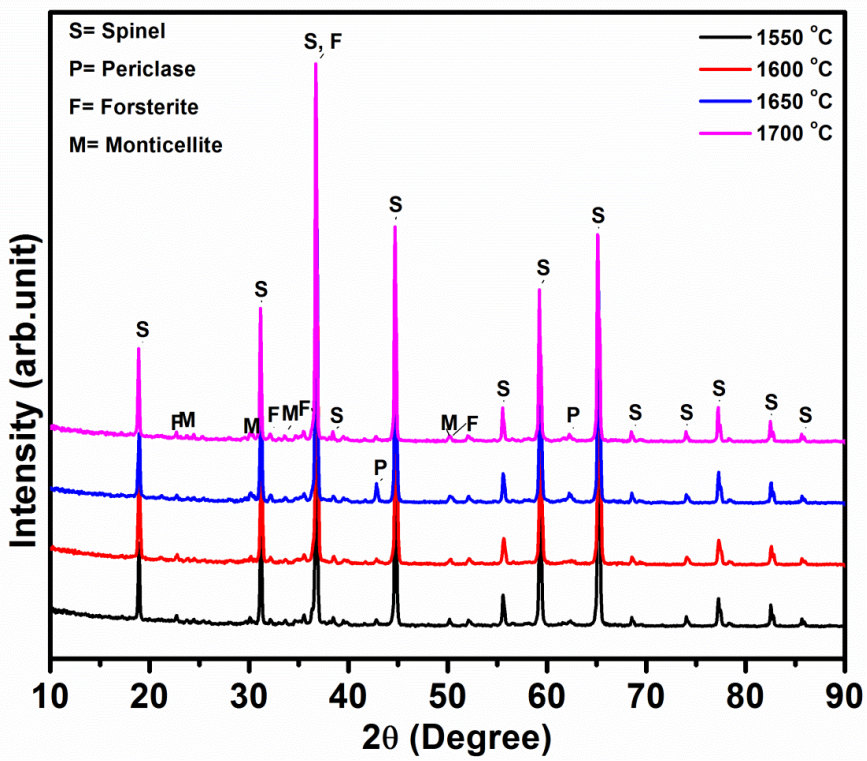

Figure 5-52: XRD pattern of MS samples sintered at different temperatures

Table 5-7: Variation in spinel content with increase in sintering temperature

Sintering temperature (^{o}C)	Spinel content (%)
1550	90.9
1600	93.3
1650	93.4
1700	95.0

5.5.3 Mechanical/thermo-mechanical properties

Flexural strength of the samples is measured using three point bending test. Figure 5-53 shows the effect of sintering temperature on flexural strength at room temperature as well as high temperature (1300 °C). Room temperature flexural strength or CMOR is highest at 1600 °C which may be due to the lowest apparent porosity at that temperature. On the other hand high temperature flexural strength or HMOR is the lowest at 1550 °C. The reason is that in the phase quantification results it is observed that spinel content is lowest at 1550 °C.

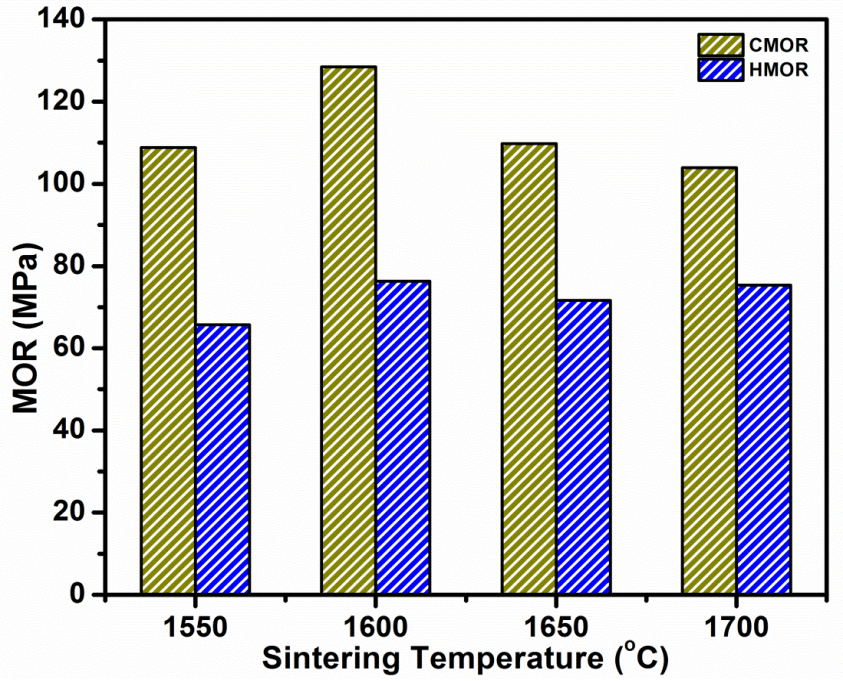

Figure 5-53: Variation in CMOR and HMOR (at 1300 °C) of magnesium aluminate spinel samples as a function of sintering temperature

Magnesium aluminate spinel has good thermal shock resistance due to its low thermal shock coefficient. Retained flexural strength after thermal shock of MS samples is depicted in Figure 5-54. It is evident that samples sintered at 1700 °C have the best thermal shock resistance. This may be due to the fact that these samples have highest spinel content. The general trend shows that thermal shock resistance increases with increasing sintering temperature. Earlier we have found that spinel content increased with temperature. Therefore the result found in thermal shock resistance test is justified.

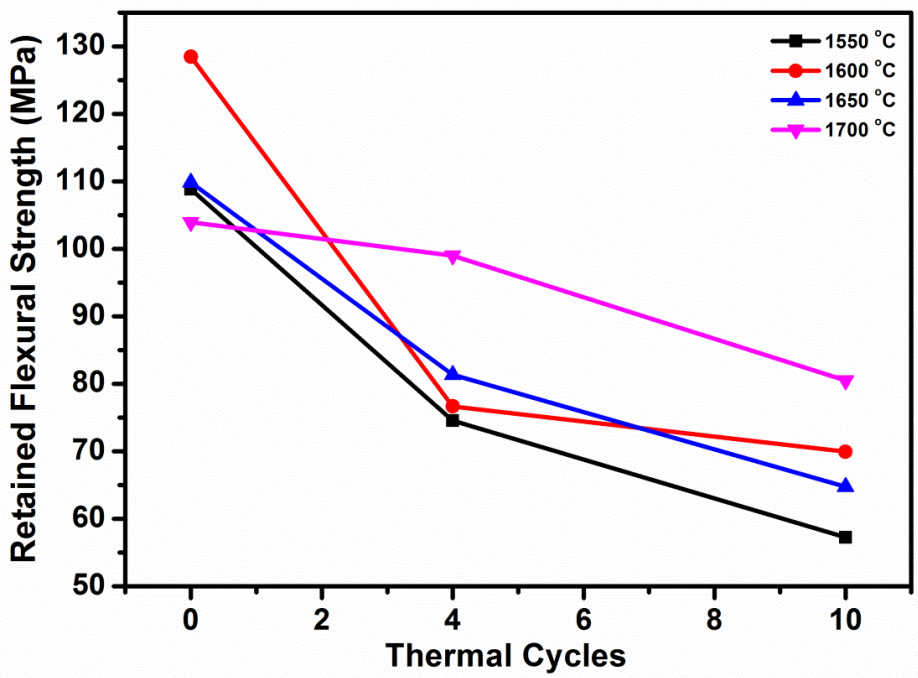

Figure 5-54: Variation in retained flexural strength of magnesium aluminate spinel samples with thermal cycles

5.5.4 Microstructure analysis

Microstructural evolution with sintering temperature is studied using FESEM. The images (Figure 5-55) show presence of angular shaped spinel grains throughout the matrix. Some grains are smaller in size and they are predicted to be forsterite grains. Periclase and monticellite grains could not be identified from the FESEM images. Grain growth from 1500 °C to 1700 °C is very much evident from the FESEM images. Variation in grain size with sintering temperature is depicted in Figure 5-56. Very high percentage of grain growth is observed in the grain size analysis report. At 1700 °C, grains are quite big which leads to increase in apparent porosity of the samples.

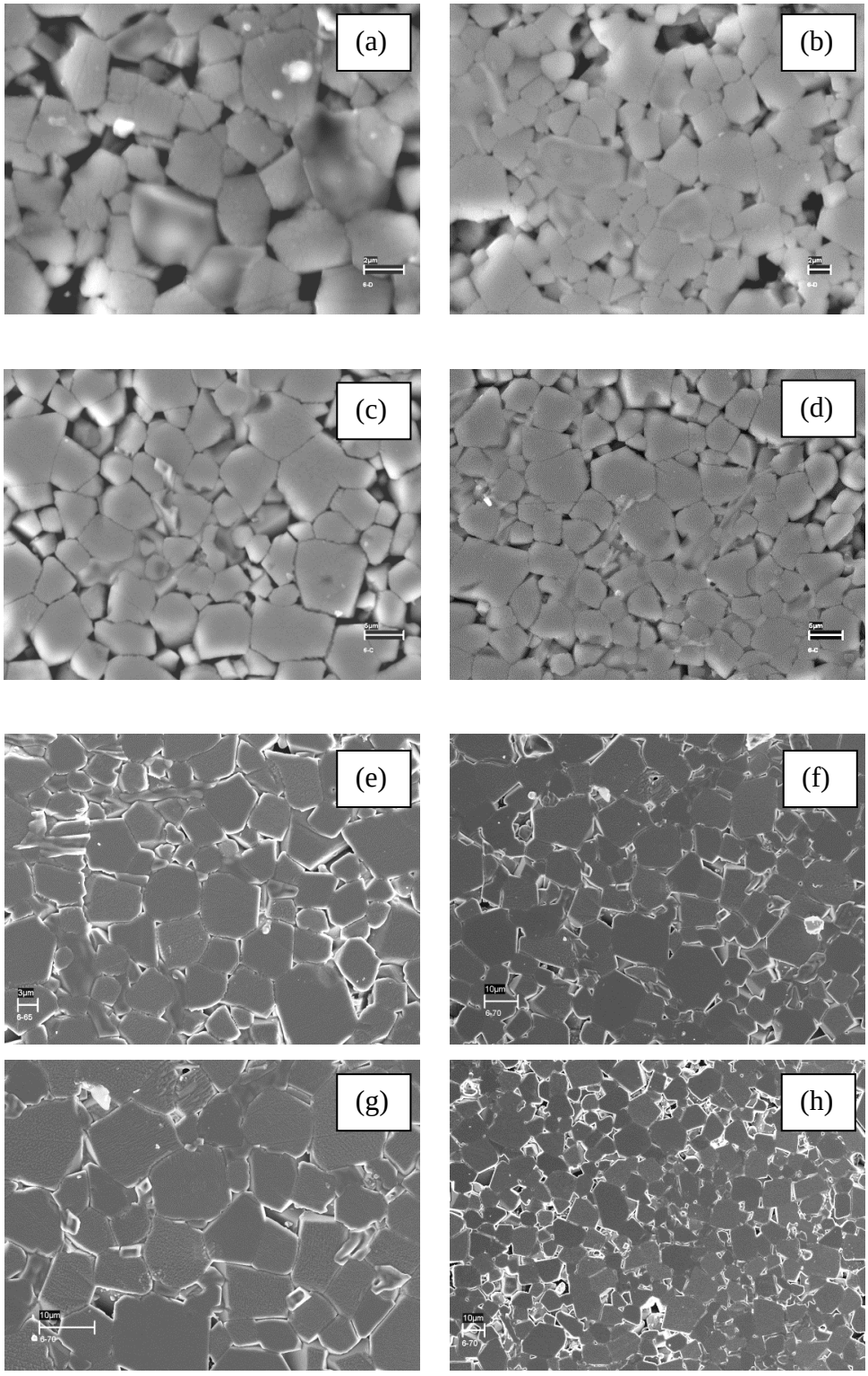

Figure 5-55: FESEM images of magnesium aluminate spinel samples sintered at (a, b) 1550 °C, (c, d) 1600 °C, (e, f) 1650 °C and (g, h) 1700 °C

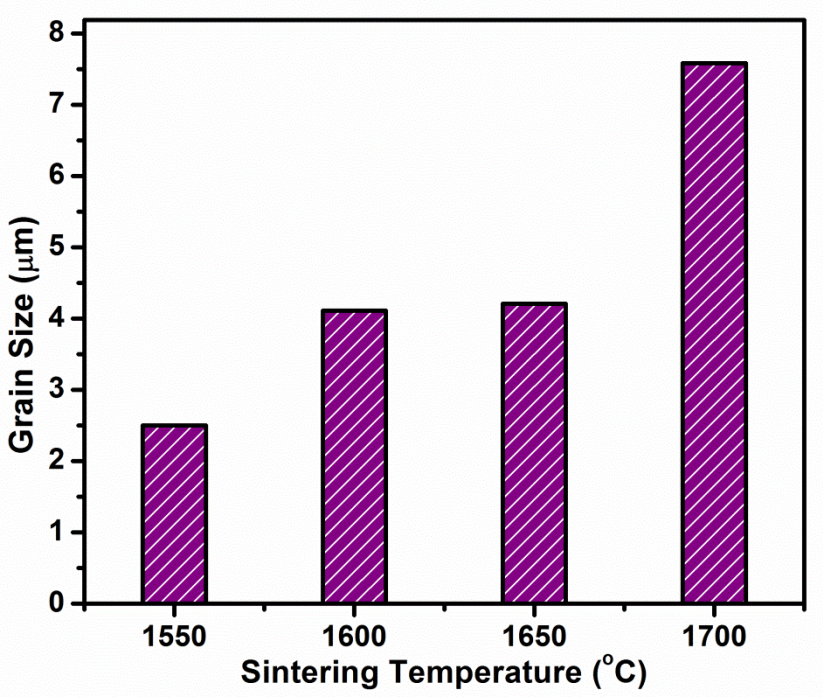

Figure 5-56: Variation in grain size of magnesium aluminate spinel with sintering temperature [179]

EDX analysis (line scan) of MS sample sintered at 1550 °C is shown in Figure 5-57. Angular shaped spinel grains can be identified. Another grain of darker shade is observed which is predicted to be forsterite. From the line scan image, presence of lime can be observed inside the spinel grains and at the grain boundary.

Figure 5-58 shows the elemental mapping of MS sample sintered at 1600 °C. Mainly spinel grains are found in this particular EDX analysis image.

EDX analysis of MS sample sintered at 1650 °C is shown in Figure 5-59. Here also the observations are similar to that of earlier EDX images. Mainly spinel grains are present all over the matrix. In the grain boundaries there is a light colored phase which is predicted to be monticellite. Presence of little amount of lime is observed inside spinel grains.

Line scan of MS sample sintered at 1700 °C (Figure 5-60) also reveals that the microstructure consists of mainly spinel grains. Here also a light colored phase is seen in the intergranular positions containing lime, silica and magnesia. This phase is predicted to be monticellite.

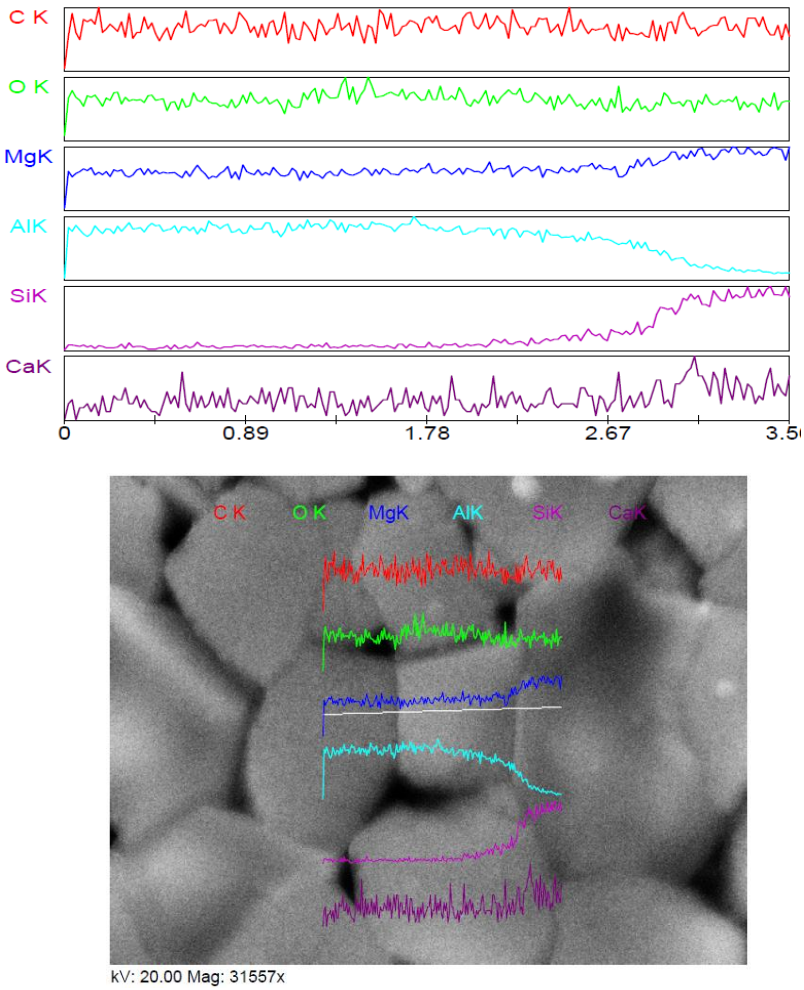

Figure 5-57: Line scan of magnesium aluminate spinel sample sintered at 1550 °C

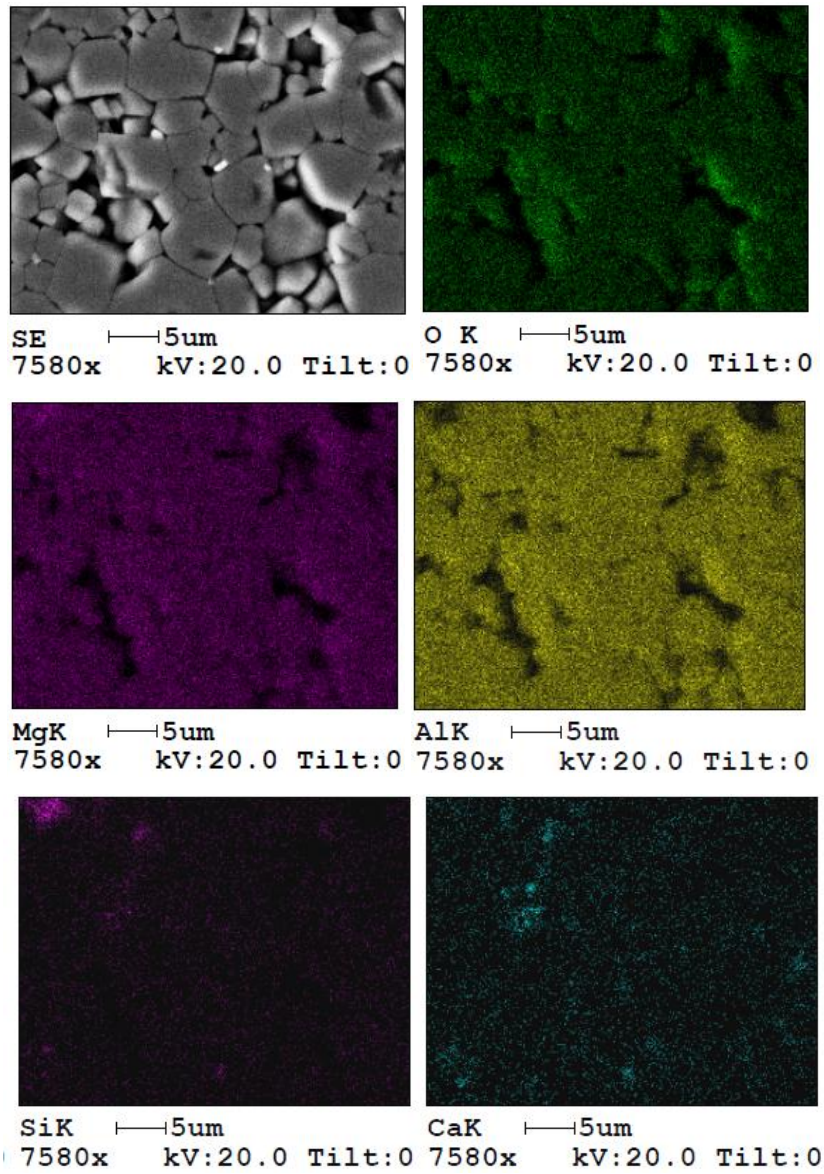

Figure 5-58: Line scan of magnesium aluminate spinel sample sintered at 1600 °C

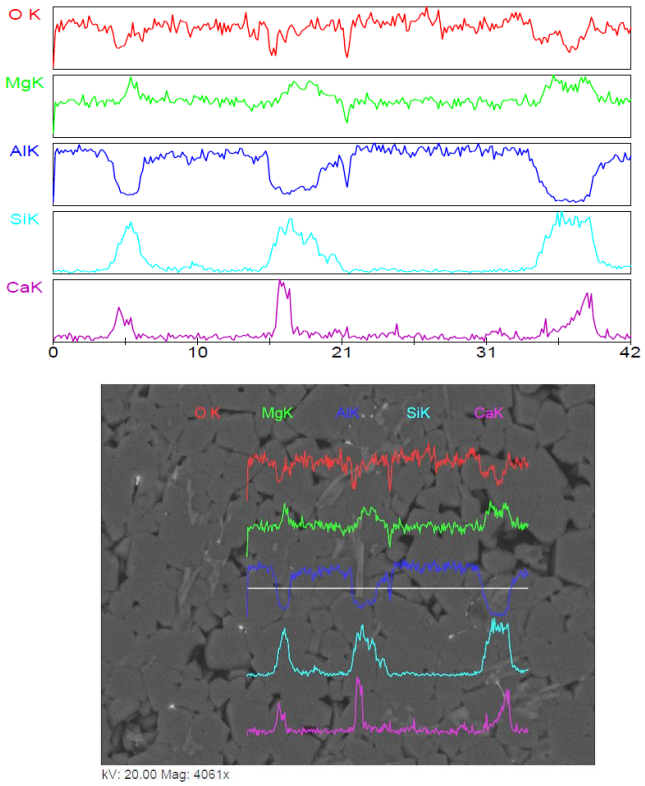

Figure 5-59: Line scan of magnesium aluminate spinel sample sintered at 1650 °C

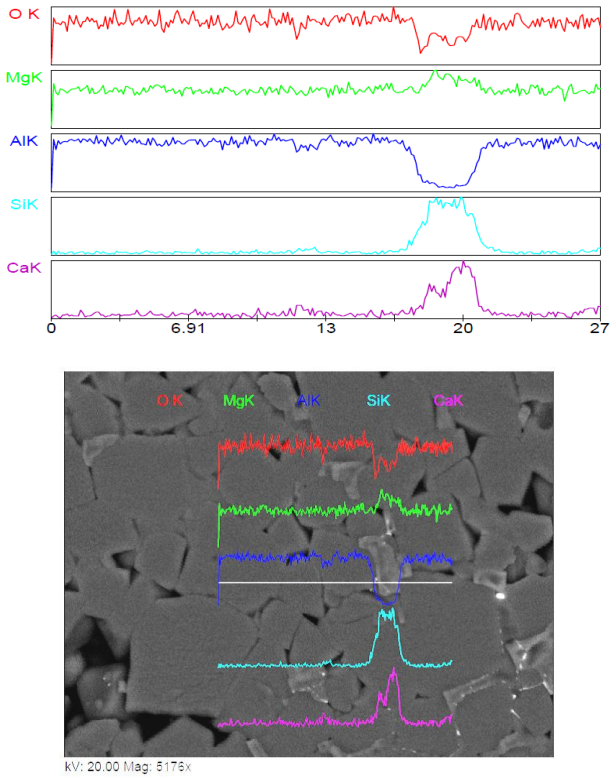

Figure 5-60: Line scan of magnesium aluminate spinel sample sintered at 1700 °C

5.5.5 Summary

- Magnesia rich magnesium aluminate spinel is developed using Indian low quality magnesite and calcined alumina in one stage sintering.
- Developed spinel aggregates show good mechanical as well as thermo-mechanical strength.
- Spinel has good thermal shock resistance due to its low thermal expansion coefficient. Therefore, the samples perform well in the thermal shock resistance test.
- Quantification of the phases by XRD analysis and Rietveld refinement confirms that spinel content gradually increases with sintering temperature.

Methodology 4

(Beneficiation by reverse flotation and process optimization using RSM)

- ***Chandrima Ghosh, S. Sinhamahapatra, H. S. Tripathi, U. Sarkar, Mining, Metallurgy & Exploration (under review)[173]***

5.6 Methodology 4

5.6.1 Particle size analysis

Particle size distribution of the froth and tailing is shown in Figure 5-61. The distribution is unimodal in both the cases. D_{50} values signify that half of the particles are below this size and half are above. For froth it is 1.918 μ and in case of tailing it is 2.618 μ. It is evident that the particles in the froth are finer as compared to the tailing. K_G value or Kurtosis of the distribution of the froth sample shows a mesokurtic distribution having a K_G value of 0.986 which indicates a normal distribution. On the other hand, analysis of the tailing gives a leptokurtic distribution with a K_G value of 1.224.

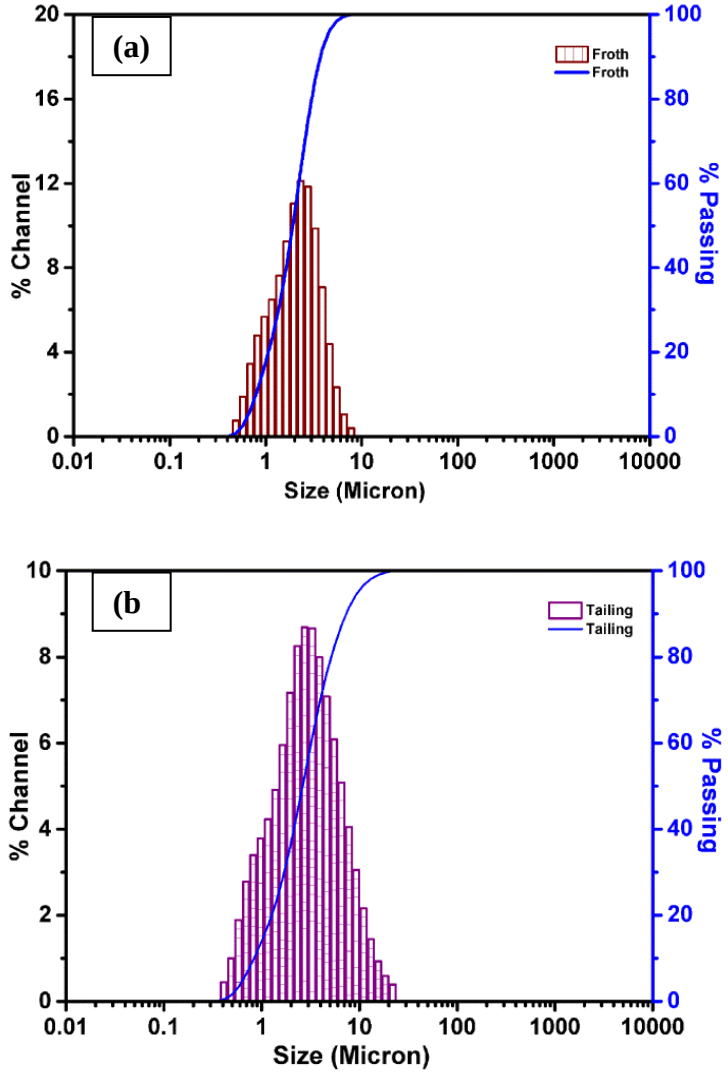

Figure 5-61: Particle size distribution in (a) froth and (b) tailing [173]

5.6.2 Box-Behnken Design (BBD) and analysis

Box-Behnken Design is applied to study the effect of air pressure, collector/frother ratio (C/F ratio) and amount of depressant on the amount of silica content in the froth. Experimental data matrix is achieved using Box-Behnken design and is presented in Table 5-8. The optimum conditions are achieved after statistical analysis of these data.

Table 5-8: Experimental design matrix and results (as per BBD)

Run	Factor 1 A: air pressure (mm water)	Factor 2 B: C/F ratio	Factor 3 C: depressant (g)	Response 1 S: silica content (%)
1	3.5	2	1.5	4.05
2	2	2	2	10.49
3	2	1.5	1.5	2.45
4	0.5	2	1.5	7.5
5	2	2	1	4.19
6	2	1	2	6.61
7	2	1.5	1.5	3.96
8	3.5	1	1.5	3.86
9	0.5	1.5	2	8.2
10	3.5	1.5	2	4.32
11	3.5	1.5	1	3.66
12	0.5	1.5	1	6.3
13	2	1	1	7.8
14	0.5	1	1.5	8.39

The suitability of different models is checked by Table 5-9. Quadratic model is suggested by the software after analyzing all other models.

Table 5-9: Summary of models tested for the response

Source	Sequential p value	Lack of fit p value	Adjusted R^2	Predicted R^2	
Linear	0.0913	0.3831	0.2991	0.0376	
2FI	0.3229	0.3908	0.3726	0.0431	
Quadratic	0.0163	0.8105	0.8960	0.6753	Suggested
Cubic	0.8105		0.7971		Aliased

Analysis of variance (ANOVA) is presented in Table 5-10. Higher values of F (13.45) for the suggested model implies that the model is significant and p-value prob>F of 0.0118 signifies that there is only 1.18% chance that the higher F-value is due to noise. If the value

of prob>F is less than 0.05, the same indicates that the model terms are significant. Hence, the significant model terms used in the quadratic model in this case are A, C, BC, B^2 and C^2. 'Lack of Fit' value of any model should not be 'significant' for a model to be significant. Here, the 'Lack of Fit F-value' of 0.35 indicates that it is not significant which in turn supports the fact that the suggested quadratic model is significant.

Table 5-10: Analysis of variance (ANOVA) for the quadratic model

Source	Sum of squares	Df	Mean square	F value	p value prob > F	
Model	70.70	9	7.86	13.45	0.0118	significant
A-air pressure	26.28	1	26.28	44.98	0.0026	
B-C/F ratio	0.023	1	0.023	0.040	0.8520	
C-depressant	7.35	1	7.35	12.59	0.0238	
AB	0.29	1	0.29	0.50	0.5189	
AC	0.38	1	0.38	0.66	0.4628	
BC	14.03	1	14.03	24.01	0.0080	
A^2	0.95	1	0.95	1.63	0.2702	
B^2	15.47	1	15.47	26.48	0.0068	
C^2	11.18	1	11.18	19.13	0.0119	
Residual	2.34	4	0.58			
Lack of Fit	1.20	3	0.40	0.35	0.8105	not significant
Pure Error	1.14	1	1.14			
Cor Total	73.03	13				

Table 5-11 shows the values of different parameters for the 'goodness of fit'. It is observed that R^2 value is 0.968 and adjusted R^2 is 0.896 with a coefficient of variation (C.V.) of 13.08 %. Importance of R^2 and adjusted R^2 is that it interprets the results of statistical analysis ad indicates how close the data are to the fitted regression line. Here, R^2 and adjusted R^2 values are close enough to signify that the predicted and actual data are in good agreement with each other. The 'Adequate Precision' value demonstrates the signal to noise

ratio. In this case a value > 4 is desirable. In the current research work adequate precision value is 10.668 which indicates that the model can be used to navigate within the design space.

Table 5-11: Goodness of fit parameters of the suggested quadratic model

Parameters	Value
R-Squared	0.9680
Adj R-Squared	0.8960
Adeq Precision	10.668
C.V. %	13.08

The final quadratic equation achieved from the model is as follows:

$$S = 3.20 - 1.81 \times A - 0.054 \times B + 0.96 \times C + 0.27 \times AB - 0.31 \times AC + 1.87 \times BC + 0.55 \times A^2 + 2.20 \times B^2 + 1.87 \times C^2 \quad \textbf{(Equation 5-1)}$$

where,

S indicates response (wt % of silica in the froth)

The above equation can be used to predict the response for given levels of each factor. The high levels are coded as +1 and the low levels are coded as -1. This equation is used to study the relative effect of the process parameters (factors) by comparing their coefficients.

Experimental and predicted data are correlated with each other (Figure 5-62) using the quadratic equation (Equation 5-1). The graphical representation of the predicted and actual data shows that the data points are well distributed near the straight line. This implies that there is a good agreement between experimental and predicted data. Figure 5-63 shows the 'Normal Plot of Residuals'. It is observed that the residual is externally studentized because the last value is an outlier and hence excluded from the calculation. It also signifies that the residuals follow a normal distribution.

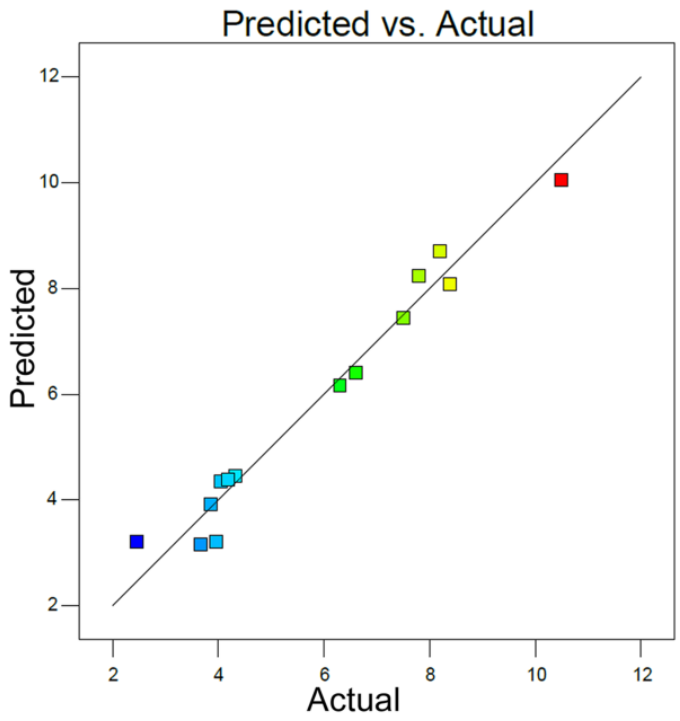

Figure 5-62: Correlation between experimental and predicted data[173]

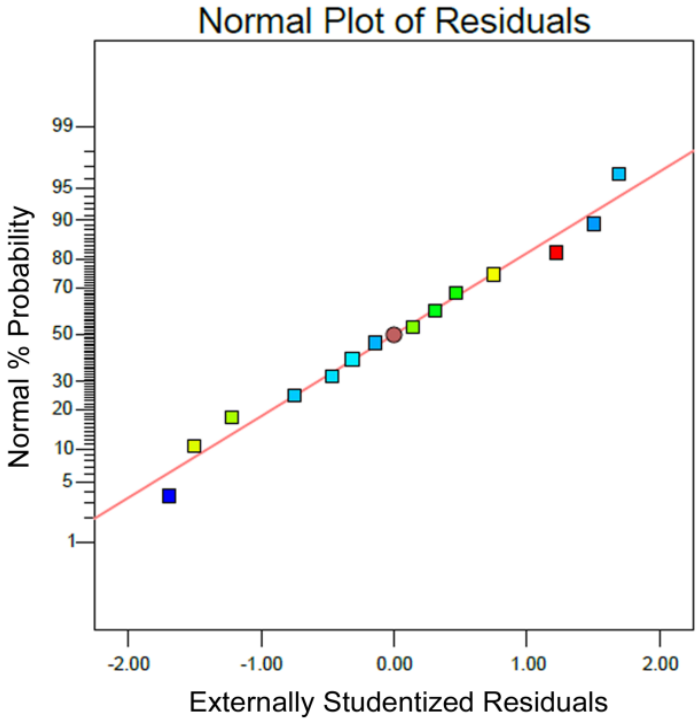

Figure 5-63: Normal plot of studentized residuals[173]

The interaction effects of the three process parameters namely air pressure, C/F ratio and amount of depressant on silica content in froth are shown in Figure 5-64(a-c) in terms of 3D response surface plots. In each figure two parameters are varied while keeping one parameter constant. Figure 5-64a shows the effect of C/F ratio and air pressure on silica content at the center level of the amount of depressant. It is found that silica content in froth is increased with increasing C/F ratio. However, air pressure has a negative impact on silica content in froth i.e. increase in air pressure reduces the silica content in froth. Figure 5-64b depicts the effect of amount of depressant and air pressure on silica content keeping the C/F ratio constant. It is observed increasing air pressure reduces the silica content in froth. On the other hand, an increase in the amount of depressant increases the silica content in froth. In Figure 5-64c, the effect of C/F ratio and amount of the depressant on silica content is presented while air pressure is kept constant. In this case, both the parameters have positive impact on silica content in froth except at lower values of the depressant amount.

After analyzing all the data, an optimum condition is suggested by RSM where the best possible operational conditions are air pressure of 0.512 mm water, C/F ratio of 1.993 and a depressant amount of 1.999 g/ 4 kg of slurry. According to the model this set of process parameters would result in 12.335 % silica in froth. A new experiment is carried out with these optimized values and 12.15 % silica in the froth is achieved.

5.6.3 Characteristic of processed magnesite

XRD patterns of Indian raw magnesite and the processed magnesite after flotation for which maximum silica removal has been achieved are compared in Figure 5-62. Magnesite is the major crystalline phase along with dolomite and quartz as secondary phases in both the samples i.e. no change in crystalline phases is found. However, quantification of the phases shows that magnesite content is increased after flotation from 94 % to 95.10 % (Table 5-12). On the other hand silica content is decreased from 2.30 % to 1.80 % and dolomite content is decreased from 3.7 to 3.1%.

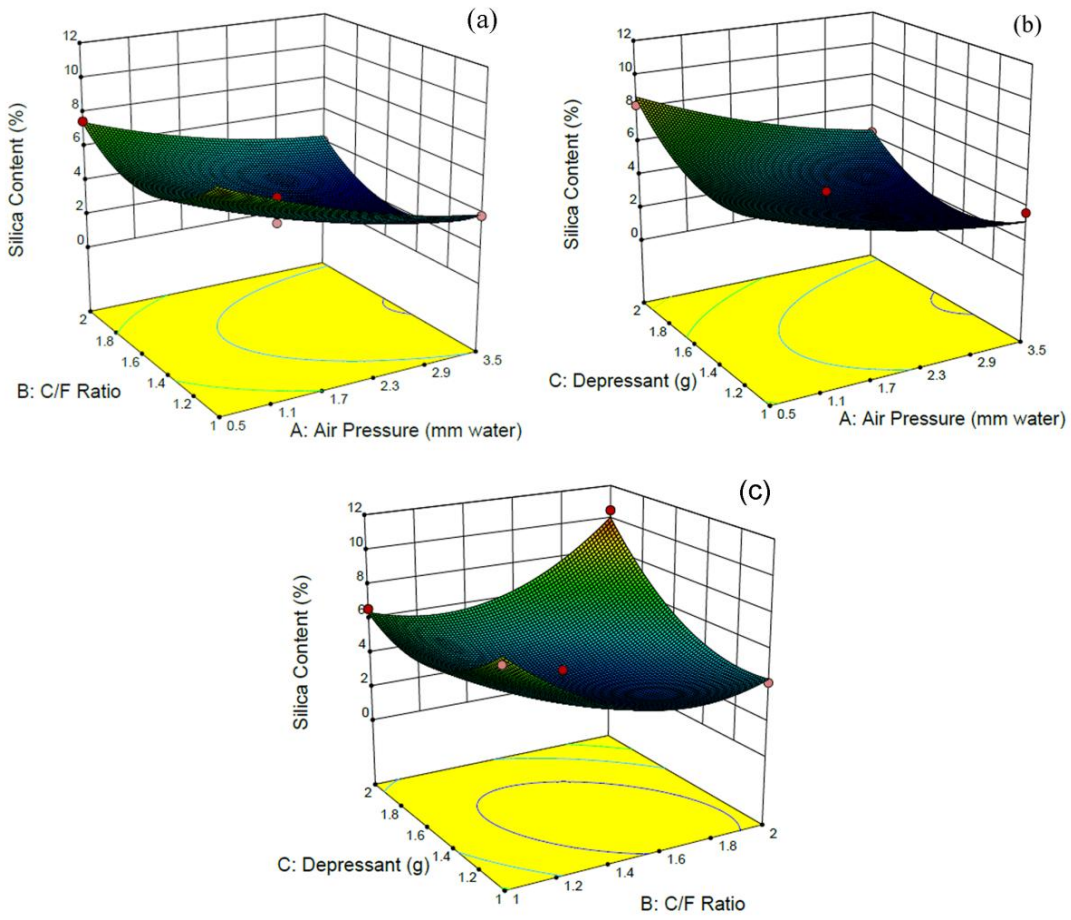

Figure 5-64: Response surface plots showing the interactive effect of C/F ratio, amount of depressant and air pressure in various combinations; (a) effect of C/F ratio and air pressure (b) effect of amount of depressant and air pressure (c) effect of amount of depressant and C/F ratio on the silica content of forth [173]

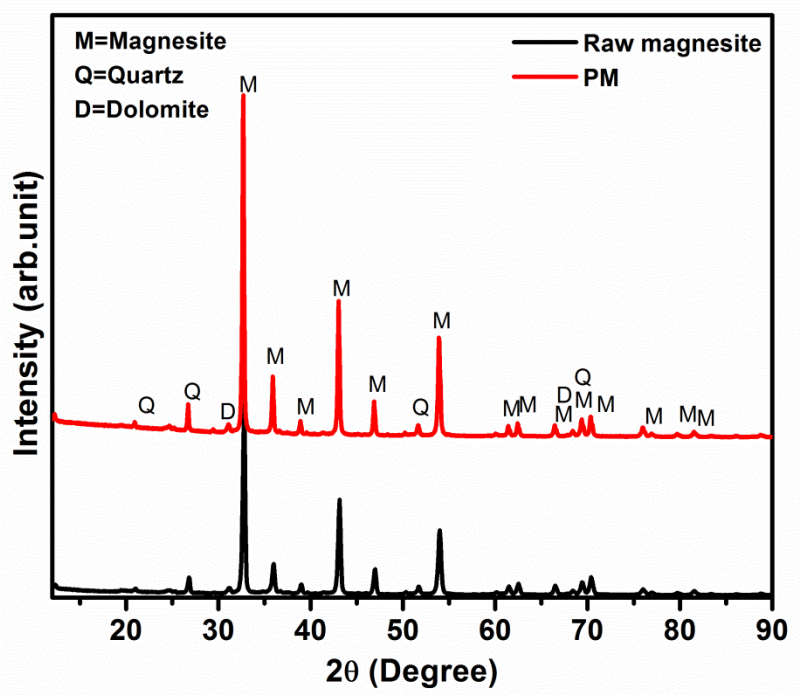

Figure 5-65: XRD pattern of raw magnesite and processed magnesite (PM)

Table 5-12: Quantification of the crystalline phases of raw and processed magnesite

Sample description	Crystalline phases (%)		
	Magnesite	Dolomite	Quartz
Raw magnesite	94	3.7	2.3
Processed magnesite (PM)	95.1	3.1	1.8

5.6.4 Summary

- Low grade Indian magnesite is beneficiated with reverse froth flotation technique using pine oil as frother, FLOTIGAM EDA as collector and SHMP as depressant.
- Effect of different process parameters was optimized using RSM and a quadratic model equation is formulated for the experiment.
- The operational conditions are optimized by RSM and they are air pressure of 0.512 mm water, C/F ratio of 1.993 and a depressant amount of 1.999 g/ 4 kg of slurry.
- The processed sample was characterized in terms of phase assemblage and chemical composition. Reduction of quartz content from 2.3 to 1.8 % was achieved by this beneficiation method which was confirmed by the quantitative phase analysis through XRD.

6. Summary and Conclusions

Indian magnesite of Salem region was the subject of this study. Chemical analysis showed that it contained 4.8 wt% silica and 2.79 wt% lime as main impurities. XRD study confirmed the presence of magnesite along with dolomite and quartz. DTA-TG curves described the thermal decomposition behavior of the sample. There were three endothermic peaks relating to the decomposition of magnesite, magnesite present in dolomite and calcite present in dolomite.

Indian magnesite of Salem region was sintered at different temperatures starting from 1550 to 1700 °C. It was observed that AP was very low in the said temperature range suggesting the presence of liquid phase in the samples. Further XRD analysis confirmed that substantial amount of low melting monticellite phase was present in the samples which was the reason behind the poor thermo-mechanical properties of the samples. Microstructural analysis showed that the periclase grains are rounded to subrounded in shape which is due to the presence of low melting phase in the matrix. EDX analysis indicated that the main bigger grains were periclase, the smaller grains were forsterite and the third phase that was present along the grain boundaries having no proper shape was monticellite.

$CaCO_3$ was added to Indian magnesite to change the C/S ratio. Initially it was 0.58 and it was changed to 1 in one batch and 2 in another batch. Samples having C/S ratio 1:1 performed well in mechanical strength test at room temperature but did not show good thermo-mechanical properties. The only secondary phase formed in this batch was monticellite which was the reason behind the poor thermal shock resistance of the samples. On the other hand, the samples having C/S ratio 2:1 showed good thermal shock resistance. C_2S phase was found in these samples in the XRD analysis. This was the phase we had aimed for as it was high melting in nature. However, some amount of low melting merwinite phase was also found in XRD analysis.

In another methodology, monoclinic zirconia was added in varying amount (1, 3, 5 wt%) to Indian magnesite. It was observed that zirconia did not react with any of the impurities. However, it transformed into tetragonal form in presence of lime. As a result, lime was

unavailable to form monticellite phase. Hence, amount of monticellite phase decreased with increasing zirconia content. 1 and 3 wt% zirconia added samples showed good thermal shock resistance than without zirconia batch and the batch having 5 wt% zirconia. Higher amount of zirconia led to more number of micro cracks which resulted in reduction of retained flexural strength.

Magnesium aluminate spinel was prepared through one stage sintering from Indian magnesite and calcined alumina. Spinel samples showed good high temperature flexural strength as well as good thermal shock resistance. Microstructure consists of mainly Mg-Al spine grains which are angular in shape. Some grains of forsterite and monticellite can also be found. Though we found periclase phase in the XRD analysis we could not identify periclase grains from the microstructure.

Finally reverse flotation technique was used to beneficiate Indian magnesite. Silica content in froth was measured by chemical analysis. Process parameters were optimized using Response Surface Methodology. Box Behneken design was applied to get the experimental data matrix. A quadratic equation was developed for the process. Quantification of the phases in the tailing was done using XRD analysis and Rietveld Refinement. A new experiment was carried out using the optimized data. The result was in good agreement with the predicted value.

7. References

[1] ASTM C71-12, Standard terminology relating to refractories, ASTM International, West Conshohocken, PA, 2012.

[2] W.E. Lee, R.E. Moore, Evolution of in situ refractories in the 20th century, J. Am. Ceram. Soc., 81 (1998) 1385-1410.

[3] C.M. Peret, J.A. Gregolin, L.I.L. Faria, V.C. Pandolfelli, Patent generation and the technological development of refractories and steelmaking, Refractories Applications and News, 12 (2007) 10 - 14.

[4] S. Banerjee, Properties of Refractories, in: C.A. Schacht (Ed.) Refractories Handbook, Marcel Dekker, Inc., New York, 2004.

[5] J.D. Panda, Planned utilization of raw materials for basic refractories, Proc. Indian Natn. Sci. Acad., 50 (1984) 428-438.

[6] Magnesite, Indian Bureau of Mines, Ministry of Mines, Govt.of India, 2017.

[7] M.A. Shand, The Chemistry and Technology of Magnesia, John Wiley & Sons, Inc., New Jersey, 2006.

[8] W.A. Hull, The position of atoms in metals, Proc. Am. Inst. Electr. Eng., 38 (1919) 1171.

[9] W.P. Davey, E.O. Hoffman, Phys. Rev, 2 (1920) 333.

[10] R.W.G. Wyckoff, The crstal structure of magnesium oxide, Am. J. Sci., 5 (1921) 138-152.

[11] R.G. Burns, Mineralogical Applications of Crystal Field Theory, Cambridge University Press, Cambridge, 1993.

[12] R.M. Hazen, Effects of temperature and pressure on the cell dimension and X-ray temperature factors of periclase T = 24 C, P = 1 atm, standard mount, Am. Mineral., 61 (1976) 266-271.

[13] W.R. Eubank, Calcination studies of magnesium oxides, J. Am. Ceram. Soc., 34 (1951) 225-229.

[14] M.S. Judd, J.A. Nelson, Interaction of molten aluminium and magnesium oxide refractories, Am. Ceram. Soc. Bull., 55 (1976) 643-644.

[15] O.M. Margulis, K.G. Romanchenko, A.V. Stovbur, Dense magnesium oxide refractories with increased spalling resistance, Refractories, 1 (1960) 106-109.

[16] D. Kocaefe, D. Karman, F.R. Steward, Comparison of the sulfation rates of calcium, magnesium and zinc oxides with SO_2 and SO_3, Can. J. Chem. Eng., 63 (1985) 971-977.

[17] B.V. Molotilov, V.G. Borisenko, E.N. Vlasova, N.G. D'yakonova, The use of magnesium oxide produced from magnesite in electrotechnical anisotropic steel making, Steel, 12 (1996) 55-58.

[18] A. Rosanoff, M.S. Seelig, Comparison of mechanism and functional effects of magnesium and statin pharmaceuticals, J. Am. Coll. Nutr., 23 (2004) 501-505.

[19] C. Wildt, O. Gibert, J.L. Cortina, G. Coscera, On-site remediation of chromium-contaminated sediments by combination of sediment washing and stabilization with magnesium oxide, J. Soils. Sediments, 4 (2004) 184-191.

[20] C.K. Chau, Z. Li, Accelerated reactivity assessment of light burnt magnesium oxide, J. Am. Ceram. Soc., 91 (2008) 1640-1645.

[21] L.C. Jackson, Magnesium Compounds, in: J. I.Kroschwitz, M.Howe-Grant. (Eds.) Kirk-Othmer Encyclopedia of Chemical Technology, John Wiley & Sons, Inc., New York, 1995, pp. 19-22.

[22] D.R.F. Spencer, Basic refractory raw materials, Trans. Br. Ceram. Soc., 71 (1972) 123-134.

[23] W.C. Gilpin, Refractories J., 45 (1969).

[24] M. Frith, T. Buffrey, I. Strawbridge, Magnesia: a refractories manufacturer perspective, Trans. Br. Ceram. Soc., 97 (1998) 29-34.

[25] Magnesite, Indian Bureau of Mines, Ministry of Mines, Government of India, 2018.

[26] R.A. Landy, Magnesia Refractories, in: C.A. Schacht (Ed.) Refractories Handbook, Marcel Dekker, Inc., New York, 2004, pp. 109-149.

[27] M.A. Serry, S. M. Hammad, M.F.M. Zawrah, Densification and microstructure of refractory periclase grains, Interceram, 46 (1997) 430-435.

[28] H.R. Zargar, C. Oprea, G. Oprea, T. Troczynski, The effect of nano-Cr_2O_3 on solid-solution assisted sintering of MgO refractories, Ceram. Int., 38 (2012) 6235-6241.

[29] J.H. Chesters, Refractories: Production And Properties, Iron and Steel Institute, London, 1973.

[30] A.Y. Borisova, É.I. Zin'ko, I.V. Fedina, Highly refractory material based on magnesia spinel, Refractories, 7 (1966) 418-420.

[31] A. Brongniart, D'une classification minéralogique des roches mélangées, Journal Des Mines, 34 (1813) 1-49.

[32] D.L.G. Karsten, Minerogische Tabellen, Rottmann, Berlin, 1808.

[33] W.A. Deer, R.A. Howie, J. Zussman, Rock Forming Minerals, in: M.E. Fleet (Ed.) Sheet Silicate: Micas, The Geological Society, London, 1997.

[34] G.W. Bain, Types of magnesite deposits and their origin, Economic Geology, 19 (1924) 412-433.

[35] The Magnesite Deposits of California, United States Geological Survey, Department of the Interior, 1908.

[36] K.D. Oh, H. Morikawa, S. Iwai, H. Aoki, The crystal structure of magnesite, Am. Mineral., 58 (1973) 1029-1033.

[37] W. Liang, Z. Li, Y. Yin, R. Li, L. Chen, Y. He, H. Dong, L. Dai, H. Li, Single crystal growth, characterization and high-pressure Raman spectroscopy of impurity-free magnesite ($MgCO_3$), Phys. Chem. Miner., 45 (2018) 423-434.

[38] Mineral commodity summaries, 2017, U. S. Geological Survey, 2017.

[39] V. Prasannakumar, C. Vikas, S.N. Kumar, Constraints on the origin of South Indian magnesite deposits, Boletim Paranaense de Geociências, 50 (2002) 15-20.

[40] C.W. Beck, Differential thermal analysis curves of carbonate minerals, Am. Mineral., 35 (1950) 985-1013.

[41] R.M. Gruver, Differential thermal-analysis studies of ceramic materials: I, characteristic heat effects of some carbonates, J. Am. Ceram. Soc., 33 (1950) 96-101.

[42] C.N.R. Rao, S.R. Yoganarasimhan, M.P. Lewis, Exothermic reactions due to annealing of defects in oxide lattices: study of the decomposition of carabonates, Can. J. Chem., 38 (1960) 2359-2362.

[43] N. Khan, D. Dollimore, K. Alexander, F.W. Wilburn, The origin of the exothermic peak in the thermal decomposition of basic magnesium carbonate, Thermochim. Acta., 367-368 (2001) 321-333.

[44] F.L. Cuthbert, R.A. Rowland, Differential thermal analysis of some carbonate minerals, Am. Mineral, 32 (1947) 111-116.

[45] D. Sheila, Thermal analysis studies on the decomposition of magnesite, Int. J. Miner. Process., 37 (1993) 73-88.

[46] M. Samtani, D. Dollimore, K.S. Alexander, Comparison of dolomite decomposition kinetics with related carbonates and the effect of procedural variables on its kinetic parameters, Thermochim. Acta., 392-393 (2002) 135-145.

[47] X.W. Liu, Y.L. Feng, H.R. Li, P. Zhang, P. Wang, Thermal decomposition kinetics of magnesite from thermogravimetric data, J. Therm. Anal. Calorim., 107 (2012) 407-412.

[48] J. Malek, The kinetic analysis of non-isothermal data, Thermochim. Acta, 200 (1992) 257 -269.

[49] L. Tian, A. Tahmasebi, J. Yu, An experimental study on thermal decomposition behavior of magnesite, J. Therm. Anal. Calorim., 118 1577-1584.

[50] S. Maitra, S. Mukherjee, N. Saha, J. Pramanik, Non-isothermal decomposition kinetics of magnesite, Cerâmica, 53 (2007) 284-287.

[51] F. Demir, B. Dönmez, H. Okur, F. Sevim, Calcination kinetic of magnesite from thermogravimetric data, Chem. Eng. Res. Des., 81 (2003) 618-622.

[52] L. Turčániová, G. Paholič, K. Mateová, Stimulating the thermal decomposition of magnesite, Thermochim. Acta, 277 (1996) 75-84.

[53] M.A. Serry, M.B. El-Kholi, M.S. Elmaghraby, R. Telle, Characterization of Egyptian dolomitic magnesite deposits for the refractories industry, Ceram. Int., 28 (2002) 575-583.

[54] J.A. Varela, O.J. Whittemore, Structural rearrangement during the sintering of MgO, J. Am. Ceram. Soc., 66 (1983) 77-82.

[55] C.E. Hoge, J.A. Pask, Thermodynamic and geometric considerations of solid state sintering, Ceramurgia Int., 3 (1977) 95-99.

[56] L.C.D. Jonghe, M.N. Rahaman, Sintering of Ceramics, in: S. Somiya, F. Aldinger, R.M. Spriggs, K. Uchino, K. Koumoto, M. Kaneno (Eds.) Handbook of Advanced Ceramics, Academic Press, USA, 2003, pp. 187-264.

[57] F.B. Swinkels, M.F. Ashby, A second report on sintering diagrams, Acta Metall., 29 (1981) 259-281.

[58] S.-J.L. Kang, Sintering: Densification, Grain Growth and Microstructure, Elsevier Butterworth-Heinemann, Oxford, UK, 2005.

[59] M.N. Rahaman, Ceramic Processing and Sintering, CRC Press, New York, USA, 2003.

[60] W.S. Treffner, Microstructure of periclase, J. Am. Ceram. Soc., 47 (1964) 401-408.

[61] A. Pande, R. Singh, Electron microscope and electron diffraction studies of sintering of magnesite, J. Am. Ceram. Soc., 41 (1958) 394-397.

[62] A.G. Allison, E.C. Sesler, N.L. Haldy, W.H. Duckworth, Sintering of high-purity magnesia, J. Am. Ceram. Soc., 39 (1956) 151-154.

[63] C. Aksel, F. Kasap, A. Sesver, Investigation of parameters affecting grain growth of sintered magnesite refractories, Ceram. Int., 31 (2005) 121-127.

[64] H.J.S. Kriek, W.F. Ford, J. White, Effect of additions on the sintering and dead-burning of magnesia, Trans. Br. Ceram. Soc., 58 (1959) 1-34.

[65] A.U. Daniels, R.C. Lowrie, R.L. Gibby, I.B. Cutler, Observations on normal grain growth of magnesia and calcia, J. Am. Ceram. Soc., 45 (1962) 282-285.

[66] G.K. Layden, M.C. Mcouarrie, Effect of minor additions on sintering of MgO, J. Am. Ceram. Soc., 42 (1959) 89–92.

[67] J.W. Nelson, I.B. Cutler, Effect of oxide additions on sintering of magnesia, J. Am. Ceram. Soc., 41 (1958) 406-409.

[68] Y.B. Lee, H.C. Park, K.D. Oh, F.L. Riley, Sintering and microstructure development in the system MgO-TiO_2, J. Mater. Sci., 33 (1998) 4321- 4325.

[69] P.S. Mamykin, T.A. Drozdova, Sintering magnesia with boron additives, Refractories, 10 (1969) 765-768.

[70] M. Chaudhuri, A. Kumar, A.K. Bhadra, G. Banerjee, Sintering and grain growth in Indian magnesites doped with titanium dioxide, Interceram, 39 (1990) 26-30.

[71] M. Chaudhuri, G. Banerjee, A. Kumar, S.L. Sarkar, Secondary phases in natural magnesite sintered with addition of titania, ilmenite and zirconia, J. Mater. Sci., 34 (1999) 5821-5825.

[72] G. Banerjee, B. Mukherjee, M.K. Chatterjee, Some studies on spalling of magnesite refractories: effect of porosity on thermal spalling in high and low silica magnesite bodies, Trans. Ind. Ceram. Soc., 45 (1986) 29-31.

[73] P. Kumar, Burhanuddin, A. Kumar, A. Ghosh, S. Sinhamahapatra, H.S. Tripathi, Effect of titania on the microstructure evolution of sintered magnesite in correlation with its properties, Ceram. Int., 41 (2015) 9003-9008.

[74] R.K. Khandal, B.M.K. Reddy, P.K. Gangopadhyay, Thermal analysis studies on Karya magnesite from Karnataka, Proc. Indian Natn. Sci. Acad., 52 (1986) 565-572.

[75] R.K. Khandal, J.K. Singh, B.M.K. Reddy, P.K. Gangopadhyay, Characterisation of Kartanaka magnesite, Proc. Indian Natn. Sci. Acad., 51 (1985) 872-875.

[76] M.R. Rao, P.C. Sen, H.V.B. Rao, Mineralogy and refractory properties of Almora magnesite, Trans. Ind. Ceram. Soc., 17 (1958) 67-71.

[77] J.C. Banerjee, N.R. Sircar, A comprehensive study of Indian magnesites as refractory material, Trans. Ind. Ceram. Soc., 23 (1964) 49-59.

[78] J.C. Banerjee, S.P. Banerjee, N.R. Sircar, Sintering characteristics of Indian magnesites up to 2000 °C, Trans. Ind. Ceram. Soc., 26 (1967) 121-130.

[79] P. Kumar, A. Ghosh, H.S. Tripathi, Study of densification behaviour, microstructure vis-à-vis high temperature properties of commercially available Indian magnesites, Trans. Ind. Ceram. Soc., 75 (2016) 250-255.

[80] P. Kumar, M. Nath, U. Roy, A. Ghosh, H.S. Tripathi, Improvement in thermomechanical properties of off-grade natural magnesite by addition of Y_2O_3, Int. J. Appl. Ceram. Tec., 14 (2017) 1197-1205.

[81] J.C. Banerjee, S.P. Banerjee, N.R. Sircar, Chemical and magnetic properties of magnesites, Trans. Ind. Ceram. Soc., 26 (1967) 93-97.

[82] V.G. Rogozina, N.I. Baranovskii, N.V. Bortnikova, Improving the quality of magnesite refractory raw materials by beneficiation, Refractories, 31 (1990) 563-565.

[83] M.J. Pearse, An overview of the use of chemical reagents in mineral processing, Miner. Eng., 18 (2005) 139-149.

[84] A.N. Santana, A.E.C. Peres, Reverse magnesite flotation, Miner. Eng., 14 (2001) 107-111.

[85] J. Yao, W. Yin, E. Gong, Depressing effect of fine hydrophilic particles on magnesite reverse flotation, Int. J. Miner. Process., 149 (2016) 84-93.

[86] S. Aslani, H.R.S.B. Hashemi, F. Arianpour, Beneficiation of Iranian magnesite ores by reverse flotation process and its effects on shaped and unshaped refractories properties, Bull. Mater. Sci., 33 (2010) 697–705.

[87] T. Gambopoulos, A. Nestoridis, "Separation of magnesite from its contaminants by reverse flotation," USA Patent 3976251, 1976.

[88] V.A. Bron, M.I. Diesperova, I.A. Stepanova, A.P. Kukuruzov, N.F. Bugaev, K.V. Simonov, A.G. Luzin, N.I. Baranovskii, N.A. Yur'eva, Obtaining dense powder from Satkinsk magnesite beneficiated by flotation, Refractories, 11 (1970) 401-404.

[89] V.A. Smertin, V.I. Samusenko, Experience and prospects for beneficiating magnesite ores from the satkinsk deposits (Review), Refractories, 26 (1985) 295-303.

[90] A.M. Vieira, A.E.C. Peres, The effect of amine type, pH, and size range in the flotation of quartz, Miner. Eng., 20 (2007) 1008-1013.

[91] A.D. Cronberg, C.N. Impola, T.H. Lentz, "Use of primary aliphatic ether amine acid salts in froth flotation process," USA Patent 3363758, 1968.

[92] A.Z. Frangiskos, "Method for beneficiation of magnesite ore," USA Patent 3936372, 1976.

[93] A.W. Fahrenwald, "Flotation of magnesite and the like magnesium ores," USA Patent 2280905, 1942.

[94] A.J. Weinig, "Treatment of magnesite ores," USA Patent 2363029, 1944.

[95] A.J. Weinig, "Flotation of magnesite," USA Patent 2363030, 1944.

[96] A.J. Weinig, "Froth flotation treatment of low grade magnesite ores," USA Patent 2363031, 1944.

[97] A.J. Weinig, J.F. Mcintosh, "Beneficiation of low grade magnesite ores," USA Patent 2831574, 1958.

[98] T.L.B. Jepsen, "Controlled reagent introduction in a magnesite ore concentration process," USA Patent 3383057, 1968.

[99] V.P. Mehrotra, "Collecting agents for use in the froth flotation of silica-containing ores," USA Patent 4725351, 1988.

[100] A.C. Araujo, P.R.M. Viana, A.E.C. Peres, Reagents in iron ores flotation, Miner. Eng., 18 (2005) 219-224.

[101] S.K. Tripathy, S.I. Angadi, N.K. Patra, D.S. Rao, Comparative separation analysis of direct and reverse flotation of dolomite fines, Min. Proc. Ext. Met. Rev., 39 (2018) 339-350.

[102] M.R. Ignjatović, N. ćAlić, Z.S. Marković, R. Ignjatović, Development of a combined gravity-magnetic sepaitation process for magnesite ORE using HGMS, Magn. Electr. Separ., 6 (1995) 161-170.

[103] K.V. Simonov, V.P. Koptelov, Y.V. Mokshantsev, V.A. Smertin, R.S. Polovinkina, Magnesite beneficiation in heavy suspensions, Refractories, 19 (1978) 31-37.

[104] A.K. Mishra, P. Roy, S.S.R. Mahapatra, B. Mohanty, S. Majumdar, Bioleaching of silica from magnesite ore, Indian J. Technol., 24 (1986) 770.

[105] B.K. Mohanty, A.K. Mishra, Physical and chemical factors affecting the release of silicafrom magnesite ore by a Bacillus sp., J. Gen. Appl. Microbiol., 34 (1988) 233-241.

[106] H. Karaoglu, D. Yanmis, S. Gurkok, Magnesite enrichment with Pseudomonas Oryzihabitans isolated from magnesite ore, Geomicrobiol. J., 33 (2016) 46-51.

[107] D. Yanmis, F. Orhan, M. Gulluce, F. Sahin, Biotechnological magnesite enrichment using a carbonate dissolving microorganism, *Lactococcus sp*, Int. J. Miner. Process., 144 (2015) 21-25.

[108] B.D. Chattaraj, M.K. Chatterjee, Beneficiation of magnesite-an alternate approach, Trans. Ind. Ceram. Soc., 38 (1979) 188-196.

[109] V.E. Potapenko, D.I. Surorova, L.G. Tyurykhanov, V.V. Tydrykhanov, E.P. Mezentsev, K.V. Simonov, Beneficiation of calcined Satkinsk magnesite through magnetic separation, Ogneupory, 10 (1981) 25-27.

[110] A.M. Urvantsev, I.D. Kashcheev, Magnesite enrichment by a dry method, Refract. Ind. Ceram., 53 (2012) 78-81.

[111] D.I. Gavrish, K.K. Strelov, Y.M. Gelkin, Chemical methods for concentrating magnesite, Ogneupory, 2 (1977) 17-23.

[112] E.K. Kozhevnikov, L.P. Chernitskii, Beneficiation of Satkinsk magnesite by photometric separation, Refractories, 21 (1980) 347-349.

[113] E. Ahmed, A. Owais, Optimization of packed bed electrolysis of zinc anode casing of spent dry cell batteries, Hydrometallurgy, 163 (2016) 176-191.

[114] V.K. Kalyani, T. Pallavika , G. Charan, S. Chaudhuri, Optimization of a laboratory-scale froth flotation process using response surface methodology, Coal Prep., 25 (2005) 141-153.

[115] M.A. Bezerra, R.E. Santelli, E.P. Oliveira, L.S. Villar, L.A. Escaleira, Response surface methodology (RSM) as a tool for optimization in analytical chemistry, Talanta, 76 (2008) 965-977.

[116] G. Ye, L. Ma, L. Li, J. Liu, S. Yuan, G. Huang, Application of Box–Behnken design and response surface methodology for modeling and optimization of batch flotation of coal, Int. J. Coal Prep. Util., (2017) 1-15.

[117] A. Banerjee, P. Sarkar, S. Banerjee, Application of statistical design of experiments for optimization of As (V) biosorption by immobilized bacterial biomass, Ecol. Eng., 86 (2016) 13-23.

[118] J.B. Ferguson, H.E. Merwin, The ternary system CaO-MgO-SiO_2, Proc. Natl.Acad. Sci. U. S. A. , 5 (1919) 16-18.

[119] R.W. Ricker, E.F. Osborn, Additional Phase Equilibrium Data for the System CaO-MgO-SiO_2, J. Am. Ceram. Soc., 37 (1954) 133-139.

[120] P. Hudon, I.-H. Jung, D.R. Baker, Experimental investigation and optimization of thermodynamic properties and phase diagrams in the systems CaO–SiO_2, MgO–SiO_2, $CaMgSi_2O_6$–SiO_2 and $CaMgSi_2O_6$–Mg_2SiO_4 to 1·0 GPa, J. Petrol., 46 (2005) 1859-1880.

[121] R. Staut, Effects of the lime-silica ratio on the physical properties of magnesia-chrome ore composition, J. Am. Ceram. Soc., 51 (1972) 901-905.

[122] P.G. Lampropoulou, C.G. Katagas, D.C. Papamantellos, Composition of periclase and calcium-silicate phases in magnesia refractories derived from natural microcrystalline magnesite, J. Am. Ceram. Soc., 88 (2005) 1568-1574.

[123] T. Hatfield, G. Richmond, W.F. Ford, J. White, Compatibility relationship between the periclase and silicate phases in magnesite refractories at high temperatures, Trans. Br. Ceram. Soc., 69 (1970) 53-58.

[124] M.R. Rao, N.V. Naidu, A correlation of chemical composition, mineralogical constitution and physical properties of magnesite refractories, Trans. Ind. Ceram. Soc., 28 (1969) 35-43.

[125] R.A. Brown, Sintering in very pure magnesium oxide and magnesium oxide containing vanadium, Am. Ceram. Soc. Bull., 44 (1965) 483-487.

[126] K. Hamano, Z.-e. Nakagawa, H. Watanabe, Effect of magnesium chloride on sintering of magnesium oxide, Advances in Ceramics, 10 (1984) 610-618.

[127] T. Lucion, P.H. Duvigneaud, A. Laudet, J.F. Stenger, E. Gueguen, Effect of TiO_2 additions on the densification of MgO and MgO–CaO mixtures, Key Eng. Mater., 264-268 (2004) 209-212.

[128] V. Martinac, M. Labor, N. Petric, Effect of TiO_2, SiO_2 and Al_2O_3 on properties of sintered magnesium oxide from sea water, Mater. Chem. Phys., 46 (1996) 23-30.

[129] T. Matsumoto, A. Kato, Effects of additives on sintering of CVD-MgO powders, Ceram. Int., 16 (1990) 325-331.

[130] J.W. Nelson, I.B. Cutler, Effect of oxide additions on sintering of magnesia, Journal of the American Ceramic Society, 41 (1958) 406-409.

[131] N. Petric, B. Petric, V. Martinac, N. Bogdanic, M. Mirosevic-Anzulovic, M. Labor, Sintering of magnesium oxide obtained from sea water, J. Am. Ceram. Soc., 13 (1994) 545–549.

[132] N. Petric, B. Petric, M. Mirosevic-Anzulovic, N. Bogdanic, Investigating the magnesium oxide sintering process, CFI- Ceramic Forum International, 65 (1988) 7-10.

[133] Z. Wang, Z. Xu, B. Zhang, X. Wang, Effect of mixture of rare earth oxides on microstructure and properties of magnesia refractory, Rare Metal Mat. Eng., 36 (2007) 373-375.

[134] B. Zhang, Z. Wang, S. Zhang, X. Wang, Z. Xu, Effects of rare earth oxides on microstructures and properties of magnesia refractories, Key Eng. Mater., 368-372 (Part 2) (2008) 1158-1160.

[135] O. Vasylkiv, Y. Sakka, V.V. Skorokhod, Hardness and fracture toughness of alumina-doped tetragonal zirconia with different yttria contents, Mater. Trans., 44 (2003) 2235-2238.

[136] K. Das, S. Mukherjee, P.K. Maiti, P.G. Pal, Microstructural and densification study of natural Indian magnesite in presence of zirconia additive, Bull. Mater. Sci., 33 (2010) 439-444.

[137] R. Kusiorowski, J. Wojsa, B. Psiuk, T. Wala, Influence of zirconia addition on the properties of magnesia refractories, Ceram. Int., 42 (2016) 11373-11386.

[138] Burhanuddin, A. Kumar, P. Kumar, A. Ghosh, S. Sinhamahapatra, H.S. Tripathi, Effect of zirconia on densification and properties of natural Indian magnesite, Int. J. Miner. Process., 144 (2015) 40-45.

[139] Z. Zhihui, L. Nan, Influence of mechanical activation of Al_2O_3 on synthesis of magnesium aluminate spinel, Sci. Sinter., 36 (2004) 73-79.

[140] J. Laming, Sintered and Chemically Bonded MgO-Chrome Ore Refractories, in: A.M. Alper (Ed.) High Temperature Oxides, Part 1, Magnesia, Lime and Chrome Refractories, Academic Press, New York, 1970, pp. 143-189.

[141] D.J. Bray, Toxicity of chromium compounds formed in refractories, Am. Ceram. Soc. Bull., 64 (1985) 1012-1016.

[142] C.G. Marvin, Chrome-bearing hazardous waste, Am. Ceram. Soc. Bull., 72 (1993) 66-68.

[143] C. Baudin, R. Martinez, P. Pena, High temperature mechanical behavior of stoichiometric magnesium spinel, J. Am. Ceram. Soc., 78 (1995) 1857-1862.

[144] W.T. Baker, J.G. Lindsay, Reactive magnesia spinel, preparation and properties, Am. Ceram. Soc. Bull., 46 (1967) 1094-1097.

[145] J.T. Baitley, R.R. Jr., "Sintered spinel ceramics"; in *Proceedings of 69th Annual Meeting of the American Ceramic Society*, New York, 1967, pp.

[146] S. Miglani, J.J. Uchno, "Resin bonded alumina-magnesia-carbon brick for ladles"; in *Proceedings of Unified International Technical Conference on Refractories (UNITECR '97)*, New Orleans, Louisiana USA, 1997, pp. 193-201

[147] W.H. Bragg, The structure of the spinel group of crystals, Philos. Mag., 30 (1915) 305-315.

[148] S. Nishikawa, Structure of some crystals of the spinel group, Proc. Math. Phys. Soc., 8 (1915) 199-209.

[149] N.F.M. Henry, K. Lonsdale, International Tables for X-ray Crystallography, Kynoch Press, Birmingham, England, 1952.

[150] K.E. Sickafus, J.M. Wills, N.W. Grimes, Structure of spinel, J. Am. Ceram. Soc., 82 (1999) 3279-3292.

[151] N. Kashii, H. Maekawa, Y. Hinatsu, Dynamics of the Cation Mixing of $MgAl_2O_4$ and $ZnAl_2O_4$ Spinel, J. Am. Ceram. Soc., 82 (2004) 1844-1848.

[152] S. Zhang, W. Lee, Spinel-Containing Refractories, 2004.

[153] G.A. Rankin, H.E. Merwin, The ternary system CaO-Al_2O_3-MgO, J. Am. Chem. Soc., 38 (1916) 568-588

[154] A.M. Alper, R.N. McNally, P.H. Ribbe, R.C. Doman, The System MgO–$MgAl_2O_4$, J. Am. Ceram. Soc., 45 (1962) 263-268.

[155] B. Hallstedt, Thermodynamic assessment of the system MgO-Al_2O_3, J. Am. Ceram. Soc., 75 (1992) 1497-1507.

[156] R. Sarkar, A. Ghosh, S.K. Das, Reaction sintered magnesia rich magnesium aluminate spinel: effect of alumina reactivity, Ceram. Int., 29 (2003) 407-411.

[157] E. Ryshkewitch, Oxide Ceramics, Academic Press, New York, 1960.

[158] I. Ganesh, S. Bhattacharjee, B.P. Saha, R. Johnson, Y.R. Mahajan, A new sintering aid for magnesium aluminate spinel, Ceram. Int., 27 (2001) 773-779.

[159] I. Ganesh, K.A. Teja, N. Thiyagarajan, R. Johnson, B.M. Reddy, Formation and densification behavior of magnesium aluminate spinel: the influence of CaO and moisture in the precursors, J. Am. Ceram. Soc., 88 (2005) 2752–2761.

[160] I. Ganesh, S.M. Olhero, A.H. Rebelo, J.M.F. Ferreira, Formation and densification behaviour of $MgAl_2O_4$ spinel: the influence of processing parameters, J. Am. Ceram. Soc., 91 (2008) 1905–1911.

[161] I. Ganesh, G.J. Reddy, G. Sundararajan, S.M. Olhero, P.M.C. Torres, J.M.F. Ferreira, Influence of processing route on microstructure and mechanical properties of $MgAl_2O_4$ spinel, Ceram. Int., 36 (2010) 473-482.

[162] F.N. Cunha-Duncan, R.C. Bradt, Synthesis of magnesium aluminate spinels from bauxites and magnesias, J. Am. Ceram. Soc., 85 (2002) 2995-3003.

[163] D. Mohapatra, D. Sarkar, Preparation of MgO-$MgAl_2O_4$ composite for refractory application, J. Mater. Process. Technol., 189 (2007) 279-283.

[164] D. Domanski, G. Urretavizcaya, F.J. Castro, F.C. Gennari, Mechanochemical synthesis of magnesium aluminate spinel powder at room temperature, J. Am. Ceram. Soc., 87 (2004) 2020-2024.

[165] L.R. Ping, A.-M. Azad, T.W. Dung, Magnesium aluminate ($MgAl_2O_4$) spinel produced via self-heat-sustained (SHS) technique, Mater. Res. Bull., 36 (2001) 1417-1430.

[166] L.B. Kong, J. Ma, H. Huang, $MgAl_2O_4$ spinel phase derived from oxide mixture activated by a high-energy ball milling process, Mater. Lett., 56 (2002) 238-243.

[167] K.T. Faber, M.D. Huang, A.G. Evans, Quantitative studies of thermal shock in ceramics based on a novel test technique, J. Am. Cer. Soc., 64 (1981) 296-301.

[168] I. Peretz, R.C. Bradt, Andalusite derived mullite matrix refractories, Ceram. Trans., 6 (1990) 613-633.

[169] H.S. Tripathi, S. Kr Das, G. Banerjee, Thermal shock behaviour of high alumina aggregates derived from sillimanite beach sand with and without Fe_2O_3 doping, Ceram. Int., 26 (2000) 1-6.

[170] B. Tuchołka-Szmeja, T.B. Wala, Thermal shock acoustic emission and microstructure of refractories I. High Alumina refractories (60–90% Al_2O_3), Ceram. Int., 20 (1994) 359-366.

[171] S.L.C. Ferreira, R.E. Bruns, H.S. Ferreira, G.D. Matos, J.M. David, G.C. Brandão, E.G.P. da Silva, L.A. Portugal, P.S. dos Reis, A.S. Souza, W.N.L. dos Santos, Box-Behnken design: An alternative for the optimization of analytical methods, Anal. Chim Acta, 597 (2007) 179-186.

[172] C. Ghosh, S. Sinhamahapatra, H.S. Tripathi, Effect of ZrO_2 on the densification behavior and properties of Indian magnesite, Int. J. Appl. Ceram. Technol., 16 (2019) 410-417.

[173] C. Ghosh, S. Sinhamahapatra, H.S. Tripathi, U. Sarkar, Reverse flotation of natural magnesite and process optimization using response surface methodology, Mining, Metallurgy & Exploration, (Under review).

[174] C. Ghosh, A. Ghosh, H.S. Tripathi, J. Ghosh, M.K. Haldar, Studies on densification, mechanical, microstructural and structure-properties relationship of refractory aggregates prepared from Indian magnesite by changing lime-silica ratio, Ceram. Int., 40 (2014) 16791-16798.

[175] M.K. Haldar, C. Ghosh, A. Ghosh, Studies on synthesis and characterization of magnesia based refractory aggregates developed from indian magnesite, J Mat Sci Chem Engg, 2 (2014) 1-8.

[176] J. Gebauer, D.A. Krohn, D.P.H. Hasselman, Thermal-stress fracture of a thermomechanically strengthened aluminosilicate ceramic, J. Am. Ceram. Soc., 55 (1972) 198-201.

[177] H.P. Kirchner, R.M. Gruver, R.E. Walker, Strngthening alumina by glazing and quenching, Bull. Am. Ceram. Soc., 47 (1968) 798-802.

[178] H.P. Kirchner, R.E. Walker, D.R. Platts, Strengthening alumina by quenching in various media, J.Appl. Phys., 42 (1971) 3685-3692.

[179] C. Ghosh, A. Ghosh, M.K. Haldar, Studies on densification, mechanical, micro-structural and structure-properties relationship of magnesium aluminate spinel refractory aggregates prepared from Indian magnesite, Mat. Char., 99 (2015) 84-91.